Investigations on the structure-toxicity relationship of different α-synuclein aggregates associated with Parkinson's disease

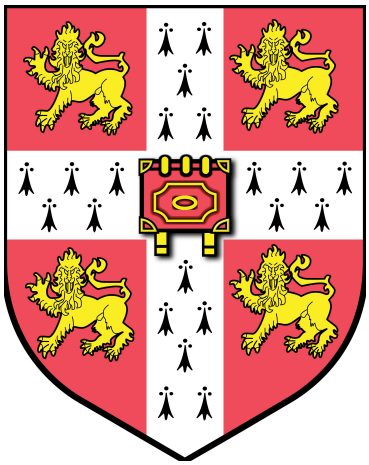

Marta Castellana Cruz

Supervised by Professor Sir Christopher Dobson and Professor Michele Vendruscolo

Wolfson College

University of Cambridge

October 2020

This thesis is submitted for the degree of *Doctor of Philosophy*

Declaration

I hereby declare that:

This thesis is the result of my own work and includes nothing which is the outcome of work done in collaboration except as declared in the preface and specified in the text.

I further state that no substantial part of my thesis has already been submitted, or, is being concurrently submitted for any such degree, diploma or other qualification at the University of Cambridge or any other University or similar institution except as declared in the Preface and specified in the text.

It does not exceed the prescribed word limit for the Physics and Chemistry Degree Committee.

Investigations on the structure-toxicity relationship of different α-synuclein aggregates associated with Parkinson's disease

Marta Castellana Cruz

Parkinson's disease is characterized by the disruption of motor functions as a consequence of the degeneration of the dopaminergic neurons of the substantia nigra pars compacta. This neuronal degeneration is preceded by the formation of α-synuclein aggregates denoted Lewy bodies and neurites. Due to their potential value for the understanding of Parkinson's disease (PD) and the development of effective treatments, a number of mouse models of PD have been developed. A particular PD model, referred to as the preformed fibrils (PFF) PD mouse model, has been shown to reproduce many features of PD, although a great variability of phenotypes has been reported. Here, we studied how the preparation and storage of different α-synuclein conformers can influence this model. We concluded that only freshly prepared short α-synuclein fibrils were able to induce a strong phenotype in mice. After this, the difference in toxicity between kinetically trapped oligomers derived from different α-synuclein variants was explored. From these experiments it was concluded that WT and G51D oligomers induce a stronger toxicity than other α-synuclein mutational variants. It was also possible to determine that different α-synuclein fibrillar species are able to recruit endogenous α-synuclein at different rates. Finally, it was intended to explore the cellular toxicity of these different fibrillar α-synuclein aggregates through the widely used MTT (3-(4,5-dimethylthiazol-2-yl)-2,5-diphenyltetrazolium bromide) assay. While performing these experiments it was observed that, α-synuclein fibrils and other unrelated amyloid aggregates were able to induce the formation of formazan crystals that resulted in a false-positive result. The nature of this phenomena, the time scale in which it happens, and which species were able to induce it were explored. It was concluded that amyloid fibrils, but not monomers or kinetically trapped oligomers, were able to induce the formation of these crystals at nanomolar

concentrations and in a timescale of hours after the initial exposure. By exploring how structural characteristics of amyloid aggregates influence cell toxicity, I have been able to identify key attributes that can be used in improving *in vivo* models of Parkinson's disease, find new secondary structural markers that correlate with cellular toxicity and to provide an insight of how to measure cell viability in a reliably way.

Acknowledgements

This PhD thesis is dedicated to the memory of Professor Sir Christopher Dobson, who gave me the opportunity to come to Cambridge and welcomed me as a PhD student in his group. He was extremely supportive and encouraging during the three years that I spent under his supervision. I also want to thank Professor Michele Vendruscolo, who kindly took me into his group and supported me during the final year of my PhD.

I am also deeply grateful for the guidance and support of Dr. Janet Kumita during these four years. She taught me how to be a better scientist and to always be kind towards others, and ultimately this work would not have been possible without her. Also essential for this work were the guidance and support form Dr. Nunilo Cremades, who welcomed me into her lab for three months and offered her inestimable advice during the whole PhD. I also want to thank our collaborators Dr. Laura Volpicelli-Daley and Jessica Froula who contributed greatly to this project. I am also grateful to José Camino, with whom I collaborated during my visit in Dr. Nunilo Cremades lab, and all the people from the BIFI (Zaragoza, Spain) who welcomed and helped me during those months. I would specially like to thank Dr. Serene Chen, who introduce me to the different biophysical techniques when I arrived to the lab, and our wonderful research assistants Ewa Klimont and Swapan Preet for all their help and support. I would also like to dedicate a special thank you to Dr. Benedetta Mannini, who introduce me to the worlds of the iPSC and trusted in me to become part of her team, I have learnt and I keep learning from her not only scientifically but also personally. Finally, I would also like to thank the whole community of the CMD.

On a more personal note, I am extremely grateful to Catherine Xu, Katarina Pisani and Swapan Preet for all the advise, support, feedback, friendship and all the fun during these four years. They became my support network within the CMD and I would not have made until the end without them.

Finally I am deeply grateful to my mum, Ana María Cruz Martín, for her unrelenting support without which I would not be here. I would also like to acknowledge my dad, Jordi Castellana Ribas, and the rest of my family, grandparents, aunts, uncle and cousins, who encouraged and supported me through this adventure.

Contents

List of Figures

List of Tables

List off abbreviations

PD: Parkinson's disease
IDP: Intrinsically disordered protein
EM: Electronic microscopy
AFM: Atomic force microscopy
ssNMR: Solid state nuclear magnetic resonance
MSA: Multiple system atrophy
SNcp: Substantia nigra pars compacta
TH: Tyronise hydroxylase
DMPS: Dimyristoyl phosphatildylserine
ROS: Reactive oxygen species
NKA: Sodium potassium ATPase
iPSC: Induced pluripotent stem cell
GFP: Green fluorescent protein
YFP: Yellow fluorescent protein
MPTP: 1-methyl-4-phenyl-1,2,3,6-tetrahydropyridine
PFF: Pre-formed fibril
WT: Wild type
rAAV: Recombinant adeno-associated virus
LPS: Lipopolysaccharide
BAC: Bacterial artificial chromosome
MTT: 3-(4,5-dimethylthiazol-2-yl)-2,5-diphenyltetrazolium bromide
DNA: Deoxyribonucleic acid
DTT: Dithiothreitol
SEC: Size exclusion chromatography
PBS: Phosphate buffered saline
RT: Room temperature
PEG: Polyethylene glycol
DMSO: Dimethyl sulfoxide
CD: Circular dichroism
FT-IR: Fourier transform infrared
TEM: Transmission electron microscopy

ThT: Thioflavin T
ATP: Adenosine triphosphate
FRET: Fluorescence resonance energy transfer
IAPP: Islet amyloid precursor protein
DLS: Dynamic light scattering
WGA: Wheat germ agglutinin
PICUP: Photo-induced cross-linking of unmodified proteins
MTS: 3-(4,5-dimethylthiazol-2-yl)-5-(3-carboxymethoxyphenyl)-2-(4-sulfophenyl)-2H-tetrazolium
LDH: Lactate dehydrogenase

Chapter 1

Introduction

Disorders such as Alzheimer's disease, Parkinson's disease (PD), spongiform encephalopathies, type II diabetes and systemic amyloidoses, amongst others, can all be classified as protein misfolding diseases. This term encompasses a variety of pathologies associated with the conversion of physiological soluble proteins, of variable primary sequences and tertiary structure, into toxic aggregates and fibrils that share a common amyloid core [1, 2].

1.1 Amyloid fibril formation

Under optimal conditions proteins find the lowest energy point in their physiological native state, being that a folded one, in the case of globular protein, or a disordered one, in the case of intrinsicaty disordered proteins (IDP). However if these conditions were to change (i.e. increment of concentration, temperature, protein fragmentation, non-physiological post-translational modifications...) states of a lower energy may arise [3] (Figure 1.1). Under these pathological conditions proteins can misfold, exposing hydrophobic residues to the solvent, and self-assemble into several aggregate structures, including large, insoluble fibrillar entities known as amyloids. The study of amyloids through different biophysical methods (electronic microscopy (EM), atomic force microscopy (AFM), Fourier transformed infrared spectroscopy (FT-IR), solid state nuclear magnetic resonance (ssNMR) and x-ray crystallography) has highlighted several features. Amyloids are unbranched thread-like structures that posses a cross-β structure in which the β strands are perpendicular to the fibrillar axis, these fibrils are composed of protofilaments that associate to form larger fibrils of 7-13 nm in diameter and microns in length [1]. Diverse proteins of different size and sequence, from IDPs as α-synuclein or Aβ to globular proteins as lysozyme or insulin, can aggregate into these amyloid structures [3]. In fact, since many

proteins, pathological or not, can form amyloid fibrils, it has been suggested that under certain conditions, any protein is capable of forming an amyloid [4, 3].

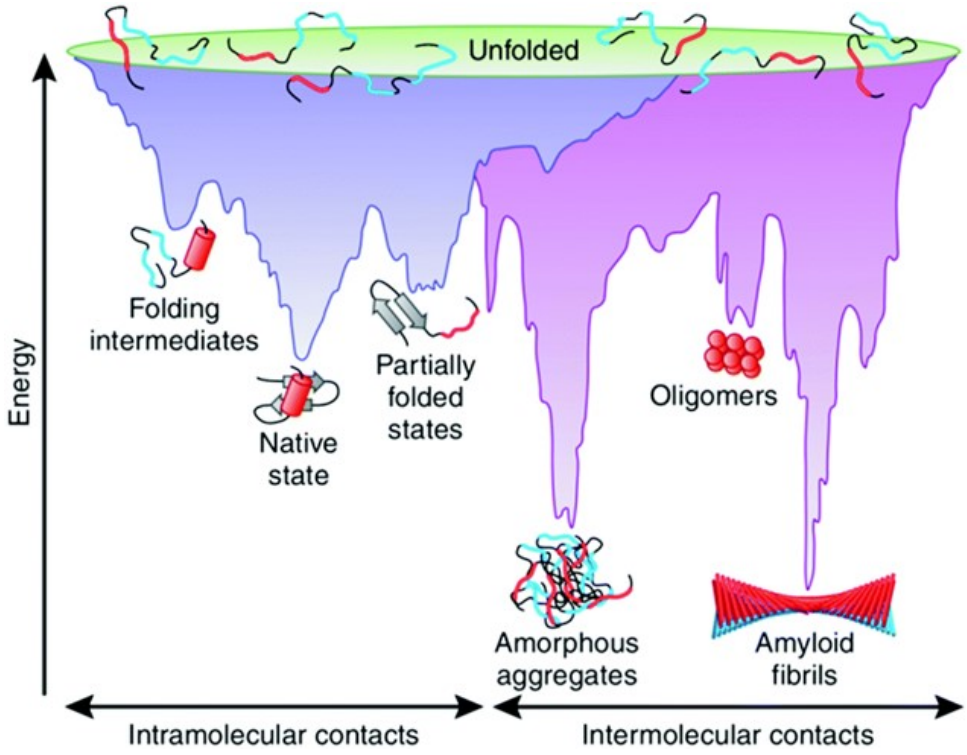

Figure 1.1: Energy landscape of protein folding and aggregation. In purple, the the multitude of conformations 'funneling' to the native state and in the pink, the conformations moving toward amorphous aggregates or amyloid fibrils. Both parts of the energy surface overlap. Reproduced from [3]

The process of the monomer aggregation into amyloid fibrils can be monitored by several compounds like Thioflavin T, a fluorescent dye that binds specifically to the amyloid structure. Although its mechanism of binding still has to be fully elucidated, the most accepted theory hypothesises that Thioflavin T binds to the surface of amyloid fibrils, specifically to the spaces left between the structures form by the interaction of the side-chains of the amino acids present in the cross-β structure. Once bound to these regions, the Thiofalvin T molecules are immobilised into specific conformations with a higher fluorescence than the free form [5]. The use of Thioflavin T has allowed the monitoring of the bulk aggregation reaction of different proteins like Aβ_{42}, Aβ_{40}, α-synuclein, tau or lysozyme. The kinetic profiles of fibril formation *in vitro* shows typically a sigmoidal behaviour characteristic of a nucleation-polymerisation process where three phases can be macroscopically differentiated: a nucleation or lag phase, characteristic of *de novo* formation of new aggregates directly from monomers, an exponential phase, that reflects the greater ease of addition of monomer onto existing aggregates, and a

plateau phase, consequence of the depletion of monomer from the solution (Figure 1.2). The application of chemical kinetics to the data obtained in bulk reaction has allowed to further study the processes that occur during the lag phase. Specifically, the kinetic analysis pointed the nucleation phase was not only dominated by primary nucleation, the process by which monomer form small nuclei, but also by secondary processes such as secondary nucleation, in which the existing amyloid fibrils act as catalytic surfaces for the formation of new amyloid nuclei, or fibril fragmentation, that directly increases the number of ends available for elongation. However, the aggregation pathway of different proteins are influenced by these processes on different ways, for example, the aggregation kinetics of Aβ_{42} is largely influenced by secondary nucleation processes while they only affects α-synuclein aggregation at acidic pHs [2, 1, 6, 7]. Recent studies [8, 9] on this small nucleai, denominated oligomers and which are in nature transient species, do not convert into fibrils but dissociate back into monomers. Moreover, this oligomer population is heterogeneous in size and probably composed by both on-pathway (oligomers with the right structure to progress into fibrils) and off-pathway oligomers(oligomers that will not covert into fibrils and that may be kinetically trapped). Together this illustrate the high complexity of the amyloid aggregation and the difficulties that may arise to successfully isolate and study specific elements of it.

1.2 Parkinson's Disease

The aggregation of α-synuclein is related to several neurodegenerative diseases called synucleinopathies, such as Parkinson's disease (PD), dementia with Lewis bodies and multiple system atrophy (MSA). PD is the second most common neurodegenerative disease in humans and its clinical symptoms include the disruption of motor functions (resting tremor, muscular rigidity, impaired postural, reflexes, and bradykinesia), depression and a general slowing of intellectual processes; although the severity of these symptoms differs between patients. Pathologically, PD is characterised by the degeneration of the dopaminergic neurons of the substantia nigra pars compacta (SNpc), which provokes a drop in the dopamine levels in its striatal projections and consequently, results in the motor impairment characteristic of the disease. This degeneration of the dopaminergic neurons is preceded by the formation of insoluble cytoplasmic (Lewy bodies) and neuritic (Lewy neurites) aggregates. These Lewys bodies and neurites are filamentous by EM, hyperphosphorylated, ubiquitinated and insoluble in anionic detergent. They are primarily composed by the amyloid form α-synuclein, although a plethora of other proteins (ubiquitin, tau, tubulin, synphilin-1, tyrosine hydroxylase, synaptophysin, p35, p38, parkin...) and lipids can also be found inside them [10, 11]. The Lewy bodies and

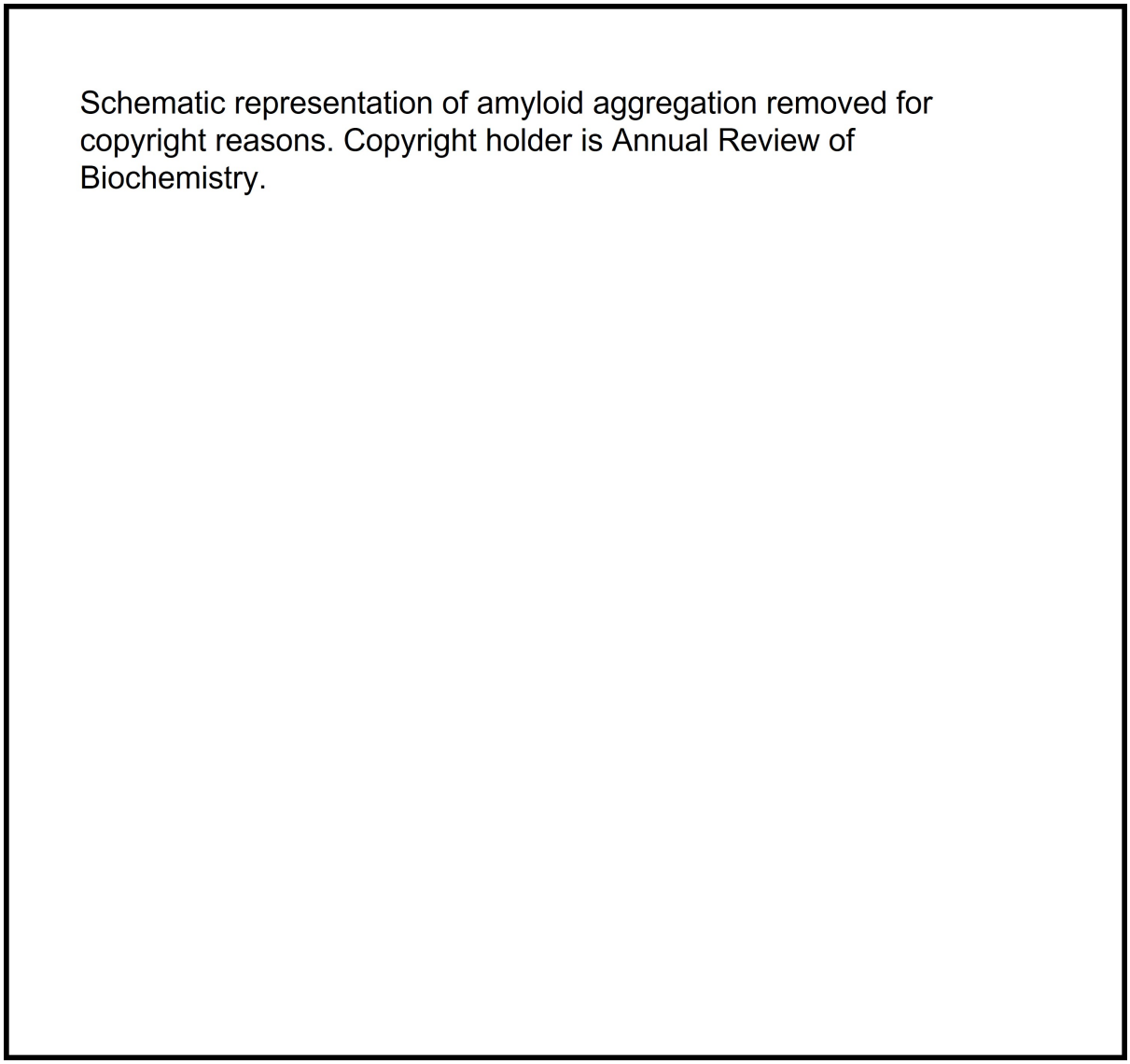

Figure 1.2: Schematic representation of the different processes that can lead to the formation of amyloid fibrils. The figure have been taken from [1].

neurites occur first in the anterior olfactory nucleus and dorsal motor nucleus, then in the pedunculopontine nucleus, raphe nucleus and SNpc and finally in the hippocampus and cortex (Figure 1.4)[12].

PD is primarily a sporadic disease in which symptoms appear between the age of 50 and 60 and its aetiology remains broadly unknown, due to the large number of predisposing genes and environmental factors involved. Although they only represent around the 10 % of the cases, there are also hereditary variants of the disease, usually with an earlier onset, caused by mutations in several genes, like SCNA (that encodes for α-synuclein, which structure and function will be addressed in section 1.3), LRRK2 (a kinase with GTPase activity involved in the regulation of a variety of cellular processes like endocytosis,

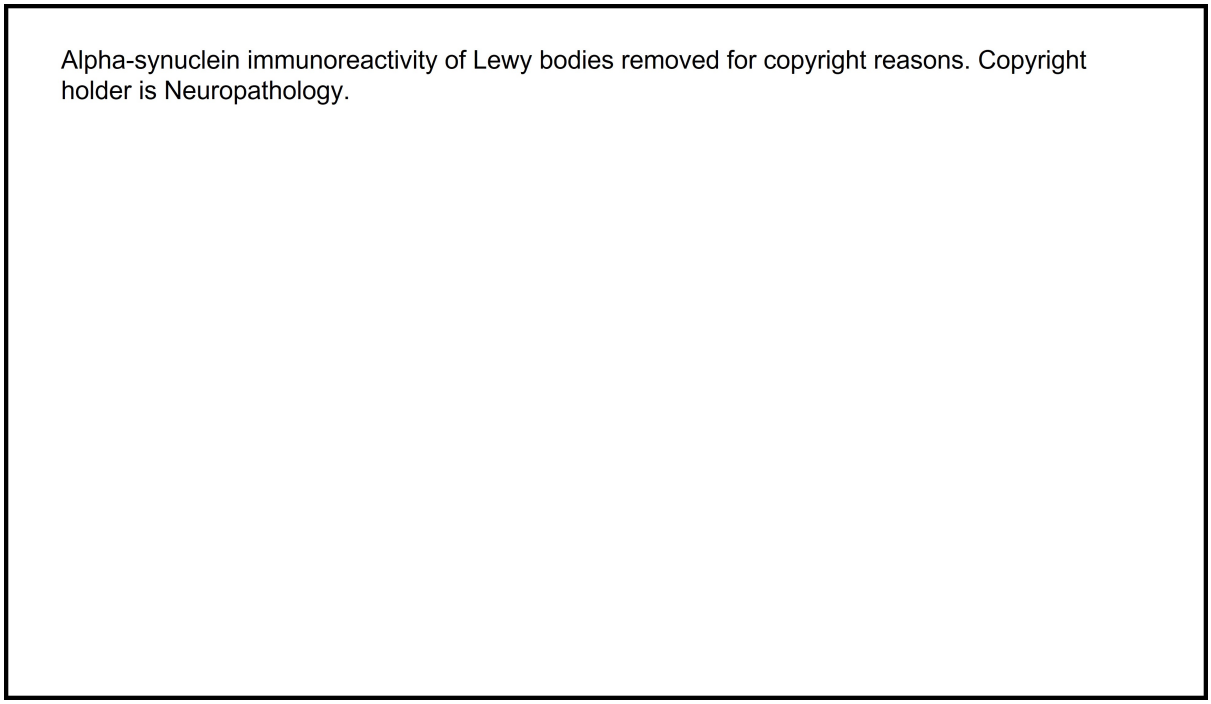

Figure 1.3: α-Synuclein immunoreactivity of Lewy bodies at different maturation stages in the substantia nigra. (A) No α-synuclein immunoreactivity. (B) Diffuse, pale cytoplasmic staining. (C) Irregularly shaped, uneven staining. (D) Discrete staining corresponding to the pale body. (E) Abnormal α-synuclein aggregate displaying both pale body (asterisk) and Lewy body (arrow). (F) Donut-shaped Lewy body. Scale bar correspond to 10 μM. Reproduced from [11]

autophagy, or the formation of the neurites cytoskeleton), PINK 1 (a serine/threonine kinase involve in the induction of autophagy of depolarised mitochondria), or Parkin (an E3 ubiquitin ligase also involved in the induction of mitophagy). In fact, several mutations in α-synuclein (A30P, E46K, A53T, G51D and H50Q) have been identified as the direct causes of the disease [13, 10]. The truncation of α-synuclein has also been related to increased aggregation and Parkinson's disease [14].

1.3 α-Synuclein and its role in disease

As it has been mention before α-synuclein is the main component of the Lewy bodies and neurites, moreover mutations in this gene have been proven to be directly linked to genetic forms of PD. Due to this direct association α-synuclein structure, function and aggregation pathway have been extensively studied.

The human physiological isoform of α-synuclein contains 140 amino acid (aa) residues. Its primary sequence can be divided into three domains: the N-terminal domain, the NAC (non-amyloid-β-component) domain and the C-terminal domain (Figure 1.5). The

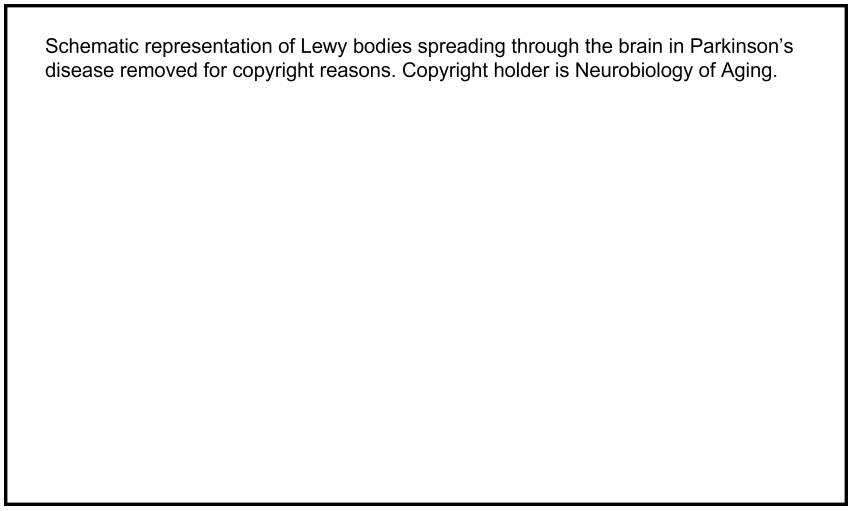

Figure 1.4: Schematic representation of Lewy bodies and neurites spreading within the brain (white arrows). The image have been adapted from [12].

N-terminal domain (aa 1-65) contains six imperfect KTKEGV repeats that allow this region to form an amphipathic α-helix able to bind lipids [15]. The amyloidogenic ability of α-synuclein resides in the NAC domain (aa 66-95) [16], which under physiological conditions remains protected by establishing intra-molecular interactions with the C-terminal domain (aa 96-140), that contains several negative charged residues [17]. α-Synuclein is abundantly expressed in the brain, and under physiological conditions, it is mainly localised in the presynaptic terminals. Although the role of α-synuclein within the cell has not been fully elucidated, in part because it is believe that other isoforms (β- and γ-synuclein) are able to partially fulfil its role, there is strong evidence that it is involved in the regulation of synaptic trafficking and homeostasis [10]. Specifically, α-synuclein has been reported to inhibit phospholipases D1 and D2 which suggest that it may be involved in the cleavage of membrane lipids and its biogenesis. It has also being identified as an inhibitor of the tyrosine hydroxylase (TH) and hence the dopamine synthesis, as well as to perturb the traffic between the endoplasmatic reticulum and the Golgi. Moreover it assists in the assembly of the synaptic SNARE complex, this function is key to the long-term functioning of neurons, as α-, β-, γ-synuclein triple-knockout mice showed reduced assembly of the SNARE complex accompanied by neurological impairment and reduced lifespan [18]. Together this suggest the α-synuclein is indeed involved in the mediation of neurotransmitter release and synaptic plasticity.

The aggregation of α-synuclein from monomer to oligomers to fibrils and bigger intracellular inclusions have been linked with several diseases including PD, dementia with Lewis bodies and multiple systemic atrophy. This highlights the importance of understanding the aggregation pathway of α-synuclein and to determine the origins of its

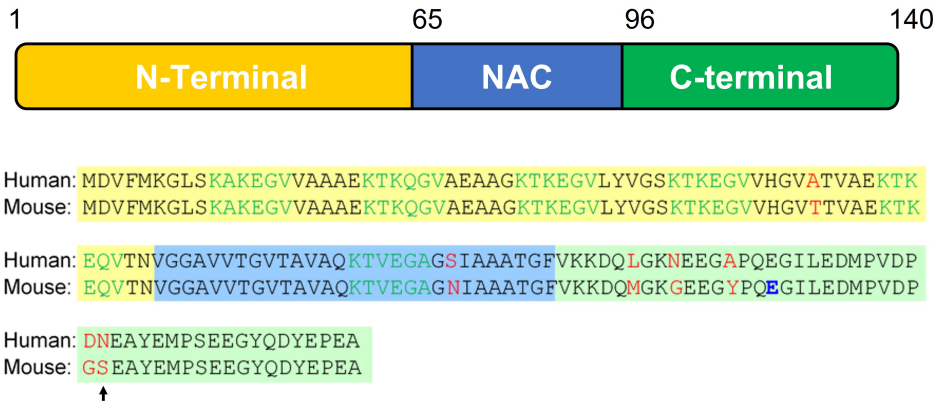

Figure 1.5: Schematic representation of α-synuclein and comparison between the human and mouse α-synuclein sequences. Amino acids which differ between the two species are coloured in red and the six imperfect KTKEGV repeats in green. The N-terminal domain is shadowed in yellow, the NAC region in blue and the C-terminal domain in green. Coloured in blue, the E used to generate the E110C α-synuclein cysteine mutants. The N used to generate the N122C human mutant of α-synuclein is colour in red since its correspond to one of the amino acids that differ between the two species (N122S) and signalised with a black arrow

toxicity. In bulk, primary nucleation of α-synuclein is extremely slow under quiescent conditions, remaining a monomeric solution even after weeks of incubation at 37 °C even at concentrations as high as 100 μM. Because of this, in order to study the aggregation pathway of α-synuclein is necessary to add external factors such us shacking conditions, negatively charge phospholipids or to seed the reaction at lower pH [7]. The study of the aggregation pathway under shacking condition gives us an idea of how prone a specific variant of α-synuclein is to aggregate. However, due to the unpredictability factor introduced by the agitation itself it is only possible to fit theses kinetics globally, but not to evaluate how different processes (primary nucleation, fragmentation and secondary nucleation) contribute to the aggregation process [19]. Using this method it has been determined that the pathological variants of α-synuclein A53T, E46K, H50Q [20, 21, 22] and several truncates (1-108, 1-124, 1-135, 1-133, 1-122) [14, 23, 24, 25] of α-synuclein accelerate aggregation compared to the WT (wild type) protein while the G51D variant slows it [26]. In order to study the primary nucleation processes in more detail it is possible to induce the aggregation of α-synuclein under quiescent conditions by the addition of negatively charge phospholipids (Dimyristoyl phosphatidylserine [DMPS]) vesicles to the mixture [27]. Under these conditions of aggregation α-synuclein A53T, A30P and 1-119 variants of α-synuclein presented an increase rate of aggregation respect of the WT while E46K, H50Q and G51D decreased it. Differences between these results and the ones observed under shacking conditions can be attributed to the enhancement of primary nuc-

leation and fragmentation induced by the shaking itself as well as to differences between the lipid-binding abilities of the different mutants [28, 29]. At mildly acidic pH 4.8, a condition relevant in the context of endocytosis or degradation of α-synuclein, it is possible to observe secondary nucleations processes driving the aggregation of α-synuclein. In this context all variants except of H50Q and G51D displayed a similar aggregation kinetics than the WT while H50Q and G51D showed very slow aggregation rates [28, 29]. Finally the last aspect to take into account when studying the aggregation process of α-synuclein is the elongation rate. All variants showed a similar elongation rates although the cross-seeding between monomers and seeds of different variants slowed the elongation process [28, 29]. This is specially relevant in a cellular context where different truncation forms of α-synuclein and in the genetic cases of PD different α-synuclein variants will coexist. Furthermore, the slower aggregation rate displayed by H50Q and G51D across the different aggregation experiments does not necessarily correlate with a lower toxicity. As it has been mentioned before, oligomers are formed during the lag phase of the aggregation pathway and a longer lag phases may translate into an increment of the number of these species, suspected to be highly toxic.

The question of which α-synuclein species presents greater cellular toxicity and triggers the development of these diseases is still a highly debated topic, with results supporting both, the oligomers [30, 31, 20] and the fibrils [32, 33] as the main toxic species. A study of the conformers present during the aggregation process of α-synuclein has allowed the isolation and characterisation of two types of oligomers, denominated “Type A” and “Type B” [30]. “Type A” oligomers appear earlier in the aggregation process, present a primarily disordered structure, are sensitive to proteinase K degradation, and are essentially benign when exposed to primary neuronal cells. In contrast, type B oligomers posses a β-sheet folding core, are resistant to proteinase K degradation and highly neurotoxic. Given the importance of the two oligomeric species types, our group developed a method to produce enriched samples of kinetically trapped oligomers that display similar structural and toxic features to the “Type B” on pathway oligomers previously identified [34]. Kinetically trapped oligomer similar to "Type A" can be generated by the incubation of α-synuclein with (-)-epigallocatechin-3-gallate (EGCG) [35, 36] (Figure 1.6). Kinetically trapped "Type B" oligomers share the same FRET pattern that on-pathway "Type B" oligomers and their biophysical characterisation showed that they posses an hydrophobic antiparallel β-sheet core with and intermediate β-sheet content (35 $\pm$ 5 %) between a fibril (65 $\pm$ 10 %) and a monomer [34]. These results were further confirmed by ss-NRM, that in addition was able to identified an unfolded free 26 residues region a the N-terminal and a 40 residues region at the C-terminal [36]. Two different populations can be identified within these stabilised oligomers, one of 10S composed by 11-25 α-synuclein

monomers, and another one of 15S composed by 19-39 α-synuclein monomers. Using cryoEM it was possible to determinate that both population are composed by cylindrical oligomers with a low electron density region running through the cylinder. EGCG stabilised "Type A" oligomers also shared the same FRET pattern than their on-pathway counterparts, however both FT-IR and ssNMR revealed that they posses an unstructured core with an exposed 43 residues region in the C-terminal. Analytical ultracentrifugation revealed that they are composed by a single population of approximately 13S [36]. Further studies revealed that both, the presence of an unstructured N-terminal and an hydrophobic core determines oligomeric toxicity; the N-terminal region is able to form an α-helical structure binding to the extracellular membrane and anchoring the hydrophobic core, that in turn gets inserted into the lipid bilayer disrupting its integrity (Figure 1.6 f and g). In fact, the blocking of the N-terminal interaction with the membrane is enough to prevent toxicity associated the kinetically trapped "Type B" oligomer [36, 37]. The permeabilisation of the membrane then provokes an influx of calcium inside the cell that with time, triggers the activation of caspase 3 and cellular death [34, 38, 36]. Moreover stabilised "Type B" oligomers but not "Type A" ones are able to induce the production of intracellular reactive oxygen species (ROS), leading to cellular stress and eventually to cellular death [34, 39, 36] (Figure 1.6 b and e).

Other species of α-synuclein extensively studied in the context of disease are fibrils. Even though the atomic structure of α-synuclein fibrils still has to be unambiguously determined, largely due to the large number of polymorphs existent, most of the experimental data support a model in which the core of the monomeric α-synuclein adopt an antiparallel in register β-sandwich fold, with both the N-terminal and the C-terminal remaining unfolded, and these monomeric units stacked in parallel to form the protofilaments, which will associate between them to form mature fibrils [40, 41]. Although in a lower degree than oligomers, fibrils have been reported to being able to disturb the plasmatic membrane and enhance the intracellular ROS production [30, 34, 39, 42]. Moreover, upon binding with the membrane α-synuclein fibrils have been shown to interact with different receptors such us heparan sulphates [43, 44], the sodium potassium ATPasa (NKA) [45] or lymphocyte-activation gene (Lag) 3 [46], that are proposed to mediate their internalisation via endocytosis. Once internalised, fibrils are able to disrupt the endocytotic vesicles [47] and release into the cytoplasm were they seed the aggregation of endogenous α-synuclein [48, 49, 50]. Furthermore, α-synuclein fibrils have been shown to have prion-like properties, being able to propagate cell to cell and thus, expanding the disease to unaffected brain areas [50, 51, 52, 53]. Another common feature with prion disease is the existence of different fibrillar polymorphs, or strains. *In vitro*, differences in the shacking conditions, pH or ion strength can lead to the formation of different

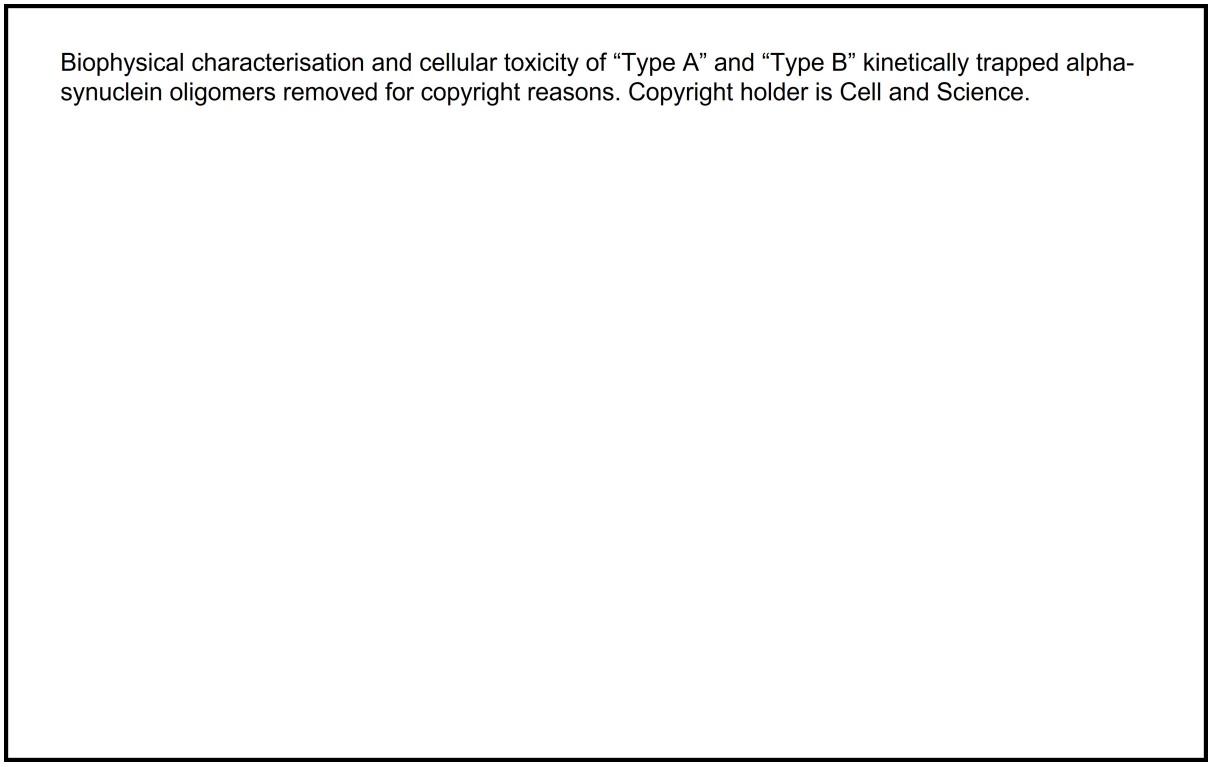

Figure 1.6: Biophysical analysis of kinetically trapped oligomers. (a) FRET profile from on-pathway "Type A" and "Type B" oligomers. (b) ROS production on the presence of on-pathway oligomers. (c) The kinetically trapped "Type A" and "Type B" oligomers share similar FRET profiles with their on-pathway counterparts of the "Type B" oligomers, indicating that they share a similar structure. (d) Secondary structure kinetically trapped "Type A" and "Type B" oligomers as determined by FT-IR. (e) Stabilised "Type A" and "Type B" oligomers induce similar ROS production levels than their on-pathway counterparts. Schematic representation of kinetically trapped "Type A" (f) and "Type B" (g) oligomers to membranes. (a and b) have been reproduce from [30], (c, d, e, f, g) have been taken from [36].

α-synuclein fibrillar polymorphs [54]. Moreover, the aggregation of different pathogenic variants of α-synuclein under the same aggregation conditions have been shown to produce different strains of fibrils [55]. This structural differences arise from differences in the packing of the protofilamets that come together to for an amyloid fibril [54]. Although these could be considered small structural changes, different α-synuclein fibrillar polymorphs have been associated with different synucleinopathies in *in vivo* models [52, 56]. Potentially, differences in cellular environments like pH, port-translational modifications or relative concentration of α-synuclein could also lead to the formation of different fibrillar strains. Indeed, the fibrillar polymorphs have been identified in patients with MSA, dementia with Lewy bodies or PD [57, 58, 59]. Moreover the injection of α-synuclein patient-derived fibrils into the brain of mice induced the development of α-synuclein ag-

gregates and neuronal degeneration [60]. Importantly, the structural analysis of these patient-derived fibrils are different to those currently generated *in vitro* [59, 61]. Since fibril polymorphism seem to be related with the development of different synucleinopathies, this highlights the importance of exploring different conditions for the aggregation of α-synuclein *in vitro*.

1.4 Modelling Parkinson's Disease

Since its aetiology has not been yet fully elucidated it is specially important to develop models of PD (from cellular to more complex *in vivo* models) that allow us to study the different characteristics of the disease (form both, the sporadic and the hereditary form of the disease) and explore different therapeutic pathways.

1.4.1 *In vitro* models of PD

Although they are not able to reproduce the disease in all its complexity, simple *in vitro* cell models allow us to study the altered cellular processes behind the development of the disease in a more simple, control environment.

Immortalised cellular lines

The use of immortalised cells lines allows for easy genetic manipulation at the same time that guarantees an homogenous population of cells. Moreover they provide a good, fast and cheap system to test new hypothesis and different conditions before taking the most promising ones to more advance models like primary neurons or human induce pluripotent stem cells (iPSC). As in PD the first cells to start degenerating and dying are dopaminergic neurons, cell lines with the potential to be differentiated into a more dopaminergic neuronal-like phenotype are usually used to study this disease. However, even though once differentiated these cells present neurites and express markers like TH, their synaptic activity is limited which impedes its use to study phenomena like synaptic plasticity. Examples of cell lines used in the study of PD include Lund human mesencephalic (LUHMES), rat pheochromocytoma PC12 and the extensively used human neuroblastoma SH-SY5Y [62, 63]. Although SH-SY5Y do not express endogenous α-synuclein they have been widely employed to explore the toxicity of extracellular aggregates like oligomers and fibrils through membrane disruption [64, 36]. Genetically modified SH-SY5Y to express an α-synuclein variant, like WT or A53T, fused to a reporter like green fluorescent protein (GFP) or yellow fluorescent protein (YFP) have also

been used to study aggregation in the presence of factors related to PD, like mitochondrial stressors [65] or proteasome inhibitors [66].

Primary neurons

Mice and rat primary neuronal cultures have been extensively used to study PD as they allow a more physiological approach. When grown in the absence of serum, they are mainly composed by neurons, with glia cells present to support the neuronal network. One of the main advantages of using this type of cultures is the possibility of detecting and study changes in synaptic activity at a single cell level. However, genetical alteration of these cultures is significantly more complicated than in immortalised cell lines. Although genetic alteration via conventional transfection methods like the use of lipofectamine or electroporation has limited results, gene modification it is still possible via viral vector like lentiviruses [63]. However, since the establishment of a cell line it is not possible this type of cultures present a higher variability than immortalised cell lines. It is important to highlight that primary dopaminergic cultures, obtained from the midbrain of E13 embryos, only contain between a 5 and a 10 % of TH positive neurons, which can lead to erroneous conclusions since specific changes occurring in the dopaminergic neurons may be masked by those happening in the non-dopaminergic ones [63]. Due to this, many groups have adopted the use of primary cortical and hippocampal neuronal cultures, better characterised in the literature, in order to study different aspects of PD. In particular, this method has been broadly used to explore the variety of effects that the addition of external α-synuclein aggregates induces in the neurons, such as impaired axonal transport [67], altered dendritic spine morphology and function [48, 68] or mitochondria fragmentation and depolarisation [69].

Human induced pluripotent stem cells derived dopaminergic neurons

The discovery in 2006 by S. Yamanaka that by delivering four genes encoding pluripotency factors (OCT4, SOX2, c-MYC and KLF-4) [70] it was possible to reprogram adult mouse cells into embryonic like pluripotent stem cells, opened the door to the use of patient-derived cells as a model for neurodegenerative diseases. Nowadays, it is possible to differentiate human induced pluripotent stem cells (iPSC) into dopaminergic neurons through a 35 days protocol that yields cultures that are both tyrosine hydroxylase (TH) and G protein-activated inward rectifier potassium channel 2 positive and show a synaptic activity characteristic of mature SNpc dopaminergic neurons [71]. Through these types of studies it has been possible to determine that iPSC-derived dopaminergic neurons carrying a triplication of α-synuclein or the A53T mutation present an increment in intracellular α-synuclein accumulation, perturbed mitochondrial function, increased

endoplasmic reticulum stress and impaired lipid homeostasis. Moreover, in iPSC-derived dopaminergic neurons carrying a triplication of α-synuclein it was possible to detect an increment in oligomeric species and α-synuclein secretion to the extracellular space [72]. This model has also been used to prove the prion-like propagation and amplification of α-synuclein fibrils in human iPSC-derived cortical neurons [52].

1.4.2 *In vivo* models of PD

Although *in vitro* models of PD allow us to study the biochemistry aspects of the disease in detail, they lack the complexity necessary to fully understand how PD affects the interaction between different types of cells, like neurons and glia, and how it spreads through the brain. It is also not possible to asses if addressing any of the particular problems that arise in the cells like elevated ROS, α-synuclein aggregation or mitochondrial dysfunction, will result in a change in phenotype. In order to solve these issues it is necessary to develop *in vivo* models of PD that give a phenotypical readout directly related to PD pathology. In the case of PD an ideal model would reproduce both, the behavioural and pathological characteristics of the disease, and it would be predictive for drug testing. Although multiple models exist, none of them has been entirely successful in the generation of this "ideal" model [73, 74].

Caenorhabditis elegans

This nematode, of just 1-2 mm length, is a extensively characterised organism. Its genome was sequenced 1998 [75], and the position and synaptic connections of each its 302 neurons have been precisely mapped [76]. Moreover, this organism is fully transparent making the direct visualisation of fluorescent reporter proteins *in vivo* easily achievable [77]. The expression of WT and A53T α-synuclein variants under a dopaminergic neurons specific promoter leads to motor deficits and loss of dopaminergic neurons and dendrites [78]. Furthermore, the expression of WT α-synuclein fused to YFP in the muscle cells of *C. elegans* also leads to α-synuclein aggregation and motor deficiencies [79]. Moreover the α-synuclein aggregation and the associated motor phenotype in this model are sensitive to drugs, like trodusquemine, which is able to affect the α-synuclein aggregation kinetics *in vitro* and hence, can be use in the screening of drugs anti-PD [80].

Drosophila melanogaster

As a model, *Drosophila melanogaster* present several advantages: it requires little space and equipment, its genome is easy to edit and has been fully sequenced and possess a relative complex nervous system with dopaminergic clusters involved in the control of motor

behaviours, such as walking, climbing or flying [77]. The expression of WT α-synuclein or the A53T and A30P mutant recapitulates the adult-onset loss of dopaminergic neurons, the formation of filamentous electron-dense intraneuronal α-synuclein inclusions resembling Lewy bodies and neurites and locomotor dysfunction [81, 82]. Moreover, the administration of dopamine agonists rescued this phenotype, proving that this model can be used as a first step in the testing of anti-PD drugs [82, 83].

Mus musculus

Over the years, multiple mouse models of PD have been developed with varying degrees of success.

One of the oldest methods to generate mice models of PD relies on the use of neurotoxins, like 6-hydroxydopamine or 1-methyl-4-phenyl-1,2,3,6-tetrahydropyridine (MPTP), that are able to specifically damage the mitochondria of the dopaminergic neurons of the SNpc and induce the death of these neurons. Although these models are able to reproduce the loss of motor functions associated with PD through the induction of the death of the dopaminergic neurons, they do not induce the aggregation of α-synuclein or the formation of Lewy bodies and neurites. Moreover, due to the fact that the neuronal damage does not extend to other areas of the brain, these models are not able to reproduce other hallmarks of PD like olfactory loss, sleep and affective disorders, and autonomic and digestive dysfunction [74, 73]. Further more, many compounds that showed neuroprotection in these models failed later on in clinical trials [77].

Another popular model is the use of transgenic mice carrying mutations in some of the genes associated with the genetic forms of the disease. For example, models that overexpress the G2019S variation of LRRK2 or the G309D one of PINK1 have been found to induce the aggregation of α-synuclein [77]. Knock-out models simulating the loss of function of Parkin or PINK1, involved in mitophagy and associated with genetic forms of PD, do not show any sign of Lewy bodies related pathology, while the knock-out of DJ-1 induces motor defects without the degradation of dopaminergic neurons [84]. However all these models failed to recapitulated all the main hallmarks of PD. Even more important is the fact that, as they are based in low prevalent hereditary forms of PD they may not be suitable to test drugs aimed to stop the progression of the sporadic form of PD.

The facts that 1) both mutations in the α-synuclein gene and protein overexpression can trigger the development of PD and 2) that the Lewy bodies and neurites are clear hallmarks of sporadic and hereditary forms of the disease, provide a link between this two forms of the disease and make α-synuclein an excellent focus for developing a mouse

model of PD. Over a number of years, several mouse models for PD based on this idea have been developed and include, the transgenic model, the recombinant adeno-associated virus (rAAv) α-synuclein model, and the pre-formed fibrils (PFF) model [85, 73].

Several transgenic models of PD expressing human wild type (WT) α-synuclein, A53T α-synuclein and A30P α-synuclein under the control of different promoters have been developed. Between these promoters the most used ones are: the tyrosine hydrolase promoter, the prion protein promoter, and the Thy promoter. Under the control of the tyrosine hydrolase promoter α-synuclein is only expressed in the catecholaminergic neurons and although the accumulation of α-synuclein within the dopaminergic neurons of the SNpc is a common finding, these mice only present some pathogenic phenotypes when they express α-synuclein carrying both, the A30P and the A53T mutations or C-terminal truncated forms of the protein [85]. The expression of α-synuclein under the prion protein promoter causes its aggregation in the spinal cord, the brainstem and parts of the midbrain but not in the SNpc, and upon age, these mice display a motor impairment [82, 85]. The use Thy1 promoter allows the expression of α-synuclein mainly in the neurons of the central nervous system which causes the apparition of granular and insoluble somatodendritic accumulations of α-synuclein across several regions of the brain, but again, not in the SNpc; the phenotypes in the mice are really variable, from a fast death due to the degeneration of neuromuscular junctions to an age-related locomotor pathology [82, 85]. Behind the lack of success of these models in reproducing the characteristic of PD lies two factors: first, due to the expression of α-synuclein from an exogenous promoter, all of them fail to reproduce the spatiotemporal expression patterns which are clinically observed; and second, the unpredictability of the transgene insert site, which directly influences the strength of the phenotype [86, 74, 87, 85]. In order to address this issues transgenic mice using bacterial artificial chromosomes (BAC) carrying the entire human α-synuclein gene and its gene expression regulatory regions have been generated. The introduction of WT α-synuclein in this manner does not lead to the formation of α-synuclein inclusions or cellular death, although these mice manifest a decrease in anxiety-like behaviours, which could correspond with non-motor symptoms typical of early PD [88]. This approach has also been used to express the E46K α-synuclein mutant, these mice present a degeneration of the dorsal striatum, innervated by the SNpc, but not of the dopaminergic neurons of the SNpc themselves. Transcriptomic analysis of the striatum revealed alterations in synaptic plasticity, neurotransmission, mitochondrial function and lipid metabolisms consistent markers of cellular dysfunction prevalent in PD [89].

Another strategy that has been widely used in model development is based on the

rAAv model in which the α-synuclein is delivered specifically into the SNpc using a viral vector inducing its constitutive expression. This model successfully reproduces the loss of dopaminergic neurons and this translates to motor defects when the neuronal loss becomes greater than 40 %. Neuroinflammation, another disease hallmark of PD, is also caused by an early activation of the microglia in this model. However, the observed α-synuclein aggregates do not entirely recapitulate the morphological features of Lewy bodies and Lewy neurites and due to its overexpression, α-synuclein is localised within the entire cytosol instead of just in the pre-synaptic terminals. In addition, the viral titer and serotype, the promoter, and the site(s) of integration influence the expression levels of α-synuclein and contribute to the high variability that can be observed in this model [73].

The third most common model system is the PFF model, in which fibrillar α-synuclein species (obtained by sonication of mature fibrils) are injected into the striatum of WT mice and act as seeds to recruit endogenous α-synuclein. This model recapitulates the loss of dopaminergic neurons and displays α-synuclein inclusions that strongly resemble the Lewy bodies and neurites: they have a fibrillar morphology observed by microscopy, are phosphorylated at serine 129, ubiquitinated and are detergent-insoluble (Figure 1.7). Furthermore, this model is able to faithfully reproduce the spreading of α-synuclein inclusion through the brain allowing the study of this process and assessment of PD therapies aimed to contain the spreading of the disease through the brain instead of its onset [73]. However, this model generally fails to show a strong motor disruption [73] and its results are not always reproducible. This may be related to several factors like the use of human instead of mouse α-synuclein seeds, the presence of lipopolysaccharide (LPS) in α-synuclein preparations that have been recombinationally expressed [90], the preparation method of the seeds or the nature of the species injected. Even though, mouse α-synuclein only differs by 7 aa compared to the human isoform (Figure 1.5), it has been shown to have faster aggregation kinetics and a shorter lag time [91]. Moreover, it has been reported that the elongation of the PFF is more efficient when both, the seeds and the monomer belong to the same species and that this has a direct influence on the number of inclusions detected in the neurons, with the amount of aggregates detected in mice injected with mouse PFF being statistically higher than the number detected in mice injected with human PFF [92, 49]. Another factor to take into account is the presence of the LPS, a component of the Gram-negative bacteria able to trigger an inflammatory cascade through the activation of some of the components of the immune system, like monocytes, macrophages and microglia [93]. Furthermore, it is known that the injection of small amounts of LPS into the SNpc or via intraperitoneal in the α-synuclein transgenic mice is able to trigger the aggregation of α-synuclein and the degeneration

of dopaminergic neurons in response to microglia activation [94, 95]. In addition, the injection of short fragments of α-synuclein fibrils have been proven to be more effective than the injection of longer ones inducing a PD-related phenotype [67, 51].

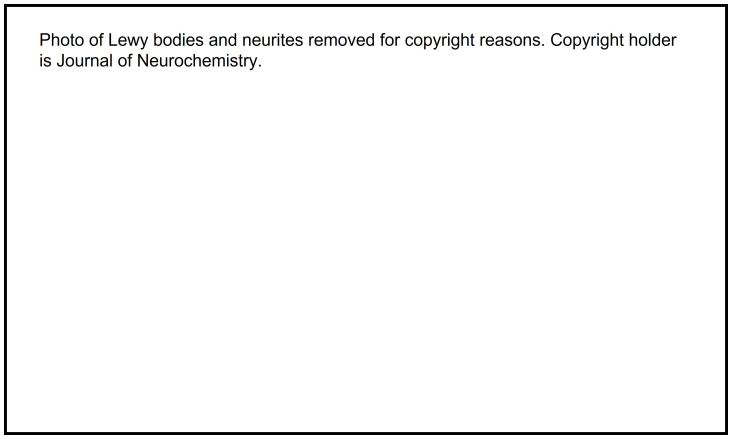

Figure 1.7: Lewy bodies and neurites in the PFF model. Example of the pS129 positives Lewy neurites-like and Lewy bodies-like in a mouse sacrifice 4 months after PFF injection. The scale bar in a is set at 30 μm. The image has been taken from [73].

1.5 Aims and objectives of this thesis

It is the aim of this thesis to investigate the possible relationship between the structural and biophysical properties of different α-synuclein species (monomer, oligomers and different strains of fibrils) and its ability to induce toxicity at a cellular and organism level. In order to evaluate this in a systematic and thorough manner several approaches were explored.

First, in collaboration with Dr. Laura Volpicelli-Daley we explored how the preparation and storage of different α-synuclein conformers (monomer, oligomers, short fibrils, medium fibrils and long fibrils) can influence the induction of a PD phenotype after its injection into the brains of mice. This study allowed us to concluded that not only the length of the fibrils could influence the phenotypical response, with the short fibrils the more successful α-synuclein species at inducing behavioural changes, but that the storage of this fibrils could influence its final length and hence the final output of the experiment.

Next, the ability of kinetically trapped oligomers derived from different α-synuclein variants to induce cellular toxicity was assessed. From these experiments it was possible to conclude that oligomers generated from WT and G51D α-synuclein variants are able

to induce a stronger cellular toxicity than oligomers generated from other α-synuclein mutational variants. Furthermore, G51D oligomers seem to have both a highly conformational variability with different degrees of α-helix present in their structure and highly variable toxic effects. Through the assessment of the toxicity of G51D oligomeric preparations with different degrees of α-helix it was possible to establish a correlation between both features, with a higher content of α-helical structure correlating with higher toxicity levels.

The study of the toxic properties of different oligomeric species was followed by the study of the efficiency with which different α-synuclein fibrillar species are able to recruit endogenous α-synuclein. With this objective fibrils with different secondary structures and dimensions were generated, and their respective seeding abilities were evaluated in mouse primary neurons. These experiments revealed that although all the different fibrillar species were able to be internalised by cells, they induce the recruitment of endogenous α-synuclein at different rates.

Finally, with the aim of exploring if the different fibrillar species were also able to induce different signatures of cellular toxicity, the viability of SH-SY5Y cells after the exposure to α-synuclein fibrils was assessed through the widely used MTT (3-(4,5-dimethylthiazol-2-yl)-2,5-diphenyltetrazolium bromide) assay. While performing these experiments it was observed that α-synuclein fibrils and other unrelated amyloid aggregates were able to induce the formation of formazan crystals that resulted in a false-positive result. After thoroughly evaluating the nature of this phenomena, the time scale in which it happens, and which species were able to induce it, it was possible to conclude that amyloid fibrils, but not monomers or kinetically trapped oligomers, are able to induce the formation of these crystals at nanomolar concentrations in a timescale of hours after the initial exposure.

Chapter 2

Methodology

All chemicals and reagents were purchased from Sigma Aldrich (UK) Ltd. (Gillingham, Dorset, UK) unless otherwise stated.

2.1 α-Synuclein variants purification

All centrifugation steps were performed in a Beckman Avanti J centrifuge (High Wycombe, UK) unless otherwise stated. *E. Coli* BL 21 cells were transformed, using standard heat shock treatment, with the pRK172 plasmid containing the gene for the mouse WT or E110C α-synuclein variants or the human WT, A30P, G51D, A53T, E46K, H50Q or N122C α-synuclein variants. A single colony containing each of the plasmids was selected according to its resistance from LB-Agar plates with 100 μg/ml ampicillin. The selected *E. Coli* cells were grown overnight as starter cultures (10 ml of LB medium, 100 μg/ml ampicillin, 37 °C, 180 rpm) and the next day 1 L 2xYT media with 100 μg/ml ampicillin was inoculated with this culture (1:1000 dilution). The larger cultures were grown in an orbital incubator to an OD_{600nm} of 0.6-0.8 (37 °C, 180 rpm). Once the desired OD was reached, expression of the protein was induced with the addition of IPTG (isopropyl-β-D-1- thiogalactopyranoside) (1 mM) and the cells were left to incubate (overnight, 28 °C). The cells were then harvested by centrifugation in a Beckman Coulter JLA-8.1000 rotor (5,000 rpm, 20 min, 4 °C). The bacterial pellet from 1 L cell culture was resuspended in 20 ml of 10 mM Tris-HCl, pH 7.7, 1 mM EDTA and 1 mM proteinase inhibitor (cOmplete(TM), EDTA-free Protease Inhibitor) and then lysed by sonication (40 % amplitude, 5 min, 15 sec on pulse, 45 sec off pulse) on a sonicator ultrasonic processor xl model XL2020 sonicator (Misonix Fisher Scientific). The cell lysate was centrifuged in a Beckman Coulter JA-25.5 rotor (15,000 rpm, 30 min, 4 °C) and the supernatant was collected. The supernatant was boiled (20 min) and further centrifuged

(15,000 rpm, 30 min, 4 °C) to remove the precipitated, heat-sensitive proteins, leaving α-synuclein in the supernatant. Streptomycin sulphate was added to the supernatant to a final concentration of 10 mg/ml for DNA precipitation and incubated with stirring (15 min, 4 °C) followed by centrifugation (15,000 rpm, 30 min, 4 °C). Finally, α-synuclein was precipitated by the addition of ammonium sulphate to a final concentration of 361 mg/ml. The solution was stirred (30 min, 4 °C) and centrifuged (15,000 rpm, 30 min, 4 °C).

The protein pellet was resuspended in 25 mM Tris-HCl, pH 7.7 (40 ml for each 1 L cell culture) and dialysed overnight in natural cellulose membrane (cut-off 3500 Da) against the same buffer to remove the excess of salts. After dialysis, the sample was purified on an anion exchange column (Hi Load 26/10 Q sepharose High Performance, GE Healthcare Lifescience, Little Chalfort UK) equilibrated with using 25 mM Tris-HCl, pH 7.7 on an AktaPrime chromatography workstation (GE Healthcare Ltd.). The protein was eluted using a NaCl gradient (0-1.5M) and the fractions containing protein (determined spectroscopically and by SDS-PAGE analysis [Figure 2.1]) pooled and further purified by size exclusion chromatography (SEC) on a HiLoad 26/60 Superdex 75 pg column (GE Healthcare Ltd) previously equilibrated with phosphate buffered saline (PBS; pH 7.4). The fractions containing only the monomeric protein (as identified by SDS-PAGE, purity above 90 % [Figure 2.1]) were collected and aliquoted, then flash frozen in liquid N_2 and stored at -80 °C. The protein concentration was determined from the absorbance at 275 nm, using a molar extinction coefficient $\epsilon = 5600$ M^{-1} cm^{-1} in case of the human α-synuclein variants and using a molar extinction coefficient $\epsilon = 7000$ M^{-1} cm^{-1} in the case of the mouse ones. For the E110C mouse and N122C human α-synuclein, all buffers used during lysis and purification contained 3 mM DTT to prevent the formation of intermolecular disulphide bonds.

2.2 Aβ_{40} purification

All centrifugation steps were performed in a Beckman Avanti J centrifuge (High Wycombe, UK) unless otherwise stated. BL21 (DE23) PlysS containing the Aβ_{40} plasmid were grown in a starter culture of 50 mL LB broth (10 g/l Bacto-tryptone, 5 g/l yeast extract, 10 g/l NaCl) containing 100 μg/ml ampicillin at 37 °C overnight, under shaking. In order the amplify the starter culture, 1 mL of the starter culture was added to 1 l of auto-induction TB medium (60 g/l) containing 10 mL/l glycerol and 100 μg/ml ampicillin and left to grow overnight, under shaking, at 37 °C. The cells were then harvested by centrifugation at 5000 rpm, at 4 °C, for 35 min (Beckman Coulter, JLA 8.1000).

The harvested cells were resuspended in 250 mL of working buffer (10 mM Tris, pH

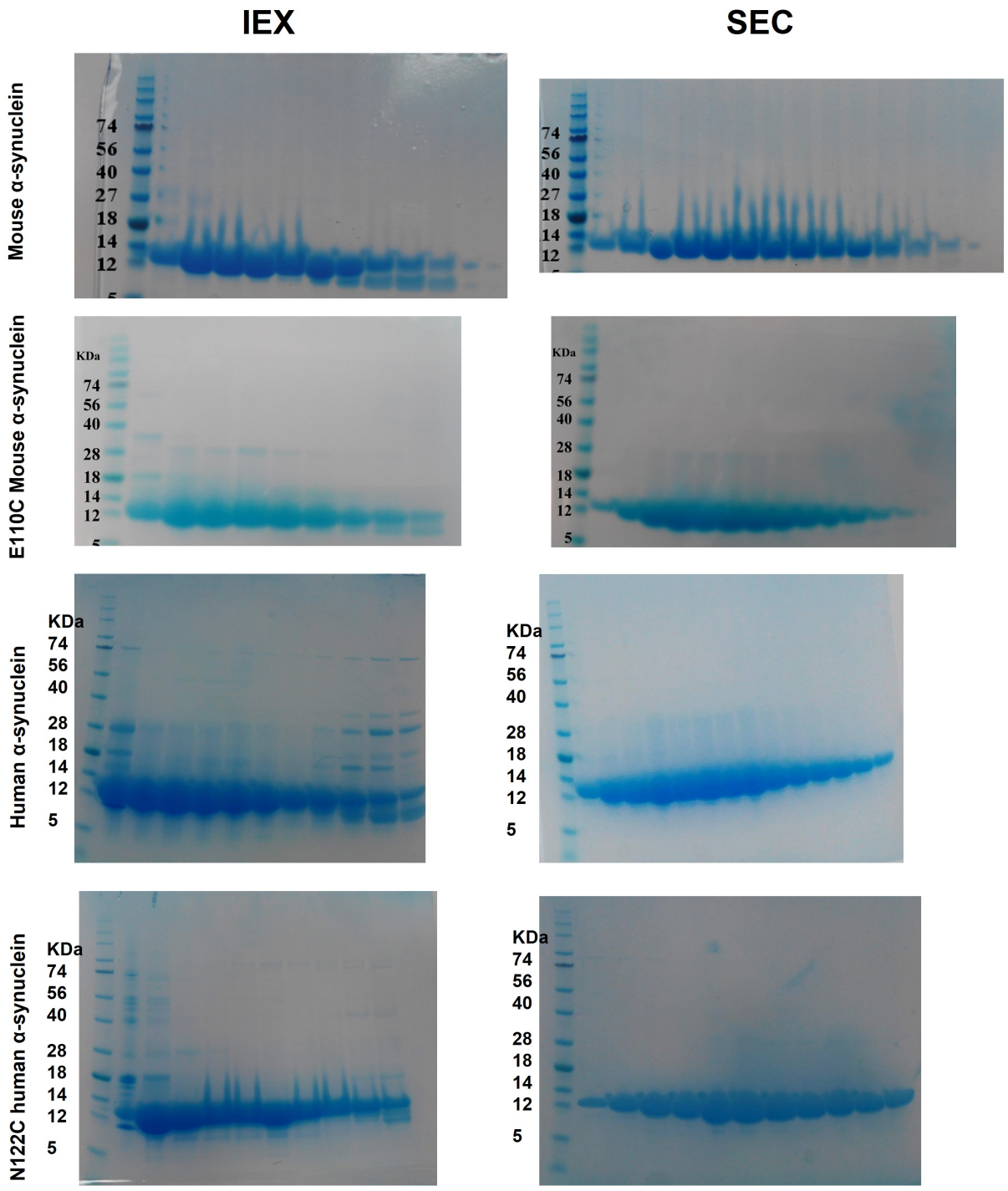

Figure 2.1: Purification of the different α-synuclein variants. SDS-PAGE analysis after the ion exchange (IEX) and size exclusion (SEC) steps of the different α-synuclein variants used in this thesis. After SEC, only pure fraction were collected.

8, 1 mM EDTA, sonicated for 3 minutes (amplitude 52, pulse on/off 1 minute) and then centrifuged (Beckman Coulter, JA-25.5, 18000 rpm, 10 min, 4 °C). This procedure was repeated for a total of three times. After the third round, the pellets were resuspended in 40 ml of 8 M urea and incubated at room temperature for 45 minutes. The solution was then sonicated again, and incubated with the DEAE Sepharose Fast flow resin (GE Healthcare) previously washed (500 mL ultrapure H_2O and three funnel volumes of working buffer) under shaking for 30 minutes at 4 °C. After the incubation time, the solution was placed into a Buchner funnel equipped with filter paper in order to remove the beads of the resin and collect the flow through. Next, one funnel volume of working buffer was run through, followed by 100 ml of 25 mM NaCl and 100 ml 125 mM NaCl. The latter two solutions were collected into pierced falcon tubes, flashed frozen in liquid nitrogen and lyophilised.

After lyophilisation Aβ_{40} was resuspended in 6 M guanidinium hydrochloride and injected in an AKTA system (GE Healthcare, Chicago, IL) connected to a Superdex 26/600 column (GE Healthcare, Buckinghamshire, U.K), previously equilibrated in 20 mM sodium phosphate buffer, pH 8. The protein containing fractions (at elution volume 180-190 ml) were then flashed frozen in liquid nitrogen and lyophilised. Finally, the lyophilized protein was resuspended again in 6 M guanidium hydrochloride and subjected to a further process of SEC using a Superdex 75 HR 26/60 column (GE Healthcare, Buckinghamshire, U.K) equilibrated in ammonium acetate buffer, 50 mM, pH 8.5. The desired protein fraction eluted at approximately 12 mL was (SDS-PAGE is performed to confirm, purity above 90 % [Figure 2.2]) flash frozen stored at -80 °C.

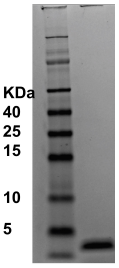

Figure 2.2: SDS-PAGE analysis of the purity of Aβ_{40} after purification. SDS-PAGE analysis of the purity of Aβ_{40} after purification. This figure was prepared by Katarina Pisani, who purified the SDS-PAGE analysis Aβ_{40} used in this study.

2.3 Removal and quantification of lipopolysaccharide levels

The protein samples (mouse WT α-synuclein and mouse E100C α-synuclein) were diluted to around 130 μM and any remaining lipopolysaccharide (LPS) was removed using

the Pierce High-Capacity Endotoxin Removal Resin (Thermo Scientific, Waltham, MA, USA) following the protocol for batch purification with spin columns (as provided by the manufacturer). The amount of LPS present in the subsequent samples was measured using the Pierce LAL Chromogenic Endotoxin Quantitation Kit (Thermo Scientific, Waltham, MA, USA), following manufacturer's instructions. After this point all the buffers were prepared with water containing less than 1 EU LPS (Water (double-processed cell culture), Sigma).

2.4 Preparation of Alexa-488 labelled α-synuclein

In order to remove the DTT, mouse E110C or human N122C α-synuclein in PBS containing 3mM DTT (1 ml) was added to a P10 desalting column (GE Healthcare Lifescience) pre-filled with Sephadex G25 resin (sigma) and equilibrated in PBS. The sample was collected in 12 aliquots (0.5 mL) and the protein concentration was determined on a nandrop UV spectrometer (Labtech International Ltd, Heathfield, East Sussex, UK). To this protein solution, Alexa Fluor 488 C5 Malemide (Life technologies, Waltham, MA, USA) was added (1.5:1 molar ratio of dye-to-protein) and the reaction was left on a rolling incubator (overnight, 4 °C) protected from light. The labelled protein was separated from the excess unreacted dye using a P10 desalting column filled with Sephadex G25 equilibrated in PBS pH 7.4. The protein was aliquoted, flash frozen in liquid nitrogen and stored at -20 °C. The labelling efficiency ($>$ 95 %) was confirmed by mass spectrometry, and the presence of dimeric protein was ruled out by SDS PAGE analysis (first batch 98 % monomer, second batch 97 %). The protein concentration was estimated from the absorbance of the Alexa flour 488 dye (ϵ_{495} = 72,000 $M^{-1}cm^{-1}$).

2.5 Preparation of purified α-synuclein oligomeric samples

The mouse and human α-synuclein oligomeric species were prepared as described previously [34]. Briefly, monomeric α-synuclein (6 mg) was dialysed against water overnight and placed in a 15 ml falcon tube (the volume must not exceed 4 ml). The sample was flash frozen in liquid nitrogen and lyophilised for at least 48 h (RT). The lyophilised protein was resuspended in PBS (pH 7.4, 0.5 mL), filtered through a 0.22 μm filter (Millipore [Watford, Hertfordshire, U.K.]) and incubated (24 h, 37 °C). In order to remove potential fibrillar species that can appear during the incubation time, the sample was placed in a 1 ml polycarbonate centrifuge tube (11 x 34 mm) and ultracentrifugated (90,000 rpm, 1 hr) in an Optima TLC Ultracentrifuge using a TLA-120.2 rotor 288,000 x g) (Beckman). After ultracentrifugation, the supernatant was recovered and passed through a 100 KDa

cut-off centrifuge filter ((Millipore (Watford, Hertfordshire, U.K.)) (4 times) to remove excess monomer. The oligomeric concentration was determined from the absorbance at 275 nm (ϵ = 7000 $M^{-1}cm^{-1}$ for human WT, A53T, H50Q, E46K; ϵ = 12444 $M^{-1}cm^{-1}$ for human G51D and A30P; and ϵ = 8750 $M^{-1}cm^{-1}$ for mouse species). The oligomeric concentration of the Alexa-488 labelled species was determined from the absorbance at 495 nm (ϵ = 72,000 $M^{-1}cm^{-1}$).

2.6 Preparation of α-synuclein fibrils

F0 anf F1 generation fibrils: 70 μM of α-synuclein (PBS pH 7.4 or 50 mM Tris-HCl pH 7.5 with 150 mM KCl) and containing 0.02 % (w/v) of sodium azide (NaN_3) in a final volume of 300 μL was incubated in an orbital incubator (37°C, 180 rpm, 5 days). Subsequently, the sample was centrifuged (10 min, 13,200 rpm, RT), and the supernatant was discarded. The pellet was washed twice with PBS and after the last centrifugation cycle, was resuspended in PBS to the final required volume. To determine the concentration, an aliquot of fibrils (40 μL) was mixed with 40 μL of 8M guanidinium chloride (in order to provoke the disaggregation of the fibrils) and the monomer concentration was determined using the absorbance at 275 nm (ϵ = 5,600 $M^{-1}cm^{-1}$). These fibrils were denoted as F(0). To generate F(1) fibrils, an aliquot of F(0) fibrils (100 μM, 300 μL) was sonicated with a Bandelin, Sonopuls HD 2070 (1 min, 3 0% cycles, 20 % maximum power) to obtain seed fibrils. These seeds (10 μM) were added to α-synuclein monomer (100 μM) in PBS, pH 7.4 to a final volume of 150 μL and this was incubated in a standard laboratory incubator (37 °C , 24 hr). After this the same procedures used for the F(0) were followed. **Fibrils injected into the mice**: The fibrils used for the mouse model project and the first stability studies were prepared as previously describe [67]. Briefly, mouse α-synuclein (5 mg/ml, final volume of 500 μL) was incubated in a Thermomixer set inside a standard laboratory incubator (37 °C, 700 rpm, 7 days). **Fibrils prepared in the presence of PEG, Dextran or 10 % methanol**: 100 μM of human monomeric α-synuclein in PBS was incubated in the presence of 300 mg/ml dextran (MW 70000), 300 mg/ml polyethylene glycol (PEG) (MW 8000) or 10 % methanol at 37 °C in a 96 well plate for seven days inside a BMG Clariostar (BMG LABTECH, Aylesbury, Bucks, UK) reading every 10 minutes. After this, the sample was ultracentrifugated at 20 °C, 120000 rpm for 1.5 h before resuspending it in PBS. In order to assure the complete removal of the crowding agent or the methanol this process was repeated three times. Final fibrillar concentration was measured as described for the F0 and f1 generation fibrils. **Fibrils prepare in the presence of 35 % methanol**: 100 μM of human monomeric α-synuclein in PBS was incubated in the presence 35 % methanol at 37 °C in an static

incubator for 24h. **Protofibrils**:Protofibrils were produced as described in [27]. Briefly, dimyristoyl phosphatidylserine (DMPS) vesicles were prepared by subjecting a dilution of 2mM DMPS in 20 mM sodium phosphate buffer, pH 6.5 to 5 freeze-thawing cycles and 2 sonication cycles of 5 min 10 % power, 50 % cycles (0.5 sec on 0.5 sec off) in a Bandelin, Sonopuls HD 2070. After centrifugation the resulting vesicles for 30 min at 15000 rpm at room temperature, 100 μM of this vesicles were incubated with 100 μM monomeric human α-synuclein in 20 mM sodium phosphate buffer, pH 6.5 at 30 °C in 96 well plate for 5 days. After collecting the samples in an eppendorf tube, this mixture was incubated for 1.5 h at 37 °C with 1 % sarkosyl in 20 mM sodium phosphate buffer, pH 6.5. Afterwards, the sample was ultracentrifugated at 20 °C, 120000 rpm for 1.5 h before resuspending it in PBS. In order to remove the lipids and detergent mixture completely this process was repeated three times. Final protofibrillar concentration was measure as described for the F0 and f1 generation fibrils.

2.7 Cross-linking of antiparallel α-synuclein fibrils

100 μl at 100 μM of 35 % methanol fibrils (antiparallel fibrils) or F1 fibrils were incubated with 0.25 % glutaraldehyde for 2 minutes at 37 °C. After this, the reaction was stopped by the addition of 10 μl of 1 M Tris-HCl, pH 8.0 The excess of glutaraldehyde was washed away by centrifugation the samples at maximum speed for 10 minutes at room temperature, discarding the supernatant and resuspending the sample in PBS. This process was repeated 3 times.

2.8 Preparation of Aβ_{40} oligomeric samples

The Aβ_{40} stabilised oligomers were prepared according to the protocol described in [96]. Briefly, the lyophilized protein was resuspended in 300 μL HFIP (Sigma, 105228), and sonicated in ultrasonic cleaner for approximately 10 seconds and incubated overnight at 4 °C. The following day, the HFIP was dried under a gentle flow of nitrogen, and the resulting film was resuspended in DMSO to a final concentration of 10 mg/ml. The sample was sonicated two times for 10 minutes and centrifuged at 13000 rpm for 5 minutes. The pellet was discarded and the supernatant was diluted in 20 mM sodium phosphate buffer, at pH 6.9, with 200 μM $ZnCl_2$ to a final concentration of 100 μM and then incubated at 20 °C for at 20 hours. Finally, the solution was centrifuged at 15000 g for 15 min at 20 °C and the pellet containing the oligomers was resuspended in 20 mM sodium phosphate buffer, at pH 6.9, with 200 μM $ZnCl_2$.

2.9 Preparation of Aβ_{40} monomers and fibrils

Aβ_{40} monomers and fibrils were prepared as decribed in [96]. Briefly, solutions of the monomeric peptide were prepared by dissolving the lyophilized Aβ_{40} peptide in 6 M guanidinium hydrocholoride. The monomers were then further purified using a Superdex 75 10/300 GL column (GE Healthcare, Chicago, IL) attached to an AKTA system (GE Healthcare, Chicago, IL) at a flow rate 0.5 mL/min and equilibrated in 20 mM sodium phosphate buffer, pH 8. The monomeric peak was collected, and the peptide concentration determined from the absorbance of the integrated peak area using $\epsilon_{280} = 1490$ M^{-1} cm^{-1}. For the preparation of Aβ_{40} fibrils, Aβ_{40} was incubated for 10 h at the concentration of 50 μM in 20 mM sodium phosphate buffer, pH 8, at 37 °C in a 96 well plate (3880, Corning B.V. Life Sciences, Tewksbury MA, USA). Part of these samples was supplemented with a solution of 20 μM ThT to monitor the aggregation of the samples with ThT kinetic. Samples not treated with ThT were then collected from the wells into low-binding eppendorf tubes.

2.10 Preparation of lysozyme fibrils

Lysozyme fibrils were generated as described in [97]. 6.8 μM monomer was incubated in 0.1 M sodium citrate buffer, pH 5.0 with stirring at 60 °C in a Cary Eclipse spectrofluorimeter (Varian Ltd) overnight. Light scattering was monitored at 500 nm in order to asses the aggregation precess. Thu buffer was exchanged to PBS by centrifugating the sample (10 min, 13,200 rpm, RT), Discarding the supernatant and resuspending in the same volume of PBS. This process was repeated twice. Finally, fibrils were sonicated (10 sec, 30 % cycles, 10 % maximum power) in a Bandelin, Sonopuls HD 2070.

2.11 Circular dichroism spectroscopy

Far-UV circular dichroism (CD) spectra (10 accumulations) of the different mouse and human α-synuclein species were acquired in PBS at 20 °C at a final protein concentration of ca. 10 μM using a 1 mm path length quartz cuvette and a J-810 Jasco spectropolarimeter (Tokyo, Japan), equipped with a thermostated cell holder. The Far-UV CD spectrum of the buffer was recorded separately and subtracted manually. For the different human α-synuclein variants 15-30 accumulations were taken using concentration ranges between 1 and 10 μM. Spectra were deconvoluted using the BestSel web server. In order to make the CD signal intensity independent of sample concentrations before comparing them the units of the CD spectra were converted from measured ellipticity (mdeg) to molar residue ellipticity (deg cm^2 dmol^{-1}).

2.12 Fourier transform infrared spectroscopy

The fourier transform infrared (FT-IR) spectra of monomeric and oligomeric mouse α-synuclein were acquired with sample concentrations of ca. 800 μM, while the fibrillar spectra were acquired with a sample concentration between 150 and 300 μM. All spectra were acquire using a Bruker VERTEX 70 FT-IR spectrophotometer (Bruker, Coventry, UK). The spectra corresponding to the characterisation of the mouse α-synuclein conformers experiments as well as the ones used to characterise the fibrils produce in the presence of 35 % methanol were acquired using a Bruker BioATRCell II. However, the spectra for the fibril fragmentation experiments and the ones pertaining the characterisation of the kinetically trapped oligomers of the different human α-synuclein variants were measure in a PLATINUM ATR accessory. For each spectrum recorded, 256 interferograms were co-added at 2 cm^{-1} resolution, the buffer background (for the BioATRCell) or air background (for the PLATINUM ATR) was subtracted and the amide I region (1720-1580 cm^{-1}) of the spectra was selected. In both cases the data were corrected by atmospheric compensation and the baseline was subtracted. All absorbance spectra were normalized for comparison. The FT-IR spectra were deconvoluted using a 6 Gaussian curves and the percentage of the different secondary structures were determined using the following ranges as a guide: α-helix/random coil (1640-1660 nm), β-sheet (1610-1639 nm, 1685-1700nm) and β-turn (1661-1684 nm).

2.13 Determining protein concentration in the soluble versus fibrillar fractions

Fibrillar samples (12 μL) were diluted in 108 μL of buffer and placed in Beckman polycarbonate centrifuge tubes (230 μL, 7 x 21 mm) and centrifuged in an Optima TLX Ultracentrifuge (90,000 rpm, 20 °C, 1 hr) using a TLA-100 Beckman rotor (436,000 x g). Following centrifugation, the supernatant was transferred to a clean 1.5 mL eppendorf tube and the fibril pellet was dissolved in 8M guanidinium chloride (120 μL). The protein concentration of both the pellet and the supernatant was then determined using the Pierce BCA Protein Assay Kit (Thermo Scientific), following the manufacturers instructions.

2.14 Transmission electron microscopy

Samples for transmission electron microscopy (TEM) analysis were diluted to a final concentration of 10 μM and applied (10 μL) to carbon coated copper grids (400 mesh) (EM resolutions, Saffron Walden UK). After incubation for 1 min, the grids were washed twice

with Milli-Q water followed by staining with a 2 % (w/v) uranyl acetate solution (10 μL). The grids were washed twice with Milli-Q water and allowed to dry for 5 min prior to storage in a grid box. The samples were imaged on a Tecnai G2 80-200 kV transmission electron microscope (Cambridge Advanced Imaging Centre (CAIC), University of Cambridge UK).

2.15 Atomic force microscopy

Samples for AFM analysis were diluted to a final concentration of 5 μM and deposited (10 μL) onto a layer of freshly cleaved mica and allowed to dry overnight. The next day, the mica was washed with Milli-Q water 5 times and left to dry. The micas for the fibrils fragmentation experiments were imaged on a Nanowizard II atomic force microscope (JPK instruments, Berlin, Germany) while the ones used in the biophysical characterisation of mouse α-synuclein conformers were imaged using a multimode 8 atomic force microscope (Bruker, Massachusetts, USA). The images were analysed with Gwyddion open source software (http://www.gwyddion.net).

2.16 Analytical ultracentrifugation

Sedimentation velocity measurements of the oligomeric samples (40 μM, 400 μM) were performed at 20 °C, 43,000 rpm using a Beckman-Coulter Optima XL-I analytical ultracentrifuge equipped with UV-visible absorbance optics and an An50Ti rotor (Department of Biochemistry, University of Cambridge, UK). The sedimentation coefficient distributions, corrected to standard conditions by using the SEDNTERP program, were calculated via least-squares boundary modelling of sedimentation velocity data using the c(s) and ls-g*(s) methods, as implemented in the SEDFIT program (www.analyticalultracentrifugation.com/default.htm).

2.17 Dot blot analysis

Dot blot assays were performed by applying drops of purified monomeric, oligomeric or fibrillar human α-synuclein (1 μg) to a 0.2 μm nitrocellulose membrane (Millipore.) The membrane was blocked with 5% (w/v) bovin serum albumin (BSA) in PBS (1 hr, RT) and then incubated (4°C, overnight) with primary antibodies for total α-synuclein (Anti-α-synuclein, Transduction Laboratories, Lexington, Kentucky, USA), oligomeric species (A11, Sigma) or fibrillar amyloids (OC, Sigma) at 1:500 v/v dilutions in PBS containing 5% (w/v) BSA. Afterwards, the membranes were washed with 0.01% (v/v) Tween-20 in

PBS (3 times, 10 min each), and subsequently incubated with Alexa Fluor-488 goat anti-mouse (in the case of the membrane incubated with anti-α-synuclein) or Alexa Fluor-488 goat ani-rabbit (in the case the membranes incubated with of A11 nd OC) secondary antibody (Invitrogen) (1 hr, RT) using a 1:5000 dilution in PBS containing 5% BSA and 0.01% Tween-20. Finally, the excess of secondary antibody was removed by washing the membranes 0.01% Tween-20 in PBS (3 times, 10 min each). Immunofluorescence quantification was performed on a Typhoon Trio scanner (Amersham Bioscience, place) and the images were analysed with ImageJ.

2.18 Assessing monomer integrity after aggregation

10 μM of α-synuclein oligomers, short fibrils, medium fibrils and long fibrils were incubated in 7M urea at overnight at RT and subsequently 10 μl of each species were loaded in a track of two SDS-PAGE gels. After gel electrophoresis one of these gels was developed with Instant Blue (Thermo Fisher Scientific, Waltham, MA, USA) while the other was developed with a silver saining kit (Thermo Fisher Scientific, Waltham, MA, USA).

2.19 Seeding aggregation experiments

Sonicated fibrils prepared with a Bandelin, Sonopuls HD 2070 (20 sec, 30 % cycles, 10 % maximum power) (10 μM, 100 μL or 5 μM, 100 μL in the case of the cross-seeding experiments) were added to monomeric α-synuclein (100 μM) in a solution containing 50 μM Thioflavin-T (ThT) and 0.02 % (w/v) sodium azide. The samples were placed in a Corning assay plate 96 wells half area (3881, CORNING B.V LIFE SCIENCES, Tewksbury MA, USA), in triplicate. The ThT fluorescence was recorded in a BMG Fluostar Optima (BMG LABTECH, Aylesbury, Bucks, UK) using an excitation filter of 440 nm and an emission filter of 480 nm, taking readings every 10 min over the course of 10 hr at a constant temperature of 37 °C.

2.20 Cellular culture

Human SH-SY5Y neuroblastoma cells (A.T.C.C., Manassas, VA) were differentiated by the addition of 10 μM all-trans-retinoid acid to the cellular media for 7 days. Cells were cultured in Dulbecco's Modified Eagles Medium (DMEM)-F12+GlutaMax supplement (Thermo Fisher Scientific, Waltham, MA, USA) with 10 % inactivated fetal bovine serum. The cell cultures were maintained in a 5.0 % CO_2 humidified atmosphere at 37 °C and grown until 80 % confluence in T75 flasks. Once cells reached confluence, they were split using a 1:10 dilution.

2.21 Primary neurons

Pregnant CD1 mice (E18) were sacrificed by cervical dislocation, after which the embryos were placed on ice and beheaded. Once the two hemispheres of the brain were extracted, the meninges were removed and the hippocampi collected in a 15 ml falcon tube containing 10 ml of Hibernate E (Thermo Fisher Scientific, Waltham, MA, USA). After this there were washed twice with Hank's balanced salt solution (HBSS) (Thermo Fisher Scientific, Waltham, MA, USA) and treated with 0.05 % trypsin (Thermo Fisher Scientific, Waltham, MA, USA) for 20 min. This reaction was stopped by the washing of the hippocampi with 10 ml of plating media (Neurobasal media [Thermo Fisher Scientific, Waltham, MA, USA], Glutamax 1/100 [Thermo Fisher Scientific, Waltham, MA, USA], FBS [5 %], B27 1/50 [Thermo Fisher Scientific, Waltham, MA, USA] and Penicillin/streptomycin 1/200 [Thermo Fisher Scientific, Waltham, MA, USA]) containing 10 U/ml of DNase, followed by other 10 ml of plating media and two washes with 10 ml of HBSS. Hippocampi were dissociated in 1 ml of HBSS using a 1000 micropipette, resuspended in 5 ml of plating media and further dissociated into a single cell state with the help of a cell strainer (Thermo Fisher Scientific, Waltham, MA, USA). Neurons were counted using a haemocytometer and plated at density of 100,000 neurons per well in a 24 well fitted with poly-d-lysine coated coverslips. After 2 h the plating media was exchanged by maintenance one (Neurobasal media [Thermo Fisher Scientific, Waltham, MA, USA], Glutamax 1/100 [Thermo Fisher Scientific, Waltham, MA, USA] and B27 supplement 1/50 [Thermo Fisher Scientific, Waltham, MA], USA).

2.22 Measurement of cell viability by MTT assay

SH-SY5Y cells were plated at a concentration of 10000 cells/well, in a flat bottom 96 well plate and placed in the incubator (37 °C , 5.0 % CO_2). After 24 hours of incubation, the medium was removed and the cells were treated with different concentration of the different samples diluted in cell culture medium. A minimum of six wells per condition were used and the volume of sample added was kept constant through the plate to guarantee that possible differences are not due to differences in the volume of PBS added. The plate was then incubated again for 24 hours or 2 hours, after which the treatment was removed and substituted with 100 μL of a 0.5 mg/mL 3-(4,5-dimethylthiazol-2-yl)-2,5-diphenyltetrazolium bromide (MTT) solution (MTT powder in RPMI for 4 hours. In the case of the 0 hours timepoint α-synuclein fibrils were added directly to this MTT solution. Pictures, at least 5 from three different wells, were taken using a 20x objective in a EVOS5000 (Thermo Fisher Scientific, Waltham, MA, USA) 2 and 4 hours after the

addition of the MTT. The percentage of cells presenting formazan crystals was quantified using ImageJ. After 4 hours incubation, 100 μL of stop solution (20 % SDS, 50 % N,N-dimethylformamide, pH 4.7) was added and the plate incubated for one hour at 37 °C under shaking. Absorbance values were acquired in the range of 500 nm and 700 nm using a plate reader (BMG Labtech, Aylesbury, UK). The difference 570-690 nm absorbance values were used to determine the cell viability, which was expressed as the percentage of MTT reduction in treated cells as compared to untreated cells (taken as 100 %). For the membrane integrity experiments, after 24 h incubation in the presence of α-synuclein fibrils, the cell media was remove and replaced by 2 μM Calcenin-AM (Thermo Fisher Scientific, Waltham, MA) dissolved in Live Cell Imaging media (Thermo Fisher Scientific, Waltham, MA, USA) for 30 minutes. After this the cells were washed twice with PBS and the MTT solution was added. Plates were imaged after 30 min and 2.5 hours using a 20x objective in a EVOS5000.

2.23 Measurement of cell viability by CellTiter-Glo assay

SH-SY5Y cells were plated at a concentration of 10000 cells/well, in a flat bottom 96 well plate and placed in the incubator (37 °C, 5.0 % CO_2). After 24 hours of incubation, the medium was removed and the cells were treated with different concentration of the different samples diluted in cell culture medium. A minimum of six wells per condition were used and the volume of sample added was kept constant through the plate to guarantee that possible differences are not due to differences in the volume of PBS added. The plate was then incubated again for 24 hours at 37 °C and further 30 minutes at romm temperature. After this 100 μL of CellTiter-Glo (Promega, Madison, WI) reagent was added and after a 10 minutes incubation the ATP (adenosine triphosphate) levels were determined by measuring the fluorescence in plate reader (BMG Labtech, Aylesbury, UK).

2.24 Measurement of cellular cholesterol levels by Flipin III assay

SH-SY5Y cells were plated at a concentration of 10000 cells/well, in a flat bottom 96 well plate and placed in the incubator (37 °C, 5.0 % CO_2). After 24 hours of incubation, the medium was removed and the cells were treated with 0.3 μM of α-synuclein fibrils diluted in cell culture medium. After this cell were treated as indicated in the Cholesterol Assay Kit (Cell-Based) (Abcam, Cambrigde, UK) protocol. Briefly, after removal of cellular media cells were fix with "fixative solution" for 10 min and subsequently washed 3 times

for 5 minutes with "wash buffer". After the last wash cells were incubated with Flipin III solution for 50 minutes, washed twice for 5 minutes and imaged using a 20x objective in a EVOS5000.

2.25 Measurement of reactive oxygen species assay

SH-SY5Y cells were plated at a concentration of 10000 cells/well, in a flat bottom 96 well plate and placed in the incubator (37 °C, 5.0 % CO_2). After 24 hours of incubation, the medium was removed and the cells were treated with 0.6 μM of α-synuclein oligomers and 5 μM CellROX-Orange (Thermo Fisher Scientific, Waltham, MA, USA) diluted in Live Cell Imaging media (Thermo Fisher Scientific, Waltham, MA, USA). After 2 h at 37 °C, images were acquire in a Cytation5 (Swindon, UK) and analysed using the Cytation5 software.

2.26 Seeding of endogenous α-synuclein

The different conformers of mouse α-synuclein (prepared as indicated in sections 2.5 and 2.6) were added at a final concentration of 70 nM to seven days old mouse hippocampal primary neuronal cultures (produced as described in section 2.21). Neurons were fixed 7 days later and immunofluorescence detection of p-α-synuclein (Abcam, Cambrigde, UK) and tau (Agilent Dako, Santa Clara, CA, USA) was performed as described in the immunocytochemistry section. The different conformers of human α-synuclein fibrils (prepared as described in section 2.6) were added to neurons at seven days *in vitro* at a final concentration of 0.3 μM. Neurons were fixed 5 days later and immunofluorescence to p-α-synuclein and neurofilament (Abcam, Cambrigde, UK) or Wheat Germ agglutinin-594 (Thermo Fisher Scientific, Waltham, MA, USA) was performed as described in the immunocytochemistry section.

2.27 Internalisation assay

In the case of the different mouse α-synuclein species, the internalisation assay was performed as described [98] with some modifications. Primary neurons were incubated for 30 minutes in cold PBS containing α-synuclein-Alexa488 fibrils or oligomers (final concentration 70 nM) allowing the species to bind the plasma membrane. The neurons were then transferred to 37 °C to allow internalisation. Extracellular α-syn-Alexa488 fibrils were quenched with freshly made trypan blue, final concentration 1 mM in PBS. Images were captured using a Zeiss Axio Observer Z1 with Colibri LED illumination. The excitation/emission was 470/550 nm for the fibrils and 560/630 nm for trypan blue. The

average intensity of each frame captured was quantified using Fiji and normalized to the fluorescence signal from trypan blue bound to the neuronal membrane. In the case of the different human α-synuclein fibrillar conformers, primary neurons were incubated for 1 h at 37 °C with media containing 0.3 μM of the different α-synuclein-Alexa488 fibrils. Images were captured using a Leica DMI 6000B and a 63x objective.

2.28 Immunocytochemistry

Primary neurons were cultured in 35 mm glass cover slips and fixed with a 4 % solution of paraformaldehydefor 20 min. If the cell membrane was going to be labelled, cells were incubated with 0.5 μg/μl Wheat Germ agglutinin-594 (Thermo Fisher Scientific, Waltham, MA, USA) for 10 min at this point. After this cells were permeabilised with a solution of 0.1 % Triton-X for 15 minutes. After washing 3 times with PBS, cells were blocked for 1 hour in 3 % BSA in PBS before incubation overnight in the presence of primary antibody (p-α-synuclein [1:5000] and neurofilament [1:1000] diluted in 3 % BSA in PBS). The next day, cell were washed 3 times with PBS before incubating for 1 hour in the presence of secondary antibody ([(AlexaFluor-488 and AlexaFluor-647], 1:1000 in 3 % BSA in PBS). Cell were mounted using ProLong-Glod (Thermo Fisher Scientific, Waltham, MA, USA) and imaged using a 63x objective in a Leica DMI 6000B microscope.
SH-SY5Y cells were cultured in 35 mm glass cover slips and fixed with a 4 % solution of paraformaldehydefor 20 min after which they were permeabilised with a solution of 0.1 % Triton-X for 15 minutes. After washing 3 times with PBS, cells were blocked for 1 hour in 3 % BSA in PBS before incubation overnight in the presence of primary antibody (0C [1:500] or A11 [1:500] diluted in 3 % BSA in PBS)). The next day, cells were washed 3 times with PBS before incubating for 1 hour in the presence of secondary antibody ([(AlexaFluor-647], 1:1000 in 3 % BSA in PBS). Following 3 washes with PBS, cell were incubated in the presence of 300 nM Nile red (Thermo Fisher Scientific, Waltham, MA, USA) for 10 min followed by 5 min incubation in the presence of hoechst. Cell were mounted using ProLong-Glod (Thermo Fisher Scientific, Waltham, MA, USA) and imaged using a 63x objective in a Leica SP8 confocal microscope.

2.29 Animals

All animal protocols were performed at AAALAC accredited sites and approved by the University of Alabama at Birmingham Institutional Animal Care and Use Committee. C57BL/6 J male mice were obtained from Jackson laboratories and housed in groups of no more than five animals per cage. Food and water were accessible 24 hours a day,

and animals were kept on a 12 hour light/dark cycle. Experiments were conducted when animals were two to four months old.

2.30 Surgeries

For duration of surgery, mice were deeply anesthetized with vaporized isoflurane on a gas mask fitted to a digital stereotaxic frame. Mouse respiration was monitored throughout the procedure. Solutions for injection were drawn to a gas-tight syringe with a 26s gauge needle (Hamilton) and controlled by a digital pump. The injection of 2 μL and subsequent withdrawal of needle occurred over the course of 12 min to prevent solution running back up the needle track. Solutions were injected into the right dorsal striatum using the following coordinates: 0.2 mm anterior and 2.0 mm lateral to the Bregma, and 2.6 mm ventral relative to the skull. Scalp incisions were closed with EZ-Clips (FisherSci).

2.31 Immunohistochemistry of brain sections

Mice injected with various α-synuclein conformations (monomers, oligomers and fibrils prepared as describes in sections 2.1, 2.5 and 2.6 respectively) were anaesthetised three months post injection with isofluorane and transcardially perfused with a saline solution (0.9 % NaCl, 0.005 % sodium nitroprusside, and 10 units/mL heparin sodium) followed by freshly prepared 4 % PFA buffered in PBS. Brains were removed, postfixed for 24 h in 4 % PFA and PBS solution, floated into 30 % sucrose PBS solution for up to three days, frozen in methylbutane solution (-50 °C), and stored at -80 °C. Brain tissue was sectioned at 40 μM with a freezing microtome. All tissues were sectioned coronally. Immunohistochemistry was performed using an antibody to p-α-synuclein EP1536Y (Abcam), at 1:5000 dilution. A biotinylated secondary antibody (goat anti Rabbit IgG), avidin-biotin complex and 3,3'diaminobenzidine (DAB) were used to develop the sections. Immunohistochemistry for Tyrosine Hydroxylase (EMD Millipore) and dopamine transporter (a generous gift from Dr.Allan Levey, Emory University) was also performed as indicated above and developed using AlexaFluor-555 goat anti-chicken and AlexaFluor-488 goat anti-rat secondary antibodies. Images were taken using a Leica TCS-SP5 Laser scanning confocal microscope.

2.32 Behaviour assays

All behavioural tests were performed with the help of the UAB (University of Alabama in Birmingham) Neuroscience Behavioural Core. At one and three months or at six

months post injection, mice were subjected to a series of different behavioural tests of gross and fine motor function. Animals were acclimated to the test environment for at least 30 minutes prior to testing and were given at least a 1 day rest between each test. **Open Field Test**: each mouse was placed at the side of a 100 × 100 × 50 cm white Plexiglass open field. A computerized tracking system (Ethovision) recorded movement for 5 minutes from which the following was derived: latency to first enter the centre of the open field, the amount of time spent in the centre and periphery of the test apparatus, velocity of movement, and the total distance travelled. **Adjusting Steps Test**: mice were placed in a covered plexiglass cylinder (dimensions) with activity recorded for five minutes by Ethovision software on a camera positioned underneath the cylinder. An experimenter blinded to the treatment conditions scored each video, which could be slowed and rewound as needed. The following behaviours were scored: number of rears, front limb steps, hind limb steps, and total steps. **Pole Test**: mice were placed on top of a wooden pole (diameter 1 cm; height) wrapped in chicken wire. Each subject completed 5 trials with a 1 minute rest between each trial. Time to turn with nose facing down and time to reach the bottom of the pole were recorded and combined to derive the total time to descend. If a mouse did not climb down the pole after 2 minutes, the trial time was not included in that animal's average total time to descend. **Cage Hang**: mice were placed on a cage top elevated 50 cm above a cage filled with bedding. The cage lid was shaken slightly and flipped over to measure latency to fall over the course of 3 trials (> 1 minute rest between each trial). A trial less than 10 seconds was redone and trials were concluded at 3 minutes if a mouse was still hanging.

2.33 Stereology

Stereology was completed using a Olympus BX51 microscope and StereoInvestigator software (MBF Biosciences) using the UAB Neuroscience Molecular Detection and Stereology Core. In each injected brain stained with TH using the methods described above, contours were drawn around 6-7 serial sections containing SNc. Unbiased stereological estimation of total TH-positive neurons in the SNc contralateral and ipsilateral to injection was performed using the Optical Fractionator probe by an investigator blinded to experimental conditions.

2.34 α-Synuclein spread mapping

Serial sections (40 μm) from the entire mice brains were stained with p α-synuclein as described above. Mapping of the location and abundance of pathology was performed

using representative brains from each type of α-synuclein conformation (oligomers and fibrils) with α-synuclein monomer as a control.

2.35 Statistical analyses

In vivo data from the mouse studies (presented in section 3.2.2) were analysed using GraphPad Prism. One-way or two-way ANOVA were performed. Outliers were identified using the ROUT method in Graphpad Prism. The only data in which 2 outliers were identified were in the cage hang motor test. The data from the remaining sections of this thesis were analysed using OriginPro. One-way ANOVA was performed to determine statistical significance.

Chapter 3

Improving the preformed fibrillar model of Parkinson's disease

This work has been done in collaboration with the lab of Dr. Nunilo Cremades (Zaragoza, Spain) and Dr. Laura Volpicelly-Daley (Birmingham, Alabama,USA). Jessica Froula, from Dr. Laura Volpicelli-Daley lab injected generated the different α-synuclein species into the mice brains and performed the in vivo experiments. I spent three weeks in the lab of Dr. Laura Volpicelli Daley in May 2017 learning primary neuronal culture and helping with immunocytochemistry and with the immunohistochemistry analysis. José Camino, from Dr. Nunilo Cremades lab took the AFM images of the different conformers injected into the mice brains. The results presented in this chapter have been partially published in the next manuscript:

Jessica M. Froula, Marta Castellana-Cruz*, Nadia M. Anabtawi, José D. Camino, Serene W. Chen, Drake R. Thrasher, Jennifer Freire, Allen A. Yazdi, Sheila Fleming, Christopher M. Dobson, Janet R. Kumita, Nunilo Cremades, and Laura A. Volpicelli-Daley. Defining α-synuclein species responsible for Parkinson disease phenotypes in mice. Journal of Biological Chemistry, 294(27):10392-10406, 2019*

3.1 Introduction

As it has been mentioned before, none of the mouse models of Parkinson's disease (PD) is able to faithfully reproduce the disease in a reliable manner. However, the preformed fibrillar (PFF) model is specially interesting as it is able to reproduce the spreading of α-synuclein inclusions through the brain and in consequence, can potentially be used to test therapies targeting the advanced states of the disease and its spreading. As nowadays

it is not possible to diagnose PD at early stages, this model becomes specially relevant. However, in order to be able to explore all of its potential, it is necessary to improve the frequency with which mice inoculated with α-synuclein fibrils develop a locomotor phenotype. Typically fibrillar species are injected in the striatum of the mice brains, as this regions present a larger and more accessible target than the substantia nigra pars compacta (SNcp), inducing a neuronal death between 40 and 50 % in this region [73]. However, this only translates into a 30 % of neuronal loss in average in the SNcp, as the threshold to develop a motor phenotype is approximately 40 % of neuronal loss in the SNcp region, locomotor phenotype in this models tends to be variable (with defects reported mainly in the rotarod and wired hang tests) [53, 73].

One of the main possible sources of variability is the type of α-synuclein (mouse or human) used to produce the seeds that are subsequently injected into the mice's brains has been extensively studied before [92, 49]. As it has been mentioned in the introductory chapter (section 1.4.1), these studies demonstrated that mice injected with human α-synuclein fibrils accumulated fewer aggregates compared to mice injected with mouse α-synuclein fibrils. This is in agreement with what can be found *in vitro*, both by monitoring the elongation of mouse α-synuclein fibrils with human or mouse α-synuclein monomer or by feeding human or mouse α-synuclein fibrils to primary neurons [92, 49]. In both cases, the cross-seeding of α-synuclein fibrillar fragments with monomer from a different specie resulted in a slower elongation rate and fewer aggregates in the neurons. However, other potential sources of variability have remained largely unexplored. Here we hypothesised that the heterogeneity of the methods used to prepare the seeds and the lack of characterisation of the fibrillar mixtures which are injected into the mice are likely contributing to the differences in phenotypes displayed by PFF model. To try to overcome some of these technical challenges, and with the collaboration of Dr. Nunilo Cremades (Department of Biochemistry and Molecular Biology, University of Zaragoza) and Dr. Laura Volpicelli-Daley (Center for Neurodegeneration and Experimental Therapeutics, Department of Neurology, The University of Alabama at Birmingham), we have biophysically characterised and isolated five mouse α-synuclein species (monomer, oligomers, short fibrils, medium fibrils and long fibrils) that may be present in the fibrillar mixtures typically used in this model. By evaluating the capacity of these α-synuclein conformers to induce the aggregation of endogenous α-synuclein *in vitro* and *in vivo* we aimed to determine which α-synuclein species are able to produce neuropathological and neurodegenerative phenotypes in mice. Moreover, another potential source of variability between the different batches of fibrils used to inject the mice cohorts is the storage of the fibrillar samples. It is common in the field to produce large batches of α-synuclein seeds and store them at -80 °C or in liquid nitrogen for long periods of time before being used

[26, 33, 67]. However, the maintenance of the structural integrity of the fibrils after these processes has not been studied before. In order to address this issue, here we performed a study comparing different structural characteristics (length and secondary structure) of fibrillar samples before and after storing them at - 80 °C.

3.2 Results

3.2.1 Study of mouse α-synuclein fibril stability

As it has been previously discussed, some researchers in the field tend to prepare large batches of fibrils and store them in liquid nitrogen or at -80 °C for long periods of time [67]. Therefore, an important question in terms of developing reproducible PFF mouse models was to determine how this process affects α-synuclein fibril stability and morphology. In order to address this question, some preliminary analysis were conducted on mouse α-synuclein fibrillar samples that our collaborator, Dr. Volpicelli-Daley had stored in either liquid nitrogen, -80 °C or room temperature for different periods of time (Table 3.1).

At the time of the analysis, the 27-june-16 LN and 21-june-16 -80 samples had been stored for around five months, the 23-sept-16 LN for 3 months and the 11-oct-16 RT and 27-oct-16 short RT for one month.

In order to determine if the α-synuclein fibrils were stable under these conditions, the amount of the protein in monomeric and fibrillar forms present in the sample was analysed. With the aim of reducing the effect of cold-denaturation on the samples [99], they were thawed at room temperature and a 1/10 dilution of each sample was ultra-centrifuged for 1 hour. After this, the amount of protein present in the supernatant and in the pellet was determined using a BCA assay (Table 3.2) using known concentrations of mouse α-synuclein monomer as a standard curve. The amount of protein present in the supernatant seems to vary greatly between the samples: in the liquid nitrogen storage conditions 74.5 % (sample 27-june-16 LN) and 7.9 % (sample 23-sept-16 LN) of the protein was detected in the soluble fraction, in the -80 °C freezer storage conditions, 30 % (sample 21-june-16 -80) of the protein was present in the supernatant, finally in the samples stored at room temperature (sample 11-oct-16 RT and sample 27-oct-16 short RT) a 9 % and 23 % of the protein was detected in the soluble fraction respectively. The amount of protein present in the supernatant seems to correlate with the age of the samples themselves, suggesting that the longer the fibrils stay frozen the more disaggregation occurs. However, these fibrils were generated by shacking 350 μM at 700 rpm for 7

Sample name	Sample description
27-june-16 LN	100 μL of mouse α-synuclein fibrils at 5 mg/ml in 10mM Tris pH 7.5, 50mM NaCl made on 27/Jun/16 and stored in liquid nitrogen
21-june-16 -80	20 μL of mouse α-synuclein fibrils at 5 mg/ml in 10mM Tris pH 7.5, 50mM NaCl made on 21/Jun/16 and stored at -80 °C
23-sept-16 LN	100 μL of mouse α-synuclein fibrils at 5 mg/ml in 10mM Tris pH 7.5, 50mM NaCl made on 23/Sept/16 and stored in liquid nitrogen
11-oct-16 RT	50 μL of mouse α-synuclein fibrils at 5 mg/ml in PBS made on 11/Oct/16 and stored at room temperature
27-oct-16 short RT	100 μL of mouse α-synuclein fibrils at 5 mg/ml in PBS made on 9/Sept/16 and stored in LN until the 27/Oct/16, when it was thawed, sonicated and passed through a 0.22 μm cut-off filter. After this, the sample was stored at room temperature

Table 3.1: Samples of mouse α-synuclein used to compare the effect of storage conditions on fibril stability.

days and the conversion rate of monomer into fibrils was not determined by our collaborators. Because of this, it is also possible that the differences between the percentage of protein found in the supernatant corresponded just to a variation in the conversion rate of different batches of fibrils. In order to asses this, the aggregation efficiencies of different α-synuclein samples generated by shacking 70 μM α-synuclein at 200 rpm for 5 days was measured. It was found that the amount of protein present in the pellet oscillated between 50.7 % and 91 % (Table 3.3) supporting, in part, the hypothesis that the differences between the amount of protein present in the supernatant of the different samples are due to the intrinsic diversity of the aggregation process.

Theoretically, the sum of the protein concentrations measured in the supernatant and the pellet should equal ca. 350 μM in all the cases; however, this value is clearly lower in most cases. Our collaborator, Dr. Laura Volpicelli-Daley, has observed that after storage in the -80 °C freezer, the concentration of the monomeric samples of α-synuclein decreases significantly [100]. A similar process may be occurring in the fibrillar samples and could

Sample	Concentration (μM)			Percentage (%)	
	Supernatant (monomer)	Pellet (fibrils)	Total (μM)	Supernatant (monomer)	Pellet (fibrils)
27-june-16 LN	99.4	34	133.4	74.5	25.5
21-june-16 -80	70.7	163.1	233.8	30.2	69.8
23-sept-16 LN	20.6	240.5	261.1	7.9	92.1
11-oct-16 RT	44.7	418.4	463.1	9.6	90.4
27-oct-16 short RT	43.5	145.5	189	23	77

Table 3.2: Total and relative amounts of protein present in the soluble fraction and in the pellet of the analysed samples.

be responsible, at least in part, for the difference between the theoretical and measured protein concentrations. The 11-oct-16 RT sample is the only one that does not follow this trend, as its concentration was above the expected amount. As we only received ca. 50 μL instead of the expected volume of 100 μL, we believe that the evaporation of the buffer may have contributed to this change in concentration.

Sample	1	2	3	4	5	6	7	8	9	10	11	12
Pellet (%)	52.05	75.2	50.7	81.4	68.5	80.5	79.1	75.8	91	86	76.9	83

Table 3.3: Conversion efficiency of monomer into fibrils of different α-synuclein samples.

After this initial characterisation we proceeded to analyse the structural characteristics of the same samples. Fourier transform infrared (FT-IR) analysis (Figure 3.1) shows that the characteristic β-sheet secondary structure present in mature fibrils is only maintained in the sample stored at room temperature (11-oct-16 RT), with a dominant peak about 1620–1630 cm^{-1}. In the other samples, although an overall β-sheet structure is observed, there is an increase in the random coil content which may indicate the presence of monomeric protein. Unfortunately, it was not possible to take the FT-IR spectra of the 21-june-16 -80 sample dues to a lack of sample volume.

To determine if any further changes occurred after thawing the samples, they were kept at room temperature for another week and re-analysed by FT-IR spectroscopy (Figure 3.1 b, c and d). It was observed that whilst the structure of the 27-june-16 LN and 23-sept-16 LN samples did not change over time, a decrease in the absorption in the random-coil

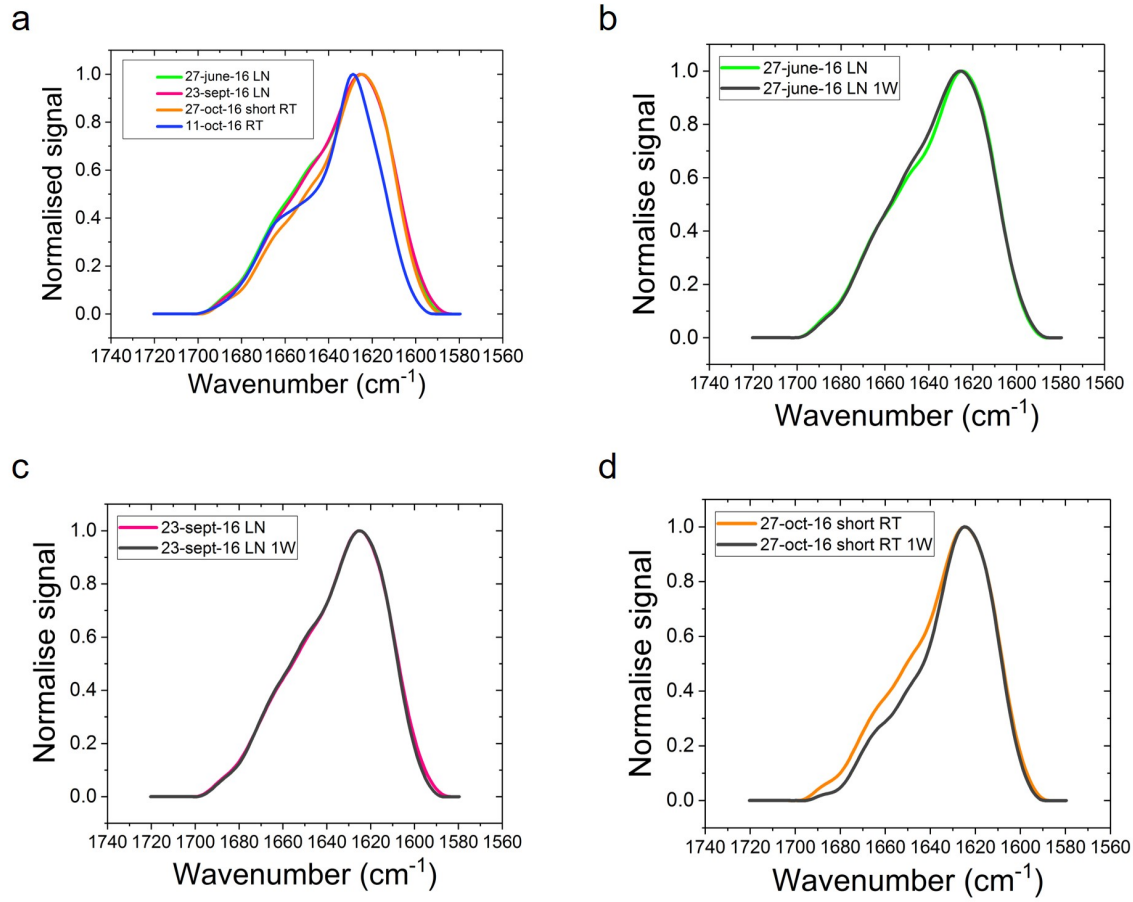

Figure 3.1: FT-IR spectra of the different samples (a) only the 11-oct-16 RT retain a fully characteristic fibrillar structure. The result from the FT-IR spectra performed after keeping the samples at room temperature show that while the structure of 27-june-16 LN (b) and 23-sept-16 LN (c) samples do not change overtime, the structure of 27-oct-16 short RT (d) sample presents decrease in the absorption in the random-coil region.

region of the 27-oct-16 short RT sample occurred. This change in the spectrum indicates that the structure of the sample has changed over time, potentially due to the elongation and re-formation of the fibrillar structure.

To confirm structural differences within the samples, microscopy techniques which could report on the fibril morphology and physical dimensions were performed. Transmission electron microscopy (TEM) and atomic force microscopy (AFM) images of all the samples were taken (Figure 3.2). In agreement with the FT-IR results, only the 11-oct-16 RT contained long mature fibrils forming networks. The TEM images showed that the 27-june-16 LN sample consisted of fibrillar fragments of different sizes and some clumps of longer fibrils, while in the AFM images only short fibrils of different sizes could eb appreciated, but as it is impossible to scan the entire mica surface, it is not possible to rule out the presence of fibrillar clumps in this analysis. Something similar happened

in the case of the 23-sept-16 LN sample where by TEM the presence of fibrillar clumps and some fragments was observed while by AFM it was only possible to appreciate a collection of fibrillar fragments of different sizes. Both the TEM and AFM images of the 21-june-16 -80 sample showed the presence of small fibrils and some very small fragments that could be oligomers. As expected, both techniques confirmed that the 27-oct-16 short RT sample was composed by short fibrillar fragments, matching the description of the sample provided for us by Dr. Laura Volpicelli-Daley (Table 3.1).

Overall, the fibrils from the 11-oct-16 RT were the only ones that maintained a typical parallel β-sheet secondary structure with a morphology characteristic of mature fibrils. Although the storage in the -80 °C freezer or liquid nitrogen did not seem to trigger the fibril disaggregation, TEM and AFM imaging indicated that the freezing of the samples triggers the fragmentation of the fibrils.

With the objective of exploring this phenomena more extensively it was hypothesised that the buffer chosen to aggregate α-synuclein may affect the fragmentation process. Accordingly, this hypothesis was tested in the experiments reported in this section of the thesis by the use of the three most commonly used buffers identified in the literature for the generation of α-synuclein. These buffers were the following: phosphate buffered saline (PBS) pH 7.3, 50 mM Tris-HCl 150 mM KCl pH 7.5 and 50 mM Tris-HCl 150 mM NaCl pH 7.5. Two different batches of α-synuclein fibrils were produced, the first one, denominated F0, was created by shaking 70 μM monomer at 200 rpm for 5 days and the second one, denominated F1, was produced by the reseeding of F0 with fresh monomer for 24 h. This process of reseeding existing fibrils with monomer has been proven to produce more homogenous fibrils that are less prone to clump [101]. Both types of fibrils were centrifuged for 10 min at 13000rpm, the soluble fraction containing unaggregated monomer was discarded and the pellet was resuspended at 350 μM, aliquoted in 125 μL aliquots and store at -80 °C for 2 months.

Upon thawing changes in fibrillar content, secondary structure and grade of fragmentation were monitored.

The analysis of the fibrillar content indicated that the amount of monomer present in the supernatant fraction after 2 month storage was increased in all the samples (Figure 3.3), although in all the cases it represented less than the 3 % of the total protein. This small increment can be explained by the process of cold denaturation that the fibrils undergo while thawing, the differences between samples seemed to indicated that fibrils produced under different conditions are not equally affected by this process. The fibrils produced in Tris KCl proved to be the least susceptible to this phenomena with the monomer content only increasing 1.24 $\pm$ 0.66 times for the F0 and 1.36 $\pm$ 0.45 for the

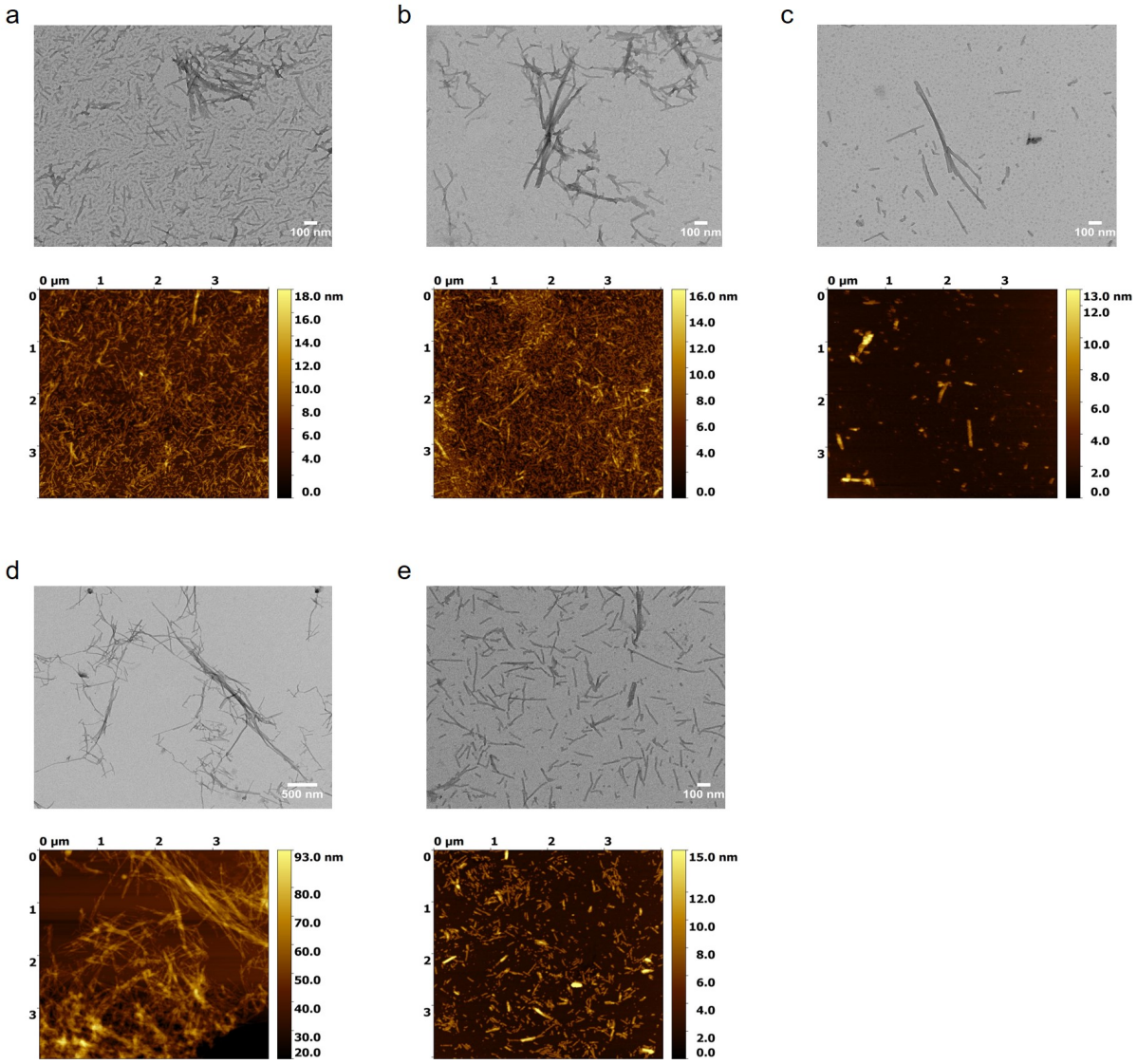

Figure 3.2: Microscopy imaging of the fibrillar samples. (a) TEM and AFM images of 27-june-16 LN show that the sample is composed by fibrillar fragments of different size and some clumps of longer fibrils. (b) TEM and AFM images of 23-sept-16 LN show that the sample is composed by fibrillar fragments of different size and some clumps of longer fibrils. (c) TEM and AFM images of 21-june-16 -80 sample show the presence of small fibrils and some very small fragments that could be oligomers (d) TEM and AFM images of 11-oct-16 RT show that the sample is composed by long mature fibrils forming networks. (e) TEM and AFM images of 27-oct-16 short RT show that the sample is composed by small fibrillar fragments.

F1. For the samples made in Tris NaCl, the amount of protein in the supernatant was incremented by a factor of 3.24 ± 0.66 in the F0 samples and 3.6 ± 0.55 in the F1. Finally the PBS samples showed the highest variability between fibril generations and a higher amount of protein in the supernatant than the samples produced in either of the Tris based buffers, with the monomer concentration elevated 9.58 ± 3.75 times in the case of the F0 and 3.59 ± 1.02 of the F1.

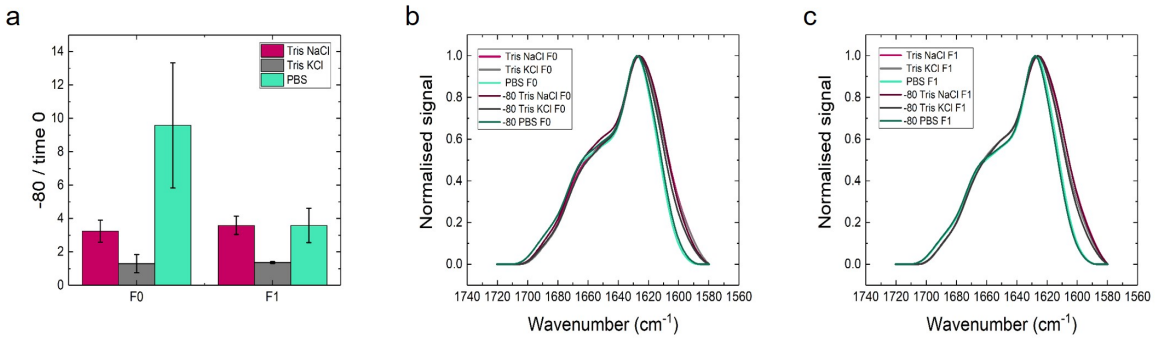

Figure 3.3: Structural characterisation of the fibrillar samples. (a) difference between the protein present in the supernatant at time 0 and after 2 months at -80 °C. (b) representative FT-IR spectra of the F0 generation samples at the two mentioned timepoints. (c) representative FT-IR spectra of the F1 generation samples at time 0 and after 2 month of storage.

Since the different susceptibilities to cold denaturation may be caused by small differences in the structure of the fibrillar samples the secondary structure of the fibrils by FT-IR (Figure 3.3) was examined. The deconvolution of the FT-IR spectra (Figure 3.4) showed that all the fibrils have similar secondary structure content. F0 fibrils made in Tris-NaCl were 62.04 % ± 5.8 β-sheet and 17.22 % ± 13.59 α-helix/random-coil and F1 61.62 % ± 0.73 and 9.66 % ± 3.21 respectively. In the case of the samples produced in Tris-KCl the percentage of β-sheet was slightly lower, 57.7 % ± 1.83 for F0 and 57.34 % ± 0.48 for F1, while the α-helix/random coil one was higher, 20.45 % ± 6.25 for F0 and 21.91 % ± 0.39 for F1. The fibrillar species formed in PBS had a similar β-sheet (57.88 % ± 2.68 for the F0 and 57.2 % ± 0.34 for the F1) and α-helix/random-coil (21.28 % ± 2.68 for F0 and 22.18 % ± 0.89 for F1) content. Although there was not significant difference between the β-sheet and α-helical/random-coil content of the different fibrillar samples, the raw spectra of the fibrils produced in Tris-based buffers were slightly different to the PBS ones. Specifically, the shape around the α-helical/random-coil region seemed to differ, with Tris-based fibrils presenting a higher signal than the PBS ones. The fact that these changes are consistent across different samples seems to indicate that although both sets of fibrils have largely the same structure there are some small differences between

them, specially in the the α-helical or random coil regions.

In agreement with the data gathered during the measuring of the protein present in the supernatant fraction of the samples, the FT-IR spectra of the different fibrillar species did not show significant changes after two months of storage at -80 °C (Figure 3.3).

As it had been previously noticed in our collaborator's samples, the storage of the samples for two month at -80 °C triggered the fragmentation of the fibrils in all the cases (Figure 3.5). With the exception of the Tris-NaCl sample, all the F0 fibrils were on average longer than the F1 ones when freshly made (Table 3.4), this fact can be attributed to the fact that the grade of clumpling in the Tris-NaCl samples hindered the proper determination of their length. Moreover, as it has been previously reported [101], the F1 fibrils were more homogeneous in length and less clumped than their counterparts. Upon thawing, all sets of fibrils experienced a significantly ($p<0.001$) decrease of length and interestingly, all the fibrils had a similar average length and display a similar distribution of sizes (Figure 3.6).This seems to indicate that the storage of fibrillar samples at -80 °C promotes the fragmentation of the fibrils to a determinate length (400-500 nm) independent of the buffer in which they were originally produced.

	Tris NaCl		Tris KCl		PBS	
	Fresh	2 moth -80 °C	Fresh	2 moth -80 °C	Fresh	2 moth -80 °C
F0	1152.42 ± 641.99	456.5 ± 320.13	966.99 ± 584.39	798.3 ± 449.4	1468.09 ± 1407.47	533.96 ± 463.24
F1	894.74 ± 439.62	451.06 ± 292.75	1192.95 ± 638.1	468.5 ± 328.12	604.55 ± 367.64	427.42 ± 281.15

Table 3.4: Average length and standard deviation of the different fibrillar samples. Samples were prepared in duplicates (n=2) and at least 5 TEM images were taken of each grid.

In conclusion, here we have demonstrated that although the freezing of the samples does not significantly alter the fibrillar structure it does promote the fragmentation of the fibrils. Because this type of samples is usually frozen with the objective of using them in different experiment separated across time, and it has been previously proven that the length of the fibrils affects the degree of cellular internalisation, this fact is of special relevance. For example, if an experimentalist were to use long fibrils freshly prepared, that have a low internalisation rate and produce a mild phenotype, in one experiment and frozen fibrils in another one, the variation in size could result in different internalisation rates and thus, a different phenotype, contributing to the great variability that we see

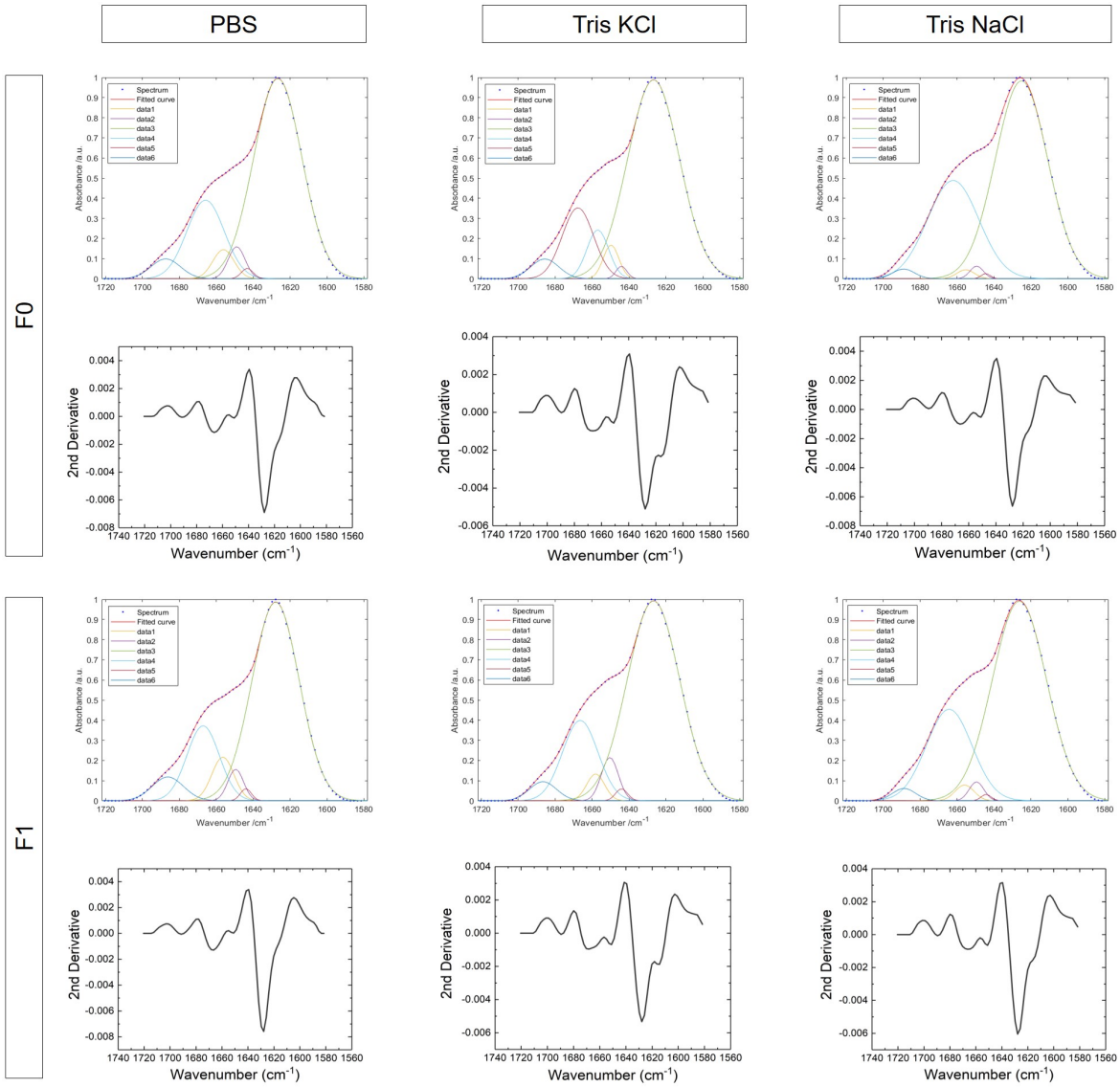

Figure 3.4: Deconvolution of the FT-IR spectra. Example of the deconvolution and second derivative of each one of the α-synuclein fibrillar species studied here. In all the cases a total of 6 Gaussian curves were used to fully reproduce the original spectra. The peaks identified by this curves were in good agreement with the ones highlighted in the second derivative functions.

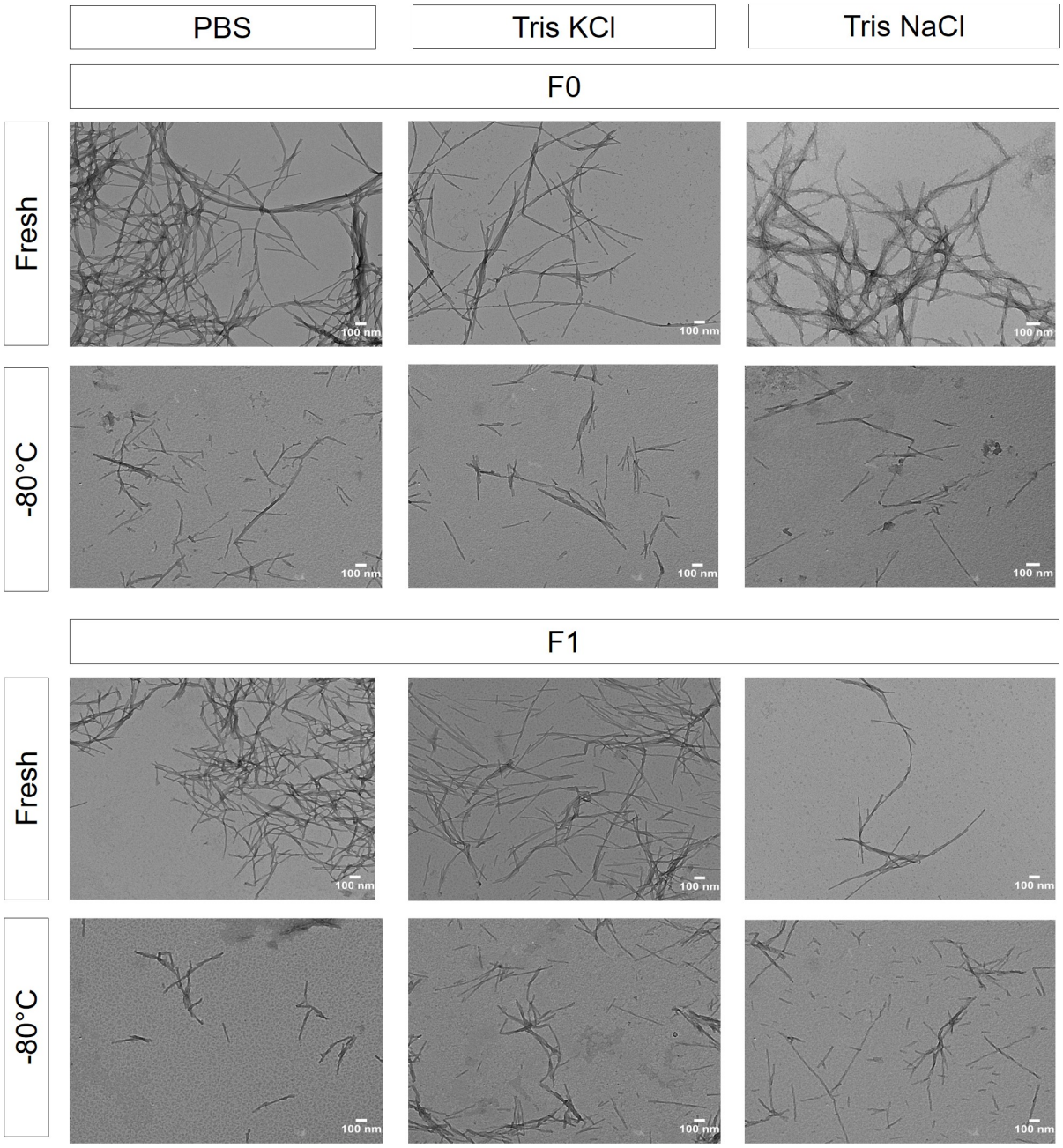

Figure 3.5: TEM images of the fibrillar samples. Here it is possible to appreciate the fragmentation that the fibrils undergo upon their freezing at -80 °C as well as the longer size and the higher degree of clumping characteristic of the F0 generation fibrils.

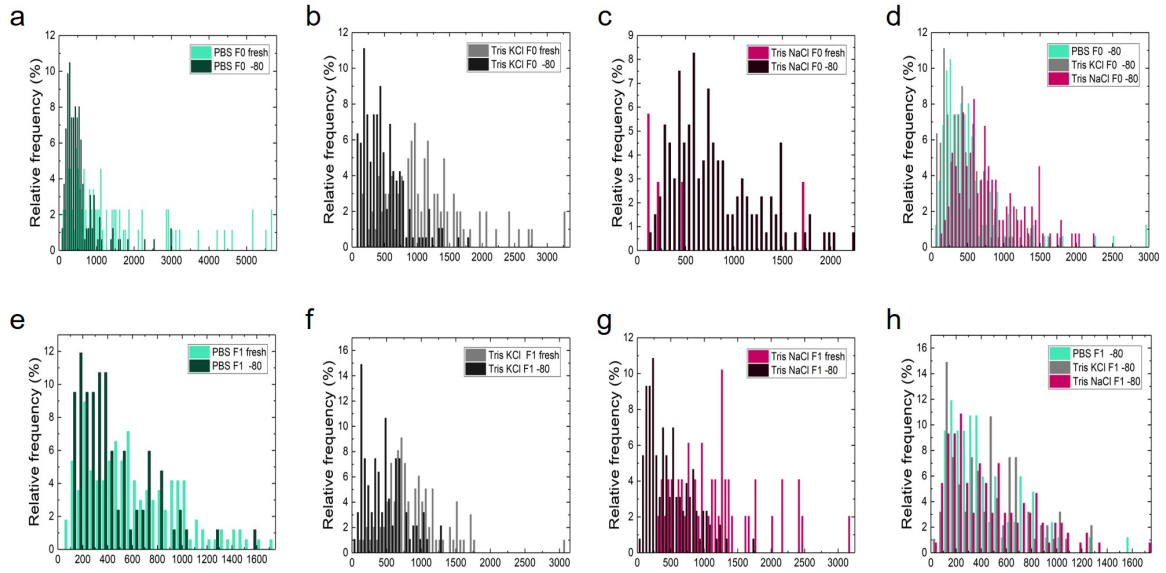

Figure 3.6: Size distribution of the different samples imaged by TEM. Samples were prepare in duplicates (n=2) and at least 5 TEM images were taken of each grid. Size distribution of (a) PBS, (b) Tris KCl, (c) Tris NaCl F0 generation fibrils at two different time points, time 0 and 2 months at -80 °C. (d) comparison between the sizes of the different α-synuclein conformers after 2 months at -80 °C, PBS and Tris KCl fibrils share the same distribution while the Tris NaCl one is slightly displaced. Size distribution of (e) PBS, (f) Tris KCl, (g) Tris NaCl F1 generation fibrils at two different time points, time 0 and 2 months at -80 °C. (e) comparison between the sizes of the different α-synuclein conformers after 2 months at -80 °C; all the fibrillar species share a similar distribution.

across this model. Due to this we believe that it is best to prepare fresh fibrils in the preferred buffer.

3.2.2 Defining α-synuclein conformers responsible for Parkinson's disease phenotypes in mice

Another main source of the phenotypical variability observed in the PFF model could be the amount of each different α-synuclein species injected into the brains of mice. The creation of α-synuclein fibrils from monomer by shacking results in a complex mixture of fibrils, monomer, oligomer and protofibrils that is often use unprocessed before being injected into the brains of mice. Moreover, the concentration of the sample is calculated assuming a 100 % conversion efficiency but, as it can be derived from (Table 3.3) the efficiency of monomer conversion into fibrils is not constant. Hence, different fibrillar batches generated this way could contain different amounts of α-synuclein fibrils, which in turn could lead to the injection of variable amounts of fibrils into the brains of mice.

This could influence the number of α-synuclein aggregates that develop in the brains of these mice and in consequence, contribute to the phenotypical variability observed across this model. As it has been explained in the introductory chapter (section 1.3) both, oligomers and fibrils, have been proposed as the toxic species responsible for PD, moreover both types of α-synuclein species are generated during the production of α-synuclein fibrils and are still present in the samples traditionally injected in this model. Here we seek to determine the seeding capacity and toxicity of these different α-synuclein species in the mouse brain through the study of five different α-synuclein conformers: monomer, kinetically trapped oligomers, long fibrils, medium size fibrils (obtained by sonication) and short fibrils (obtained after filtering the medium size fibrils through a 0.22 μm membrane). Because the cross-seeding between human α-synuclein seeds and mouse monomer is not as efficient as the seeding of mouse α-synuclein monomer with mouse α-synuclein fibrils ([49], Figure 3.10 a), we decided to use mouse recombinant α-synuclein for these experiments. It is a well known fact that the lipopolysaccharide (LPS) present in the membrane of *E. Coli* binds to recombinantly expressed proteins, contaminating the sample. As LPS is a potent activator of microglia, with the injection of 5 μg of LPS into the mouse brain have been proven to trigger this process [95], our first step was to clean the purified mouse α-synuclein with the Pierce High Capacity Endotoxin Removal Spin Column, which brought the LPS levels down from 0.77 EU per milligram of protein to less than 0.035 EU/mg.

Since mouse α-synuclein aggregated species have not been extensively characterised before, our first step was to biophysically characterise the different conformers and to compare them to their human counterparts [34]. After preparation, the secondary structure of the mouse α-synuclein monomer and oligomers, long, medium and short fibrils were determined using far-UV CD and FT-IR spectroscopies. CD spectroscopy in the far-UV region is able to define secondary structure elements such as random coil, α-helix and β-sheet structures whereas FT-IR analysis of the amide I region can, in addition, provide information of the arrangement of the β-sheet structures (i.e. parallel versus anti-parallel) which are present. The spectra of the mouse α-synuclein species revealed that the overall secondary structure is similar to their human homologues (Figure 3.7 a and b). As expected, the far UV-CD spectra of the monomer showed a typical random coil shape with a strong negative peak at 200 nm and the FT-IR presented a peak around 1650 -1640 cm^{-1} that can be attributed to a random coil conformation. All the fibrillar species produced similar spectra in both FT-IR and far-UV CD, showing an absorption band at the 1620-1630 cm^{-1} region in the FT-IR and a clear minimum at 220 nm in the far-UV CD. Deconvolution of the FT-IR spectra showed that long fibrils were 72.0 % $\pm$ 4.9 β-sheet, the medium ones were 70.0 % $\pm$ 3.2 and the short ones were 73.0 % $\pm$ 6.2,

which is in line with the values previously reported for human α-synuclein fibrils (65 % $\pm$ 10 [34]). In the case of the oligomers, both the FT-IR and far-UV CD indicated that in a similar manner to the human α-synuclein oligomers, the mouse species possessed an intermediate structure between a fibril and a monomer. The FT-IR spectrum displays an absorption peak at 1650 -1640 cm^{-1} that could be attributed to random coil content, and another one at 1620–1630 that, together with the shoulder present at 1695 cm^{-1}, indicates the presence of antiparallel β-sheet structure. In this spectrum, we can also observe that the percentage of β-sheet content seems to be higher in the case of the mouse α-synuclein oligomers (56.23 % $\pm$ 3 instead of the 35 % $\pm$ 5 reported for the human α-synuclein oligomers [34]). Finally, Thioflavin T (ThT) binding data showed that only the fibrils have a mature amyloid structure, in contrast to oligomers which showed a marginal ability to bind ThT molecules (Figure 3.7 d). Long, medium and short fibrils show similar ThT binding and thus had equivalent amyloid conformation.

In order to determine the morphology and size of the different mouse α-synuclein conformers TEM and AFM images of the different species (Figure 3.8) were taken. Due to the time constraints of the projects, the injection of the different α-synuclein species into the mouse brains was performed by our collaborator Dr. Laura Volpicelli-Daley before the characterisation of fibrillar stability upon different storage conditions could be performed, and fibrils stored in liquid nitrogen for several months were used for this purpose. As it has been shown before, fibrils made in PBS by shacking α-synuclein monomer should have had an approximated length of 1400 nm, but our long fibrillar sample shown an average height of 7 nm and an average length of 266 nm, which is indicative of the fragmentation process that has taken place upon the freezing of the samples. As expected, sonication of the samples to create medium sized fibrils created an heterogeneous population with a length rage between 40-225 nm and an average length of 120 nm. The filtration of this medium size population through an 0.22 μm filter resulted in an enriched population of the smaller fibrillar fragments with an average length of 70 nm and a more homogenous distribution of 40-125 nm. In agreement with what has been previously shown for human α-synuclein oligomers [34], mouse α-synuclein oligomers had a spherical-like morphology, an average length of 54 nm and an average height of 5.5 nm. Finally, the analysis of the sedimentation velocity measurements of the mouse α-synuclein oligomeric sample obtained by analytical ultracentrifugation (Figure 3.7 c) also reflects a similar size distribution to human α-synuclein oligomers [34]. In both cases, it is possible to observe two oligomeric populations, the first with a maximum peak at 10 S, and the second maximum peak at 15 S. This second peak is slightly higher in the case of the mouse α-synuclein oligomers, as this population has been previously shown to be increased likely due to the enrichment of β-sheet structure in this the oligomeric population [34]; therefore,

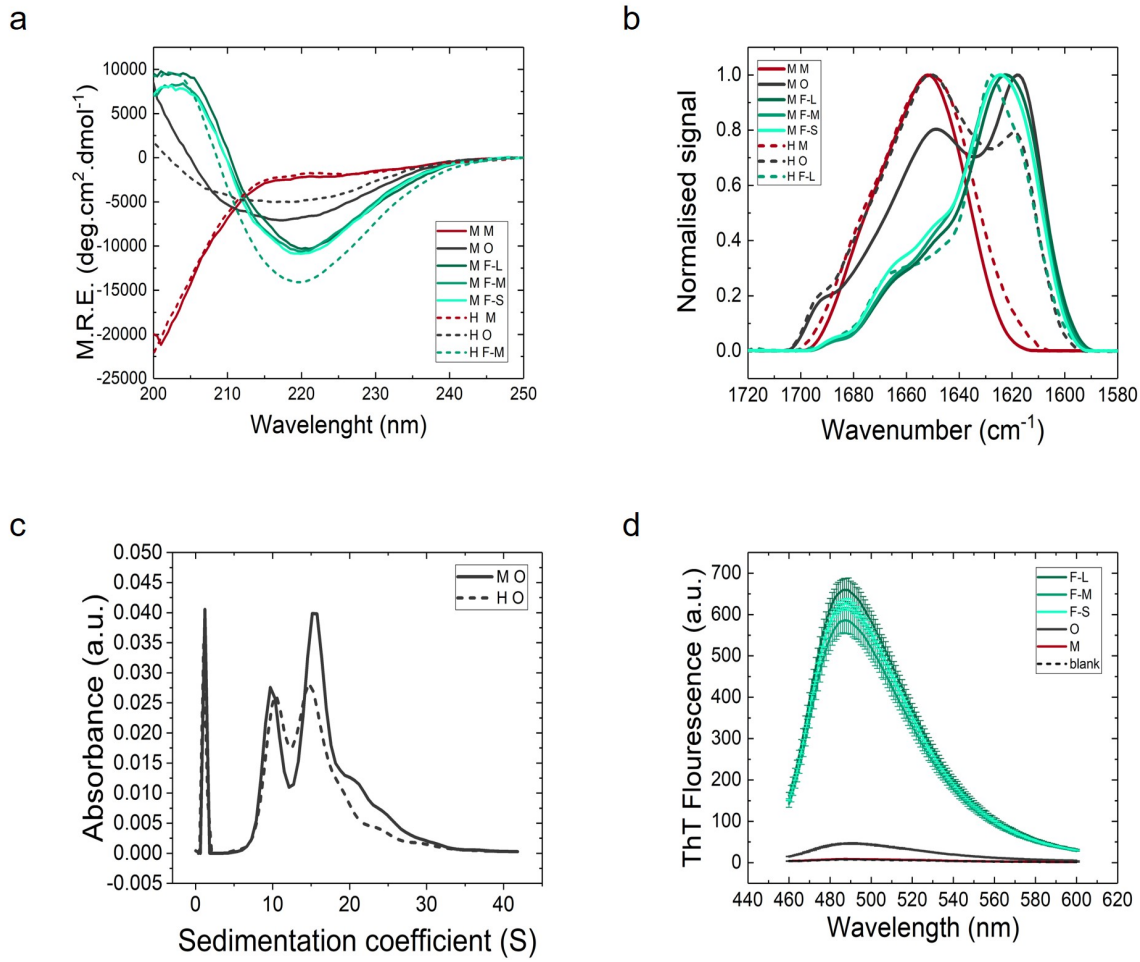

Figure 3.7: Structural characterisation of α-synuclein species used in the *in vivo* mouse studies. (a) representative far-UV CD spectra of an n=3. Oligomers (mouse and human) have a β-sheet content intermediate between monomer and fibrils. (b) representative FT-IR of an n=3. FT-IR spectra shows that long (M F-L), medium (M F-M), and short (M F-S) fibrils species are primarily composed of parallel β-sheet (band at 1620-1630 cm^{-1}) and similar to their human (H F-M) counterparts, and that the oligomeric (mouse (M O) and human (H O)) species are primarily antiparallel (band at 1620-1630 cm^{-1} and shoulder at 1695^{cm-1}). (c) analytical ultracentifuge sedimentation velocity measurement of human (grey dashed line) and mouse oligomers (grey continuous line) (n=3) shows 10S and 15S species. (d) ThT binding assay shows that all fibrillar adopt a similar amyloid conformation, the oligomers show limited ThT binding and monomer shows no ThT binding (n=3). [102]

this result is in line with our previous observation of an increased β-sheet content in the mouse oligomeric samples with respect to its human counterpart. In order to further confirm the nature of these α-synuclein conformers a dot bolt against total synuclein, oligomeric speceies and fibirllar species was performed. As expected OC, an antibody raised against amyloids, preferentially recognised the fibrillar form of α-synuclein, while A11, an antibody designed to recognise oligomers, preferentially recognised the oligomeric species (Figure 3.9 b and c). Because the antibody A11 has been previously shown to be able to recognise other conformers of α-synuclein [103], the partial recognition of monomeric and fibrillar samples by A11 observed in the dot blot does not necessarily imply a contamination of oligomeric species in these samples. As the rest of the tests performed to characterise these samples (FT-IR, CD, TEM, AUC, AFM) supported a correct isolation of the different α-synuclein conformers, it can be concluded that the different α-synuclein species were generated and purified successfully.

With the objective of assessing the integrity of the α-synuclein monomer after the aggregation process 5 μM of monomer, oligomer, short fibrils, medium fibrils and long fibrils were disaggregated by incubating overnight in 7M urea and the degree of fragmentation was assessed by SDS-PAGE. After developing the gel with silver stain, a band below the monomeric molecular weight was detected in the oligomeric sample (Figure 3.9 a), the fact that this could not be appreciated after staining with Instant Blue means that the this band contains less than 0.25 ng of protein (0.8 μM of each species were loaded into the gels). Based on this, the integrity of the α-synuclein monomer after aggregation into the different conformers was judged to be conserved.

In conclusion, the biophysical characterisation of the different mouse α-synuclein conformers reveals that they share similar structures and properties with their human homologues and hence, they can be used in this project as a model to reliable study the seeding capacity and toxicity of this different α-synuclein species *in vivo*.

Our next step was to assess the seeding efficiency of the different α-synuclein conformers *in vitro*. This was first investigated by following the time-dependent incremental change in ThT fluorescence at 37 °C of a mixture of 100 μM mouse α-synuclein and 10 μM of the different species (Figure 3.10 b). Neither the monomer nor the oligomers were able to seed the formation of amyloid fibrils, this is consistent with the fact that oligomers produced following this protocol are kinetically trapped and hence off-pathway [34]. The kinetics of seeded fibril formation was similar when medium or short fibrils were used as seeds and slightly slower for the long fibrils, this can mainly be explain by the fact that sonication of the long fibrils results in a more fragmented population and as a consequence produces more fibrillar ends capable of inducing elongation [51]. To

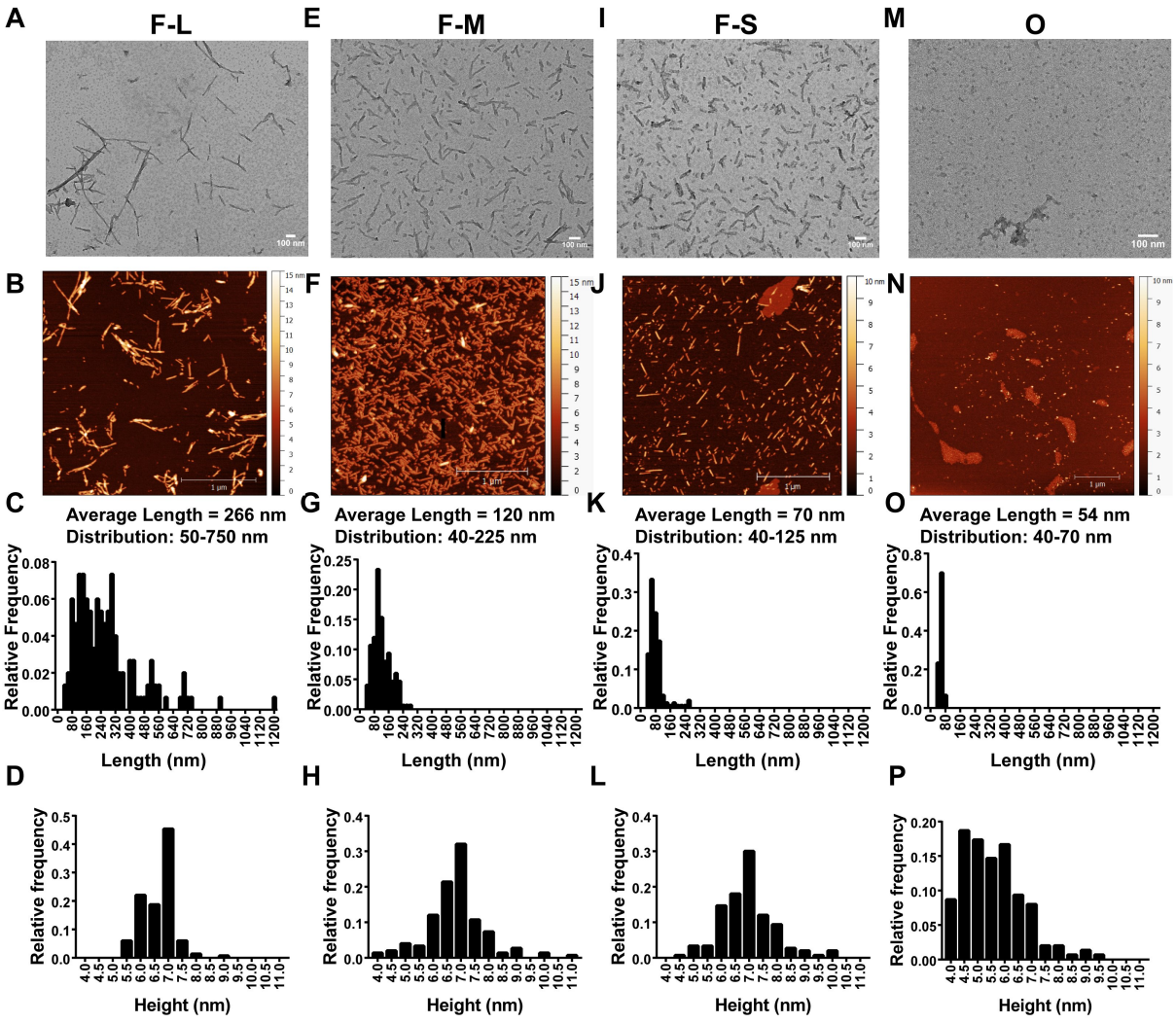

Figure 3.8: Morphological characterisation of the mouse α-synuclein species used in the *in vivo* mouse studies. TEM and AFM images of long fibrils (F-L) (a, b), medium fibrils (F-M) (e, f), sonicated fibrils enriched in short fragments (F-S) (i, j), and oligomers (O) (m, n). (c-p) AFM was used to quantify the length and height of each species shown in the histograms. [102]

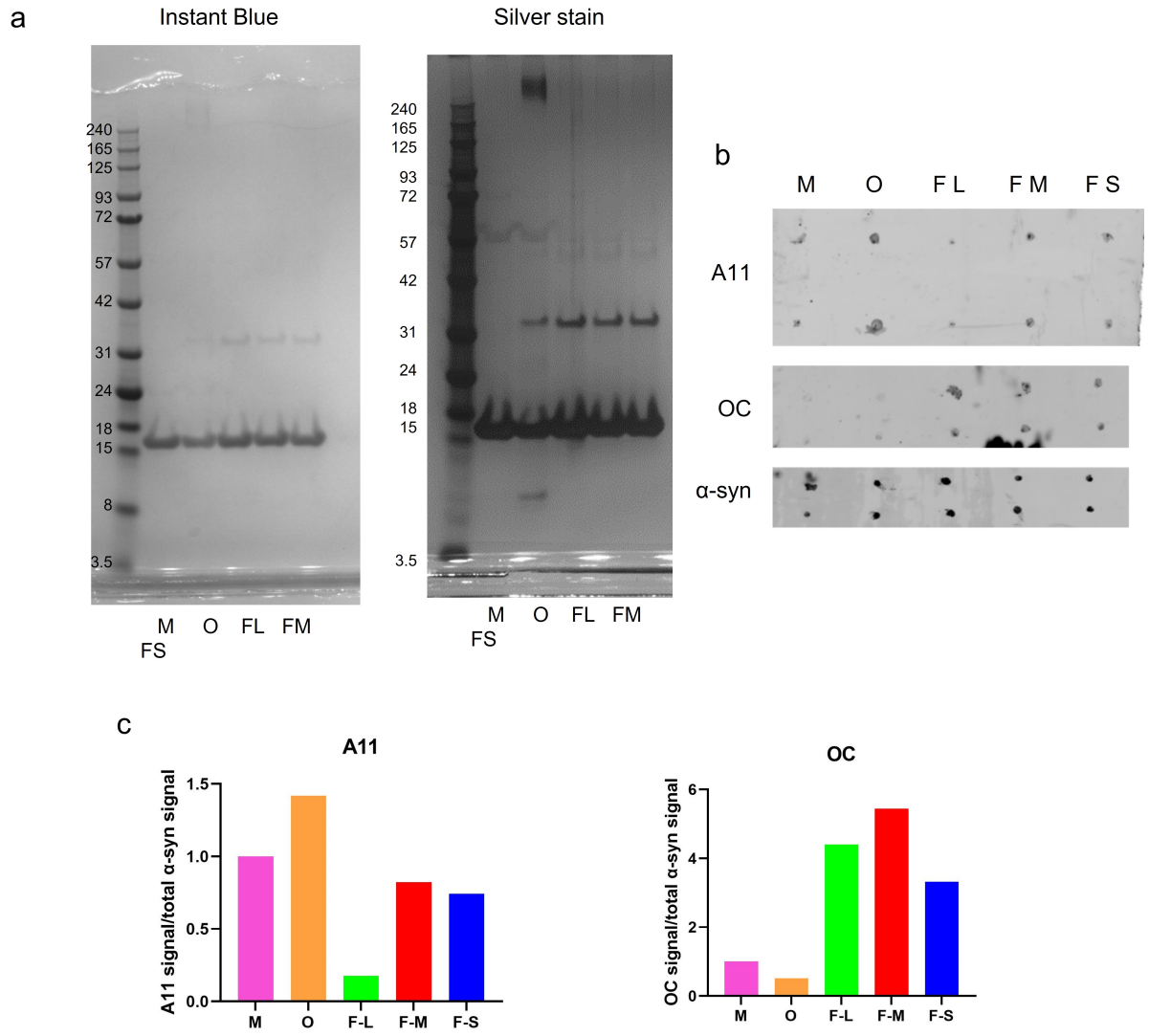

Figure 3.9: Structural integrity of mouse α-synuclein species and characterisation by structural antibodies. (a) The structural integrity of the mouse α-synuclein monomer after its aggregation into oligomer and fibrils was assessed by SDS-PAGE after incubation of 10 μM of each species with 7 M urea overnight. (b) Dot blot of the monomer, oligomer, short fibrils, medium fibrils and long fibrils against a total anti-α-synuclein antibody (syn1), oligomeric species (A11) and fibrillar species (OC). (c) Quantification of the signal from the dot blot displayed in (b). The relative intensity derived from each mouse α-synuclein species was normalised to the signal of the monomer and corrected by the total amoun of mouse α-synuclein

examine the ability of different α-synuclein fibrils to seed inclusion formation in neurons, our collaborator Dr. Laura Volpicelli-Daley added 50 nM of monomeric, oligomers, long, medium or short fibrils to wild type primary hippocampal neurons and quantified the abundance of phosphorylated α-synuclein, a marker of inclusion formation [104], seven days later (Figure 3.10 c and d). Consistent with the *in vitro* ThT binding assays, neither monomeric nor oligomeric α-synuclein produced p-α-synuclein inclusions while both short and medium fibrils produced significantly more inclusions that the long fibrils. The majority of inclusions appeared as bright, and thread-like similar to Lewy-neurites found in synucleinopathy brains. To determine if these differences in inclusion formation were a consequence of the different seeding efficiencies and if it is related to the internalisation rate of each species, an internalisation assay using α-synuclein labelled with Alexa488 was performed [98]. For this experiment a cysteine variant of mouse α-synuclein, E110C, was labelled with Alexa-488 through a malemide bond and the different mouse α-synuclein conformers were produced. The mouse E110C α-synuclein monomer was purified, LPS-cleaned, labelled with Alexa-488 and aggregated into the different conforms in Cambridge before shipping to our collaborator in Alabama. Previous studies [36, 105] have demonstrated that the labelling of α-synuclein through this method does not alter the monomer conformation nor the structure of kinetically trapped oligomers or fibrils. With the objective of assessing the internalisation of the different conformers, the 70 nM of Alexa-488 labelled α-synuclein species was added to primary hippocampal neurons for one hour, after which the extracellular fluorescence was quenched with trypan blue and the samples were imaged. Both Alexa-488 labelled short α-synuclein fibrils and oligomers were readily internalised, while long fibrils remained mainly in the extracellular region (Figure 3.10 e). As it has been previously demonstrated [106], this correlates with a low number of inclusion formations, however the addition of kinetically trapped oligomers, that are both efficiently internalised and toxic by themselves [34], was not able to induce the aggregation of endogenous α-synuclein. Taken together these results indicate that both the size and the seeding competency of the aggregates are factors that affect the formation of α-synuclein inclusions.

To determine the extent to which monomer, oligomers and different length fibrils seed formation of α-synuclein inclusions in the brain, our collaborator performed unilateral striatal injections of each conformer in 15 male C57BL/6 L male mice. In order to generate each of the conformers three different batches of monomeric protein were used to generate three independent batches of each conformer. The exact concentration of the samples was determined later during the biophysical characterisation and was 300 μM for the oligomers and monomer and 150 μM for all the fibrillar samples. This last data was surprising since the fibrils have been prepared using 300 μM monomer. Although

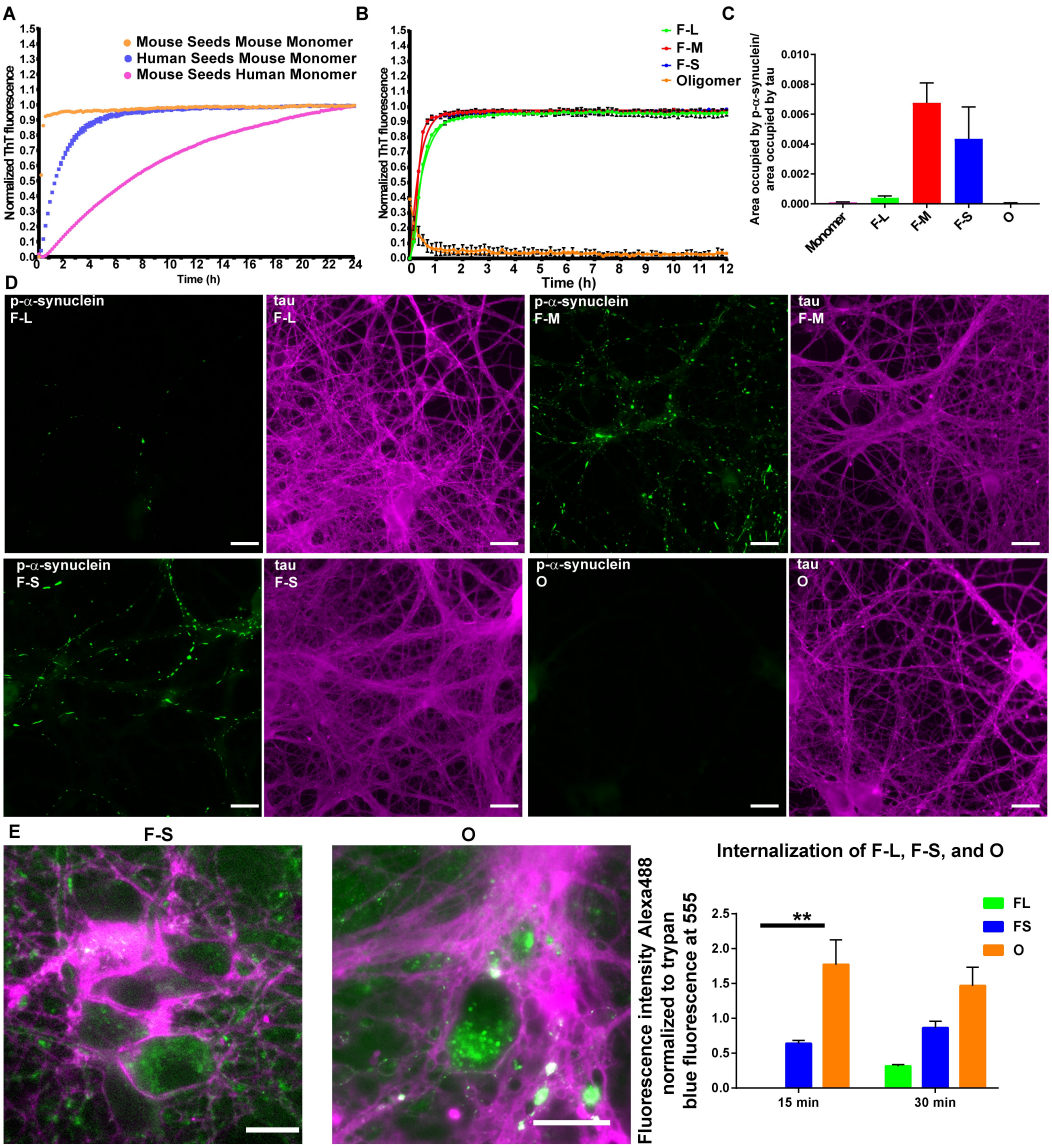

Figure 3.10: Seeding ability of the different assembled forms of α-synuclein species *in vitro* and in primary neurons. (a, b) monomer (100 μM) was incubated with 5 μM fibrillar or oligomeric seeds in the presence of ThT and the ThT fluorescence was monitored over time. The figure represent the average of n=3. (c, d) for the primary hippocampal neurons, 70 nM of long (F-L), medium (F-M), short (F-S) fibrils or oligomers (O) were added to the neurons and after seven days, the neurons were fixed and inclusion formation was visualized using an antibody to p-α-synuclein (green). Immunofluorescence for tau (magenta) shows the distribution of axons (scale bar = 50 μM). Image J was used to quantify the percent area occupied by p-α-synuclein. The data are presented as the mean ± SEM. (e) Primary hippocampal neurons were pre-incubated with Alexa-488 tagged long (F-L), short (F-S) fibrils or oligomers (O) 1 h at 37 °C to allow internalisation. Fluorescence of external α-synuclein-Alexa 488 was quenched using trypan blue. Images show representative α-synuclein-Alexa 488 fibrils or oligomers (scale bar = 50 μM). The fluorescence intensity of Alexa 488 from 10 fields per condition was quantified and normalized to trypan blue immunofluorescence. The internalisation experiments were repeated two times. [102]

the oligomers were prepared in Cambridge and shipped to Alabama, the fibrillar samples were prepared by our collaborator to avoid the clumping of the sonicated fragment during the transport [101, 100] and the concentration of the monomer used to produce the fibrils was determined by a BCA assay instead of the absorbance at 280 nm, which is known to significantly overestimate the concentration on mouse α-synuclein [107]. This could explain the differences between the expected fibrillar concentration and the observed one. Thus, the concentration of oligomers injected was two times more than fibrils in terms of mass concentration.

Mice were perfused 3 months later and the exact localisation of the injection site was evaluated via immunohistochemistry. Signs of a successful injection into the striatum were found in 12 mice injected with monomer, 15 injected with oligomers, 11 injected with long fibrils, 12 injected with medium fibrils and 11 injected with short fibrils. The remaining mice were excluded from further analysis. Immunohistochemistry was performed using an antibody specific for α-synuclein phosphorylated at serine-129 that has been characterised and validated using α-synuclein knockout mice [108, 109]. Mice injected with long medium and short fibrils presented p-α-synuclein positive inclusions while mice injected with oligomers and monomers presented a more diffuse and less intense signal in the cytosol, indicating that none inclusions had been formed (Figure 3.11). The inclusions appeared as Lewy-neurite like threads in the neuropil and skein-like inclusions in the soma. The abundance of inclusions in different areas of the brain was quantified using a semi-quantitative rating scale (Table 3.5) and the average score from the animals in each group was calculated (Table 3.5). The areas of the brain that presented more inclusions included the cortex, amygdala and striatum. In all the cases, the inclusions had a higher prevalence in the ipsilateral side to the injection, but with the exception of the SNc, the aggregates were also present in the contralateral side (Figure 3.11 c). As it had been observed *in vitro*, medium and short fibrils produced a similar number of inclusions while long fibrils produced significantly less aggregates (Figure 3.11 c).

The fact that the most abundant inclusions appear in region that project to the striatum (cortex, amygdala, and SNc)[110], suggested that the fibrils are internalised into the axon terminals and then transported to the soma. This is consistent with findings that after addition of fibrils to WT mice, inclusions appear first in axons and later in the the soma [48] and with the preferential localisation of α-synuclein at the presynaptic terminal [111]. To test this theory, we co-injected short fibrils with retrotracer beads into the right dorsal-lateral striatum. These beads are internalised and travel via axons to the neuronal soma allowing the tracing of connections in the brain. Two weeks after injections, p-α-synuclein positive inclusions were visible in the SNc, cortex and amygdala

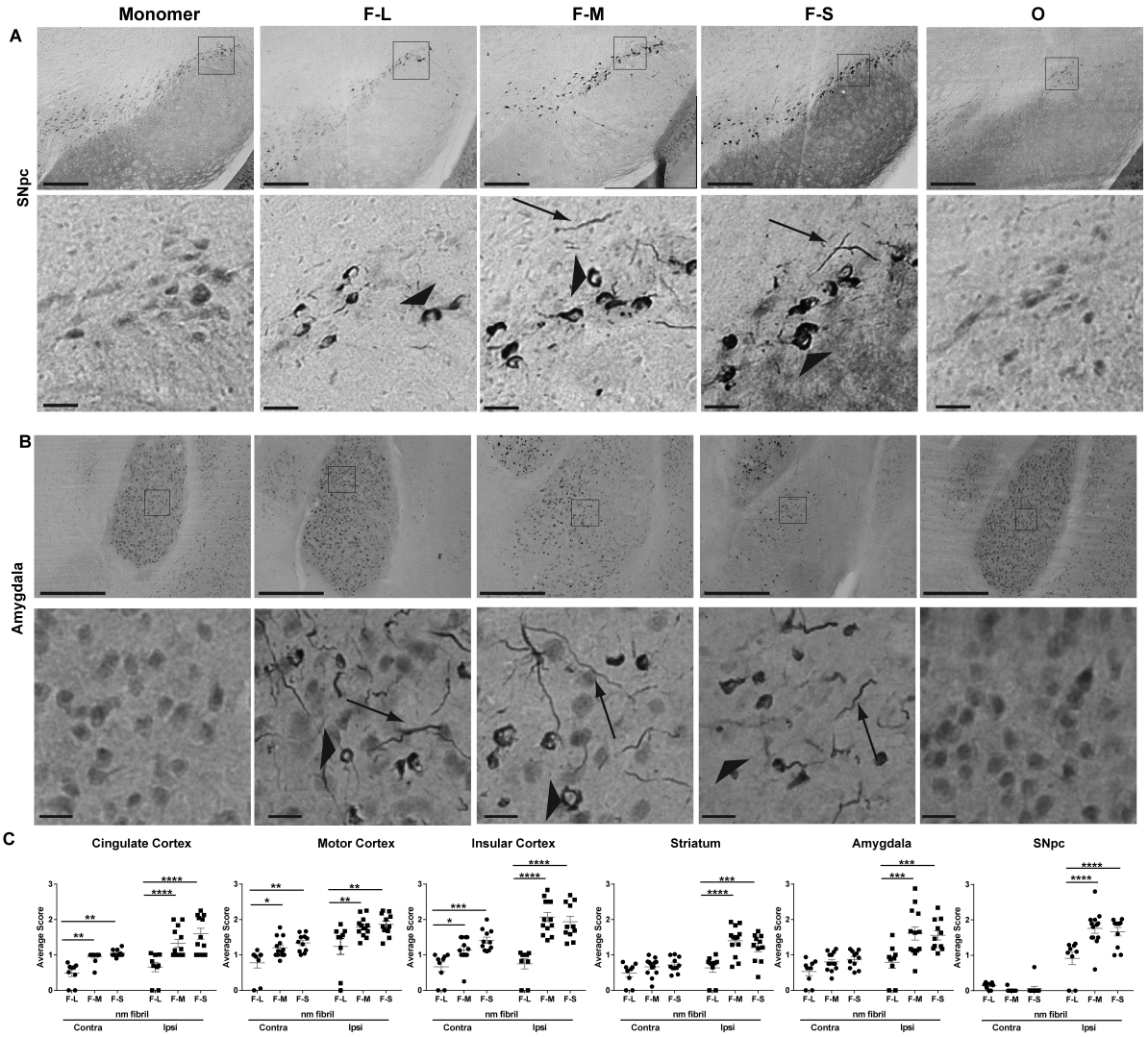

Figure 3.11: Inclusion formation in the mouse brain after injection of different forms of α-synuclein. C57BL/6J mice received unilateral striatal injections of two μL of soluble monomer (300 μM), long (F-L) (150 μM), medium (F-M) (150 μM), short (F-S) fibrils (150 μM) and oligomers (O) (300 μM). After three months, mice were perfused and immunohistochemistry was performed using an antibody to p-α-synuclein. Representative images from the SNc (a) and amygdala (b) are shown. Arrowheads indicate inclusions in the soma and arrows indicate Lewy neurite-like inclusions. (c) Quantification of the abundance of inclusions by an investigator blinded to experimental conditions. Numbers of mice: monomer (12), long (F-L) (11), medium (F-M) (12), short (F-S) fibrils (11), oligomers (O) (15). Data are shown as the mean score ± SEM and were analysed using a two-way ANOVA, α-synuclein species/cingulate $F(2,30) = 37.85$, $p < 0.0001$; α-synuclein species/motor cortex $F(2,30) = 7.9$, $p < 0.002$; α-synuclein species/insular cortex $F(2,30) = 22.3$, $p < 0.0001$; α-synuclein species/striatum $F(2,30) = 8.5$, $p < 0.001$; α-synuclein species/amygdala $F(2,30) = 6.6$, $p = 0.004$; α-synuclein species/SNc $F(2,30) = 6.2$, $p < 0.005$. *p<0.05, **p<0.01, ***p<0.001, ****p<0.0001. Scale bar = 100 μm (top panels); 20 μm (bottom panels). [102]

Brain area	Ipsilateral score	Contralateral score
Motor Cortex	1.6	1.1
Somatosensory Cortex	1.6	1
Insular Cortex	1.6	1
SNc	1.6	0
Auditory Cortex	1.4	0.9
Lateral Orbital Cortex	1.3	0.9
Amygdala	1.3	0.6
Ectorhinal Cortex	1.3	0.9
Striatum	1.1	0.5
Cingulate Cortex	1.0	1.0
Visual Cortex	1.0	0.4
Piriform Cortex	1.0	0.5
Nucleus Accumbens	0.4	0.4
Retrosplenal Cortex	0.7	0.3
Subiculum	0.6	0
Hippocampus	0.4	0
Mammillary nucleus	0.5	0.1
Olfactory Tubercle	0.2	0
Fimbria	0	0
Cerebellar Flocculus	0	0
Colliculus	0	0

Table 3.5: Quantification of inclusions present in different brain areas after the injection of short fibrils. The abundance of inclusion was rated on a scale from 0 to 3 (0:no inclusion in soma or neurites. 1: less than 10 aggregates in the soma and none in the neurites. 2: between 10 and 50 inclusion in the soma and less than 10 in the neurites. 3: more than 50 aggregates in the soma and more than 10 in the neurites). Brains from nine independent mice were scored to obtain the average score.

in the same area as the retrotracer beads and four weeks after injections, p-α-synuclein positive inclusions were abundant in all three brain regions (Figure 3.12). These data suggest that as we had hypothesized, the α-synuclein seeds are internalised in the striatum by axons projecting into this region and subsequently transported to the soma of neurons, efficiently spreading the aggregates through different areas of the brain.

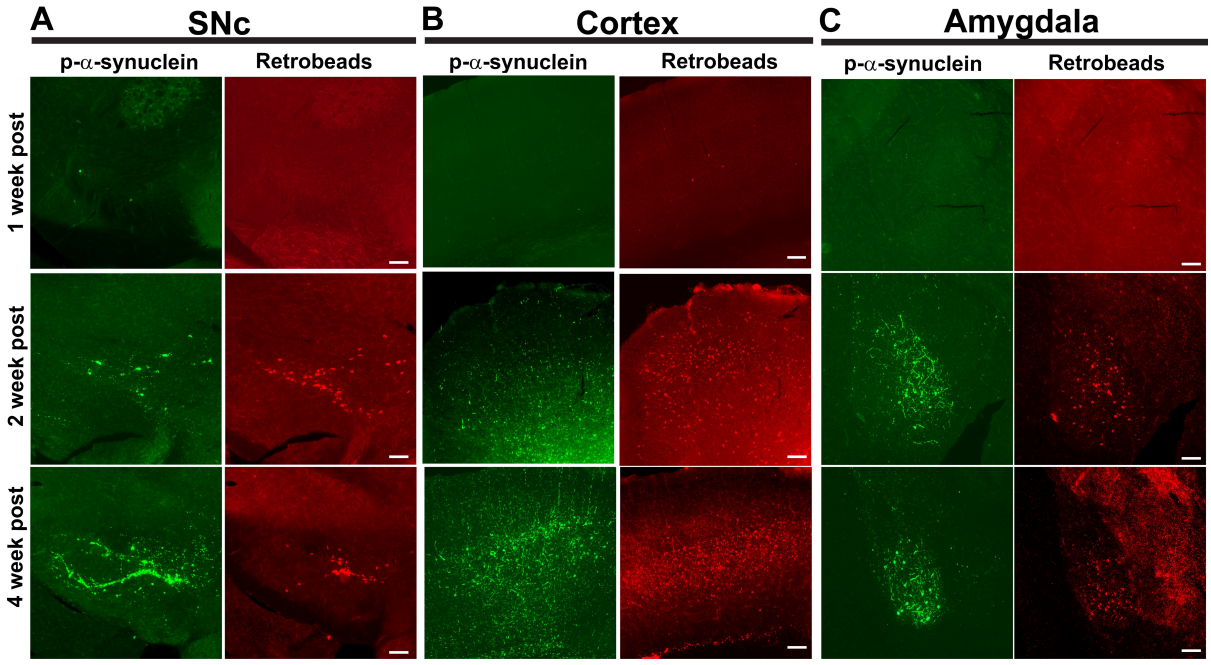

Figure 3.12: Appearance of p-α-synuclein inclusions in brain areas that project to the striatum. Fibrils and retrotracer beads were co-injected unilaterally into the striatum. After, one (N=3), two (N=3) or 4 weeks (N=3), mice were perfused and immunofluorescence to p-α-synuclein (green) was performed. The retrotracer beads are shown in red. Representative images from the SNc, motor cortex and amygdala are shown. [102]

In order to quantify dopaminergic neuronal loss in the ipsilateral and contralateral injection side of the SNc unbiased stereology the numbers against tyrosine hydroxylase (TH), a marker of dopaminergic neurons was performed. Three months after injection, only short fibrils produced a significant, approximately 30 % loss of dopaminergic neurons in the ipsilateral SNc compared to monomer injected mice (Figure 3.13). This reduction was also significant with respect to the contralateral injection side (Figure 3.13 b). Interestingly, the oligomers produced a significant reduction in the number of neurons on the side ipsilateral to the injection site relative to the non-injected side, which correlates with previous findings of kinetically trapped oligomers being toxic to neurons ([34, 38]. Although a reduction of TH positive neurons is generally accepted as an indicator of neuronal loss, another possible explanation is that the TH levels are simply being down-regulated. To address this possibility, we performed immunofluorescence measurements

against NeuN, a marker of neuronal nuclei, (Figure 3.14) in the SNc. Compared to mice injected with monomeric α-synuclein, there was a slight, but not statistically significant, reduction in the number of NeuN positive neurons in the mice that received injections of short fibrils. However, the TH-immunofluorescence in the short fibrils and oligomers injected mice appeared beaded compared to monomer injected mice, suggesting the presence of dying neurons. The loss of dopamine terminals was determined by immunofluorescence detection of the dopamine transporter (DAT) in the striatum (Figure 3.13 c, d). Mice injected with either medium and short fibrils showed an approximately 30 % reduction in DAT-positive dopamine terminals relative to the control. In addition, unlike the unilateral loss of dopamine neurons in the SNc, the loss of dopamine terminals in the striatum was bilateral. This correlates with the fact that no p-α-synuclein positive inclusions were detected in the contralateral side of the injection in the case of the SNc while α-synuclein aggregates were detected bilaterally in the case of the striatum. Although unilateral injection of unpurified sonicated fibrils into the striatum has been previously shown to produce a 35 % loss of dopaminergic neurons in the SNc [112] 6 months post injection, no statistically significant differences in the numbers of TH-positive dopamine neurons were detected 3 months after injection. As we have been able to shown a comparable reduction in the TH levels at only 3 months post-injection, this supports our theory that the generation of pure homogeneous well characterised fibrils is important to work towards the improvement of the PFF model.

Finally, we investigated if the formation of α-synuclein inclusions and the loss of dopamine neurons and terminals was translated in defects in motor behaviours. After 3 months only the mice injected with short fibrils showed changes in motor behaviour (Figure 3.15). Specifically, this mice showed an increment of the amount of time needed to descend a pole, a well establish test for "bradykinesia" [113], and reduction in the amount of time that the mice could hang from the lid of a cage, a test for motor strength [112]. However, no significant differences among any groups were found in the open field test for time spent in centre (a measure of "anxiety) or velocities of movement. A cylinder test modified specifically for mice [106] also showed no differences between mice injected with different α-synuclein conformers in the average number of hind limb steps or the average number of rears. Therefore, and in line with our previous results, only the injections of short fibrils is able to cause defects in motor strength and induce bradykinesia. This further highlights the fact that the best method to produce a strong robust phenotype in this model is to inject small seeding competent α-synuclein species.

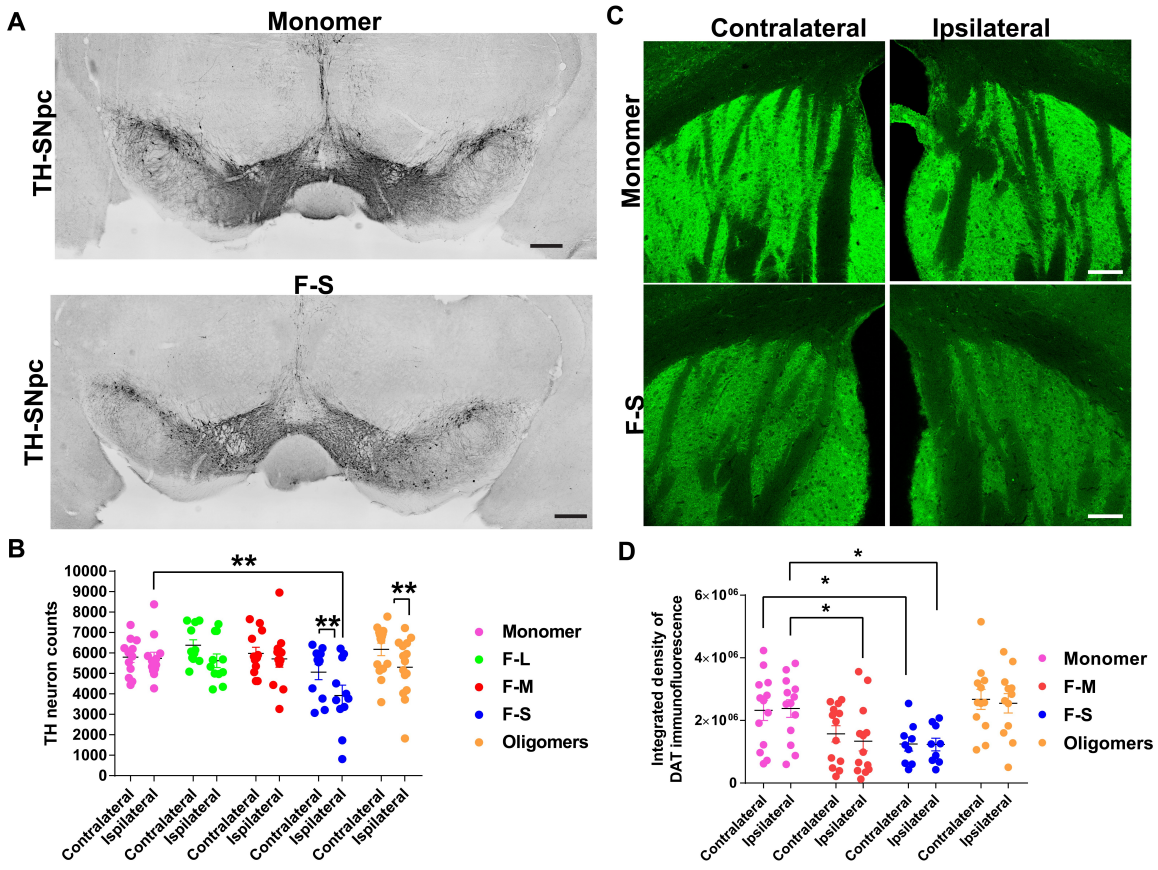

Figure 3.13: Quantification of TH-positive neurons in the SNc, and DAT terminals in striatum following unilateral striatal injections of different α-synuclein species. C57BL/6J mice received unilateral striatal injections of two μL of soluble monomer (300 μM), long (F-L) (150 μM), medium (F-M) (150 μM), short (F-S) fibrils (150 μM) and oligomers (O) (300 μM). After three months, the mice were perfused and immunostaining was performed. Numbers of mice: monomer (12), long (F-L) (11), medium (F-M) (12), short (F-S) fibrils (11), oligomers (O) (15) (a) representative images of tyrosine hydroxylase immunohistochemistry in the SNc of monomer and short fibrils injected mice. (b) unbiased stereology of tyrosine hydroxylase positive neurons performed by an investigator blinded to experimental conditions. Data are shown as the mean counts $\pm$ SEM and analysed using a two-way ANOVA, α-synuclein species $F(5,67) = 2.7$, $p = 0.03$. (c) representative images of immunofluorescence for DAT in the striatum from monomer and short fibrils injected mice are shown. (d) Image J was used to quantify the integrated fluorescence intensity of DAT in the striatum. Data are shown as the mean counts $\pm$ SEM and analysed using a two-way ANOVA, α-synuclein species $F(3,43) = 5.7$, $p = 0.002$. *p<0.05, **p<0.01, ***p<0.001, ****p<0.0001. Scale bar = 100 μm. [102]

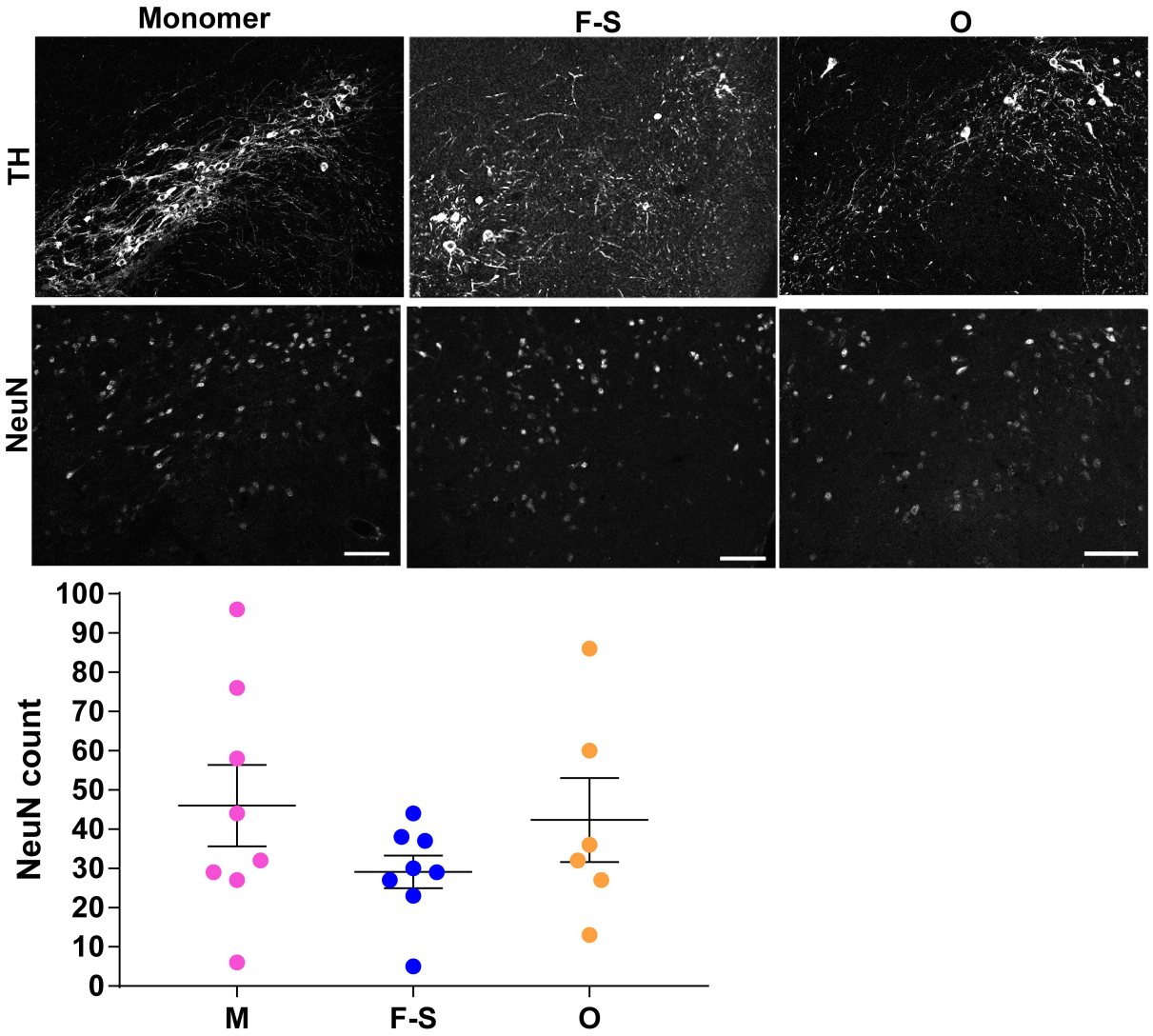

Figure 3.14: Double labeling immunofluorescence for TH and NeuN was performed using sections of SNc from mice that received unilateral injections of monomer (M), short fibrils (F-S), or oligomer (O). Images were captured using confocal microscopy. In image J, the colours were separated and thresholded using MaxEntropy autothreshold. The TH images was used to outline the SNc and the outline was transferred to the NeuN image. NeuN was converted to a binary image and "Analyze Particles" was used to count neurons. Data is presented as the mean NeuN count ± SEM (N, monomer = 8, N, short fibrils = 8, N, oligomer = 6. ANOVA revealed no significant differences between groups. Scale bar = 100 μM [102]

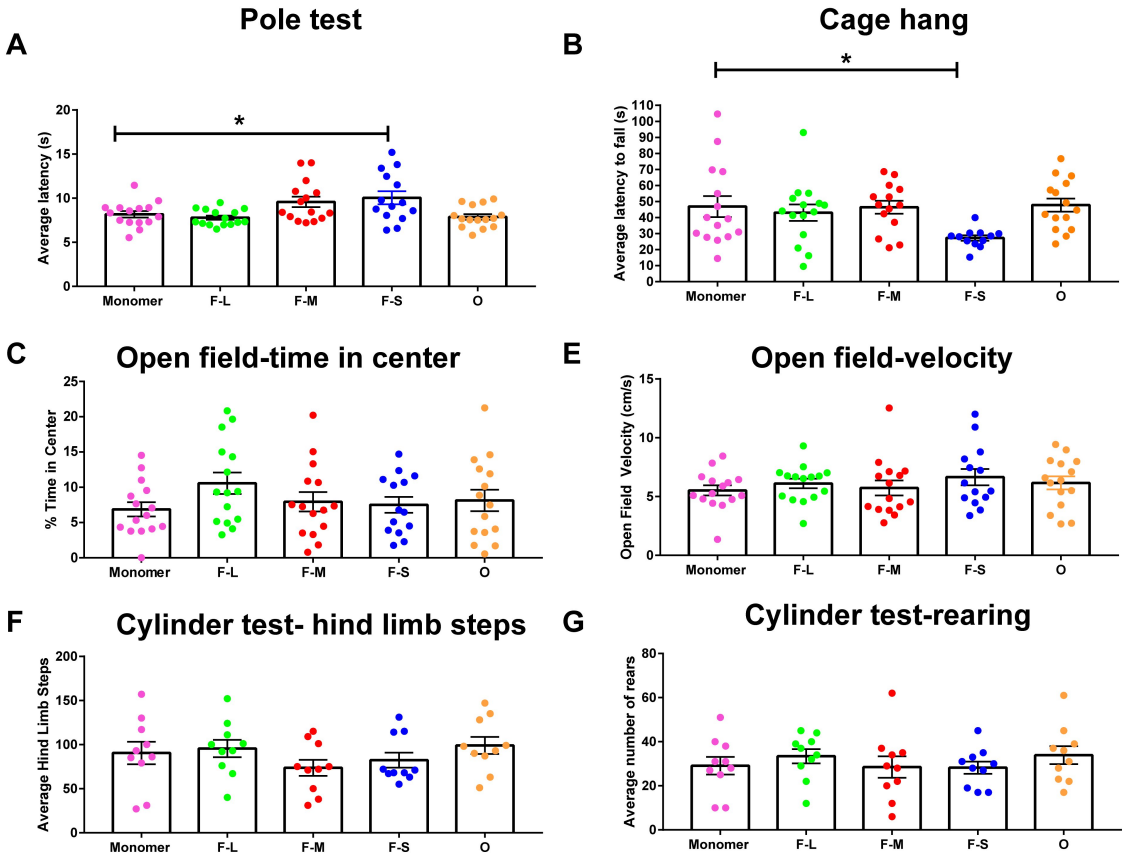

Figure 3.15: Motor behavior of mice following unilateral striatal injections of different α-synuclein species. C57BL/6J mice received unilateral striatal injections of two μL of soluble monomer (300 μM), long (F-L) (150 μM), medium (F-M) (150 μM), short (F-S) fibrils (150 μM) and oligomers (O) (300 μM). Three months later, mice were subjected to the following behavioural tests: open field, pole test, cage hang, cylinder test (modified for mice). Numbers of mice for pole test, cage hang, open field: monomer (12), long fibrils (11), medium fibrils (12), short fibrils (11), oligomers (15). Numbers of mice for cylinder test: monomer (10), long fibrils (10), medium fibrils (10), short fibrils (10), oligomers (10). The data were analysed by one-way ANOVA: pole test $F(4,69) = 4.7$, $p = 0.002$; cage hang $F(4,66) = 2.86$, $p = 0.03$; open field/% time center $F(4,69) = 1{,}1$, $p =$ NS; open field/velocity $F(4,69) = 0.6$, $p =$ NS; hind limb steps $F(4,45) = 1.1$, $p =$ NS; rearing $F(4,45) = 0.5$, $p =$ NS. [102]

3.3 Discussion

The development of good models of Parkinson's disease is key in the designing and testing of therapeutic strategies to halt the progression and spread of the disease. Although the PFF model does not reproduce the onset of the disease, it does reliably mimic its spreading state. Since there is not currently any test to detect the early stages of PD, this makes this model especially useful to test therapies focused on later stages of the disease that can currently be diagnosed. The successful targeting of the spreading state of PD requires the characterisation of the α-synuclein conformations responsible for PD phenotypes, including inclusion formation in multiple brain areas, dopamine terminal loss, neuronal death in the SNc and motor behaviours. Here, we used a combination of techniques from biophysics to immunohistochemistry to behaviour to demonstrate that small, 70 nm fragments of α-synuclein fibrils are the most efficient molecular species capable of inducing PD-like pathology features when injected into the brain of healthy mice. These aggregates are able to grow and recruit endogenous monomeric α-synuclein, suggesting that these species are important agents for the spreading of toxicity and disease. Stabilised α-synuclein oligomers are, in agreement with previous reports, able to induce a significant 14 % loss of dopamine neurons in the SNc on the side ipsilateral to the injection compared to the contralateral side [34, 36, 38, 114], but due to fact that their are kinetically trapped they were unable to seed the formation of endogenous α-synuclein inclusions, cause loss of dopamine terminals in the striatum or cause motor behaviour phenotypes. Thus our results suggest that the ability of aggregated species to recruit endogenous monomeric protein and to generate new toxic aggregates has a higher impact than the inherent toxicity of the injected species in the probability of inducing the development of PD-related phenotypes. In addition, our results suggest that the major disease spreading agents consist of small, seeding-competent α-synuclein fibrillar aggregates.

Whether fibrils or oligomers are the most toxic species of aggregated protein has been extensively studied in multiple neurodegenerative diseases including Alzheimer's disease, Huntingtin's disease and PD. As the oligomers used in this study are kinetically trapped and hence are unable to seed the formation of inclusions and spread the disease, it is not possible to discard that on-pathway oligomers play a role in the induction of PD-related phenotypes in the mice injected with short fibrils. In fact, the loss of dopaminergic neurons induced by oligomeric species has been shown *in vivo* by using lentivirus to express human α-synuclein variants prone to oligomerize [115]. Moreover, the release of on-pathway oligomers upon the interaction of small α-synuclein fibrillar samples with the cellular membrane has been recently observed [116]. As the aggregation cascade of α-synuclein is complex and the fibrils do not necessarily represent its end-point, there are

other mechanisms by which on-pathway oligomers can be formed in mice injected with short fibrils. These mechanisms include the possibility that the sonication of the fibrils pre-injection could produce some oligomers as a by-product, and that oligomeric species could be generated by the fragmentation of longer α-synuclein fibrils or by the induction of secondary nucleation processes. Although these on-pathway oligomers are expected to be toxic [30], due to their low concentration and lack of a defined amyloid structure [34], they are probably not the main species responsible of the spreading of the disease through the brain. In contrast with these oligomers, small fibrils are more stable and are composed by several α-synuclein protofilaments arranged in a specific conformation, which constitutes a fibrillar polymorph. This could potentially allow small fibrils to spread through the brain seeding the formation of new α-synuclein fibrils from a specific polymorph, which would be in line with the recent findings of specific α-synuclein fibrillar polymorphs being present in different synucleinopathies [57, 58, 59].

Our results suggest that targetting the small fibrillar α-synuclein fragments generated by the aggregation of monomeric protein or by the fragmentation or disaggregation of longer fibrils, have the potential to be a therapeutic strategy in the treatment of PD. However, antibodies that are not selective for fibrillar α-synuclein also reduce its total concentration inside the cell, and may result in the impairment of the synaptical function [117, 118]. However, antibodies that selectively target α-synuclein fibrils can potentially hinder their ability to spread from cell-to-cell and therefore reduce the rate of disease propagation. Antibodies that target the N-terminal region of α-synuclein have been proven more efficient in impairing the interaction of the fibrillar aggregates with the cellular membrane and abrogating the downstream toxic affects [37]. One example is BIIB054 which selectively binds the N-terminal region of fibrillar α-synuclein [119], and using the PFF mouse models of PD was able to inhibit inclusion formation, dopaminergic neuronal loss, and defects in motor behaviour.

Overall, our data highlights the importance of biophysically characterising in a methodological way, the species of α-synuclein responsible for the major events of dysfunction related to PD. In this study, injection of short fibrillar fragments of approximately 70 nm in length induced the formation of p-α-synuclein inclusions, neuron loss and motor dysfunction 3 months after the injection, while previous studies were not able to detect neuronal loss until 6 months post injection [112]. Interestingly, the injection of fibrillar fragments with a similar length (40-225 nm) as used in this previous studies [112, 53] was able to induce the formation of inclusions but not to trigger neuronal loss or behavioural phenotypes. This suggests that differences in the fibrillar length of the α-synuclein fragments might be the origin of some of the phenotypical variability reported within this

model. Since we have previously established the freezing of the fibrils will induce their fragmentation and therefore affect their size, this highlights the importance of preparing fresh fibrils before each round of injections.

Chapter 4

Exploring the correlation between structural polymorphism of α-synuclein oligomers and cellular toxicity

These experiments have been developed in collaboration with Catherine Xu, who performed the biophysical characterisation of the different oligomeric species.

4.1 Introduction

The misfolding of proteins and their aggregation into amyloid fibrils has been implicated in numerous neurodegenerative disorders, including Parkinson's and Alzheimer's diseases. As it has been previously discussed, α-synuclein is an intrinsically disordered protein that upon binding with lipid membranes is able to adopt an α-helical structure in the N-terminal region [120]. This association with lipid membranes is likely to have biological relevance [121] and it has been found to be a key trigger of aggregation [27, 122]. Once aggregated, α-synuclein adopts a cross-beta structure characteristic of amyloid aggregates [1]. During this aggregation process a heterogeneous mixture of species, including different populations of oligomeric species with varying percentage of β-sheet structure, can be detected [30]. It is believed that these oligomers are one of the main α-synuclein species responsible for cellular toxicity *in vivo* [36], recently using solution and solid NMR-state experiments, it has been proposed that this toxicity its mediated by both, the interaction of the N-terminal region with the cell membrane and the insertion of the β-sheet hydrophobic core into the lipid bilayer [36] which disrupts membrane integrity (Figure 1.6 g). Experiments with oligomeric species from other proteins suggest the presence of a key link between hydrophobicity, size and toxicity [36, 115, 34, 123], were more toxicity is

linked to those oligomers that are small and have a higher degree of exposed hydrophobic regions.

Since the oligomers are especially relevant to explaining the α-synuclein aggregation toxicity *in vivo*, an effort has been made to study the oligomeric populations formed during the aggregation of the α-synuclein mutants related with the genetic form of Parkinson's disease (PD) (Figure 4.1). As it has been mentioned before, some of these mutations (A53T and A30P) are able to accelerate the aggregation of α-synuclein while others (E46K, H50Q and G51D) slow it. However, this does not necessarily reflex changes in the oligomeric populations. Due to the lowly populated nature of oligomers they are difficult to characterise, one possible approach to solve this is the use of single-molecule techniques like measuring of intermolecular FRET efficiency. This technique has allow the detection of two different oligomeric species, "Type A" and "Type B", present during the aggregation of α-synuclein [30] (Figure 1.6). As it has been explained before, "Type A" oligomers form fist during the aggregation process and present a reduced toxicity, while "Type B" oligomers are able to induce higher levels of cellular toxicity. Single molecule FRET studies of the oligomerisation of the A53T, A30P and E46K variants of α-synuclein revealed significant differences between the A53T and A30P oligomeric population respect to the wild-type [124]. In addition, the concentration of oligomers during the lag-phase of the aggregation of wild-type and mutated alpha-synuclein is similar, suggesting that the properties of the oligomers generated during the aggregation process might be more relevant than their absolute concentration for triggering neurodegeneration. Due to the transient and rapidly changing nature of the on-pathway oligomers, it is extremely challenging to study their structure in a detailed manner. In order to address this problem, stabilised oligomers, similar to "Type B" oligomers, of the different α-synuclein variant related to PD, A53T, E46K, H50Q, A30P and G51D were produced. Moreover, the formation of oligomers that are not able to progress into fibrils have been detected during the aggregation of WT, A5T, E43K and A30P α-synuclein variants [125, 126]. This highlights the importance of understanding the role that kinetically-trapped oligomers in cell toxicity, not just as a model of on-pathway oligomers, but also as part of the aggregation process. Since these α-synuclein mutations (A53T, E46K, H50Q, A30P and G51D) are pathogenic and oligomers have been identified as one of the toxic species of the aggregation pathway, this work seeks to study the possible relationship between oligomeric structure and cellular toxicity using kinetically trapped oligomers as a model.

MDVFMKGLSKAKEGVVAAAEKTKQGVAEAAGKTKEGVLYVGSKTKEG
VVHGVATVAEKTKEQVTNVGGAVVTGVTAVAQKTVEGAGSIAAATGFV
KKDQLGKNEEGAPQEGILEDMPVDPDNEAYEMPSEEGYQDYEPEA

Figure 4.1: Human α-synuclein sequence showing in red mutation associated with genetic forms of PD. In order: A30P, E46K, H50Q, G51D and A53T

4.2 Results

Oligomers from the familial PD associated α-synuclein variants, A30P, E46K, H50Q, G51D and A53T were successfully generated using our previously described protocols [34]. Briefly 6 mg of lyophilised monomeric α-synuclein were resuspended in 500 μL of PBS, incubated overnight at 37 °C, ultracentrifugated to eliminate possible fibrils and concentrated using a 100 kDa filter in order to eliminate excess monomer. First, we compared the size of this variants oligomers with the WT. Transmission electron microscopy (TEM) images showed that they had a similar size and morphology to the WT oligomers, being all of them approximately spherical with a diameter of around 5-15 nm (Figure 4.2). This measures were confirmed using dynamic light scattering (DLS), which showed a major peak for the oligomers around 20 nm diameter, in contrast to 4 nm peak of the monomers (Figure 4.2). This difference in the estimate size obtained from the DLS measures and the TEM is probably due to the effects of solvation and bias towards larger species of the DLS. [127]

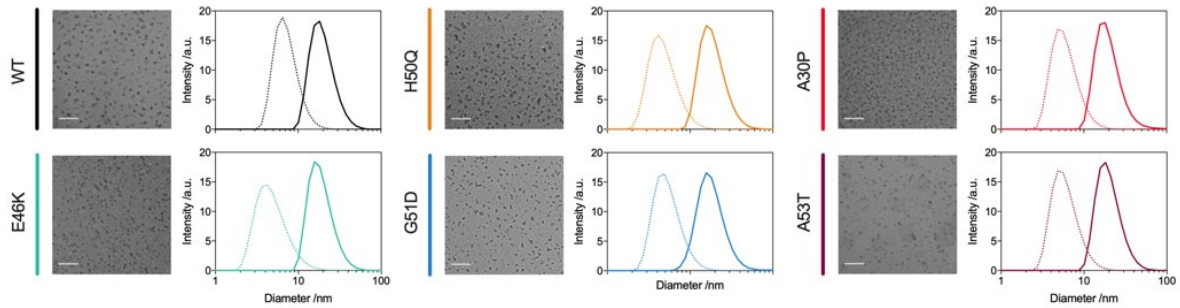

Figure 4.2: All α-synuclein variants form oligomers with similar size and morphology. TEM images of variant oligomers, confirming that relatively homogeneous oligomer populations are produced in all cases, with roughly spherical shape and 5-15 nm diameter (scale bar = 100 nm). DLS profiles of all variant oligomers (solid), are shown alongside the profiles for their corresponding monomeric species (dotted).

As all the oligomeric variants had a similar size we next investigated if they also shared a similar secondary structure. Using fourier transform infrared (FT-IR) spectroscopy, we

were able to determined that, as the WT oligomers, all the oligomers variants possessed an antiparallel β-sheet core (Figure 4.3), intermediate between the one of a fibril and a monomer. This was further confirm by far-UV circular dichroism (CD) spectroscopy (Figure 4.4). Interestingly, the analysis of far-UV CD revealed that, the structure of the G51D oligomers shifted greatly within different batches, with some of them showing standard β-sheet oligomeric properties and others showing different degrees of α-helical structure (Figure 4.4). Although the origin of this structural variability could not be experimentally determined, it was possible to establish a link between the lyophilisation process and the acquisitions of a particular secondary structure, with batches of monomeric α-synuclein lyophilised at the same time consistently showing the same secondary structure. As the FT-IR spectra remains largely unchanged between different G51D batches, indication the β-sheet structural element is largely conserved, the α-helical structure was likely to arise from regions that remain disordered in the WT and other variant oligomers.

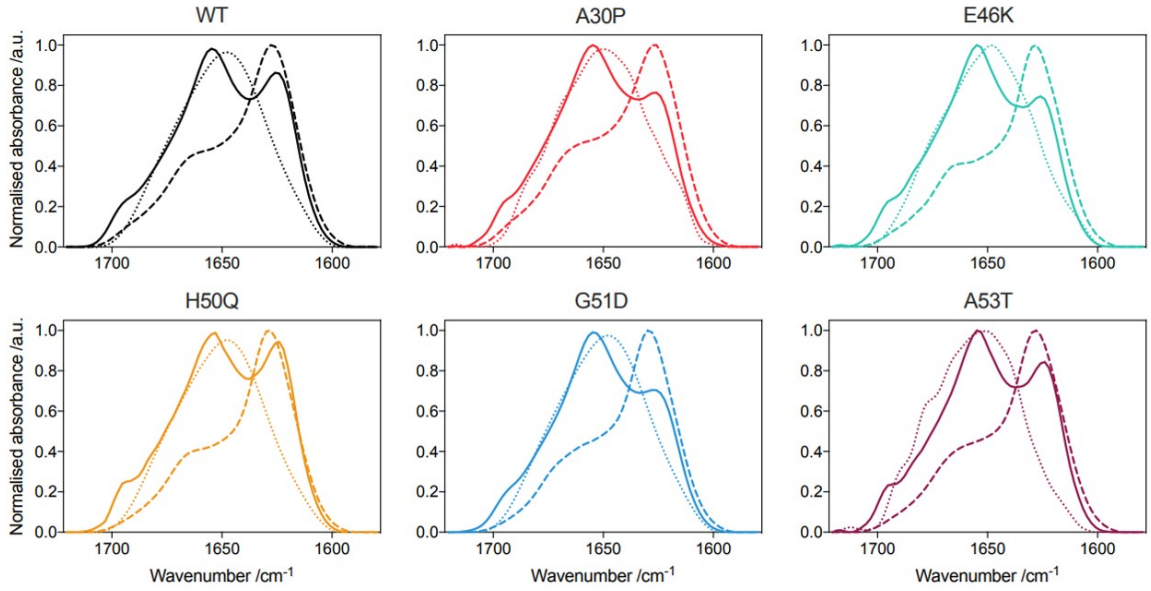

Figure 4.3: FT-IR spectra of the different variants and conformers of α-synuclein. Representative (n > 5) FT-IR spectra of all α-synuclein variants. Oligomers display β-sheet content intermediate between that of the respective monomers and fibrils and display a clear anti-parallel peak at 1695 cm^{-1}. (Solid line: oligomer; Dotted line: monomer; Dashed line: fibril).

Since the WT oligomers had been proven to cause oxidative stress, membrane disruption and cell death [34, 38, 39, 36], the next step was to explore the cellular toxicity of these oligomeric variants. It was first decided to study their effect in cell viability, with this purposed we performed the MTT assay, which monitors the MTT (3-(4,5-dimethylthiazol-2-yl)-2,5-diphenyltetrazolium bromide) reduction to formazan by

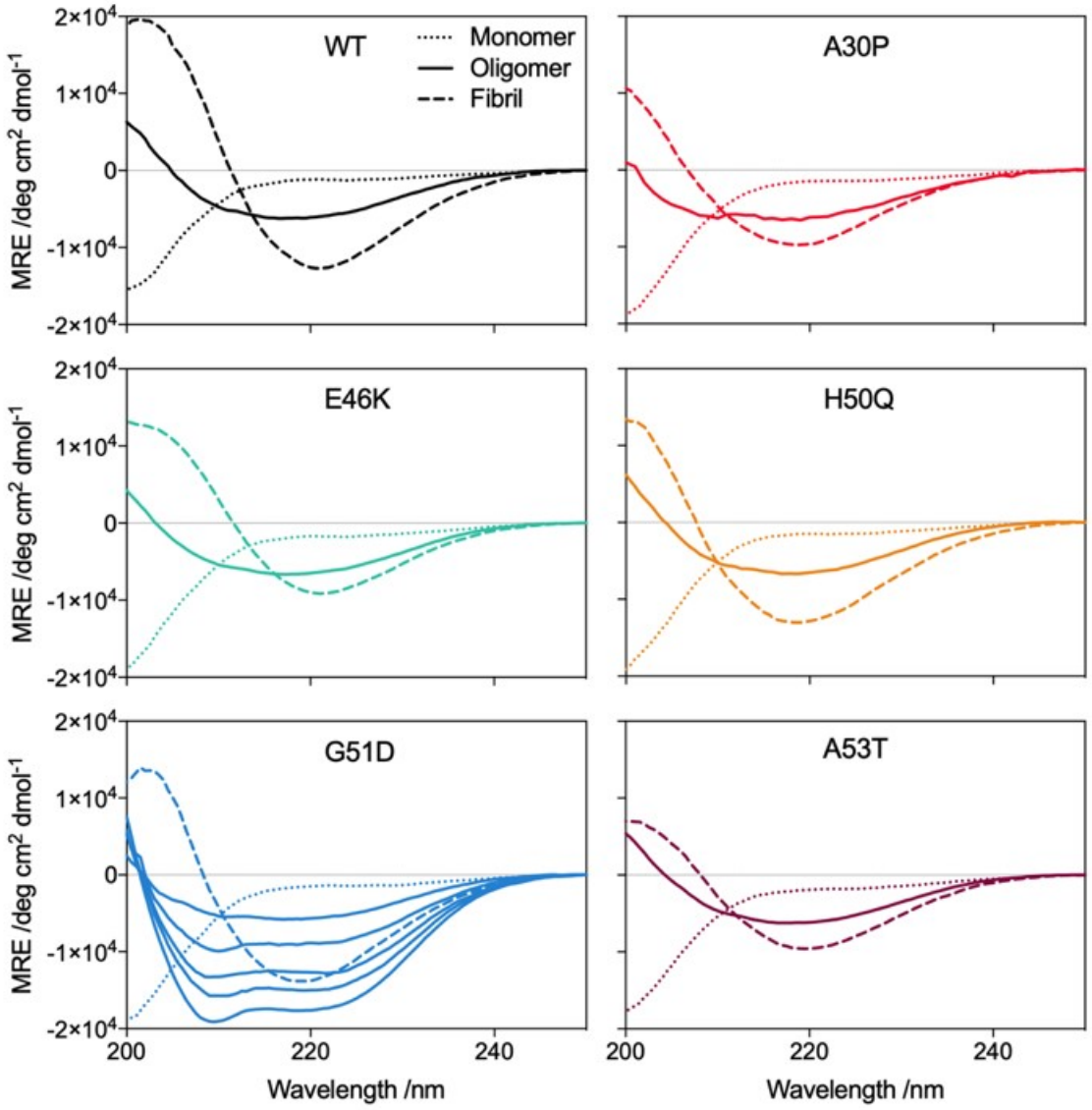

Figure 4.4: Far-UV CD spectra of the different variants and conformers of α-synuclein. All variant oligomers display β-sheet content intermediate between that of the respective monomers and fibrils. Representative (n > 5) CD spectra of variant α-synuclein species, with several different preparations of G51D oligomers shown. (Solid line: oligomer; Dotted line: monomer; Dashed line: fibril).

the NAD(P)H-dependent oxidoreductases present in the cytosol. A lower reduction of MTT can be attributed to a decrease in metabolic activity and hence to a reduction of cell viability [128]. Here SH-SY5Y were incubated cells with 0.3 μM of oligomers for 24h, after this the media was removed and replaced with a solution of 0.5 mg/mL of MTT that was allowed to be reduced for 4 hours. In agreement with previous reports the WT oligomers reduced the cell viability by 17 % $\pm$ 9 compared to the control. Surprisingly A30P, E46K, H50Q, and A53T oligomeric variants, that have apparently identical structural properties to the WT oligomers, did not show decreased levels of MTT reduction with respect to the control (Figure 4.5 a). Interestingly, although in average the G51D samples did not induce a significant reduction in cell viability, a great variability between batches of oligomers could be appreciated, with values ranging from 5 % reduction of cell viability to a 50 % reduction. In order to reduce this variability and to better determine the true toxicity of the G51D variants, more replicas of the MTT test (initaly only three different batches of each oligomeric variant were tested) were performed. For each one of these replicas a different oligomeric batch was used and 6 wells of a 96 well plate were used in each case as technical replicates. In general, at least 5 batches of every oligomeric species were tested, and this number was increased to 11 in the case of G51D. Although G51D samples continued to show the greatest variability within the oligomers variants, this strategy allowed us to determine that the G51D oligomers are in fact, able to induce a significant reduction in cell viability compared to its PBS control (Figure 4.5 b). It is important to take note here of a few considerations regarding the technical set-up of the experiments: first, due to the low concentration at which the oligomeric α-synuclein mutants are purified (form 70 μM - 1 μM), the volume of PBS added to the wells varies between experiments, secondly in order to be able to compare between samples the MTT results were normalised to untreated values and compared via an ANOVA statistical analysis to their own PBS controls. In general, it was possible to dilute all variants to the lowest concentration within the plate in order to avoid variability, but the low yield of G51D oligomers made it necessary to treat them differently and add a specific PBS controls (Figure 4.5 a and b). This change in the volume of PBS added per well can explain the higher toxicity found in the cells treated with PBS volumes equivalent to the G51D samples. Another element that could potentially influence the toxicity readout is the amount of lipopolysaccharide (LPS) present in the samples, in order to explore this possibility a solution of 1 μM of each of the variants monomeric stocks was tested. Although the levels of LPS change between stocks, the samples that register the higher levels, A30P (1.8 EU/ml) and A53T (3 EU/mL), do not correspond with the species that showed a decrease in cellular viability in the MTT test. This suggest that the MTT results are indeed independent from the LPS present in the samples (Figure 4.5 c). The

contamination of monomeric α-synuclein with LPS occurs during the purification process, hence the different levels of LPS observed in the different stocks of the α-synuclein variants could be due to the presence of higher levels of LPS during the purification process (which could be caused by differences in the number of bacteria harvested) or to different mutants of α-synuclein presenting different affinities for LPS.

In view of the differences in toxicity showed by the different oligomeric variants and since WT oligomers have been shown to be able to increase the intracellular reactive oxygen species (ROS) production levels in a consistent way [34, 38, 36], we next assessed if other oligomeric variants also shared this ability. As G51D had shown the greatest variability in the MTT test, 3 different preparations of it were included in each set of experiments. SH-SY5Y cells were treated with 0.6 μM oligomers in the presence of CellRox-Orange, a probe that becomes fluorescence in the present of ROS, after 2 hours incubation the fluorescence levels of each sample were determined. Interestingly, the ROS levels in the G51D treated cells were higher and more variable that the ones induced by any of the other α-synuclein oligomeric variants (Figure 4.6). Generally, the ROS levels are increased in the cells exposed to any of the oligomeric variants, this is especially obvious in the case of the WT (Figure 4.6), however this increment is only statistically significant in the case of G51D. This can be explained by the fact that, in order to acquire the G51D data without saturating the image, the laser setting of the microscope had to be kept at a relative low intensity, which can potentially place the ROS signal derived by cell exposure to the other oligomeric variants of α-synuclein bellow the detection threshold (Figure 4.6 b).

Since high surface hydrophobicity has been reported to be a predictor for oligomer toxicity [64, 129, 130] (an elevated number of hydrophobic residues exposed to the solvent could increase oligomers' affinity for lipid membranes facilitating membrane disruption [123, 64, 131, 132]) we investigated if changes in the hydrophobicity of the kinetically trapped α-synuclein oligomeric variants could explain the differences observed in cellular toxicity. Using 8-anilino-naphthalene sulphate (ANS), a dye whose fluorescence emission is enhanced upon binding to hydrophobic regions, we determined that A30P, E46K, H50Q and A53T oligomers showed similar amounts of solvent-accessible hydrophobic residues as the WT oligomers (Figure 4.7 a). However, the oligomers generated by the G51D variant, independently of their secondary structure content, exhibited a significantly lower ANS fluorescence, which is indicative of a reduced hydrophobic surface with respect to the WT oligomers (Figure 4.7 b). Thus, according to this model, and in line with previous reports showing that G51D oligomers induced less membrane disruption than other PD variants [133], G51D kinetically trapped oligomers should induce less cellular toxicity than other

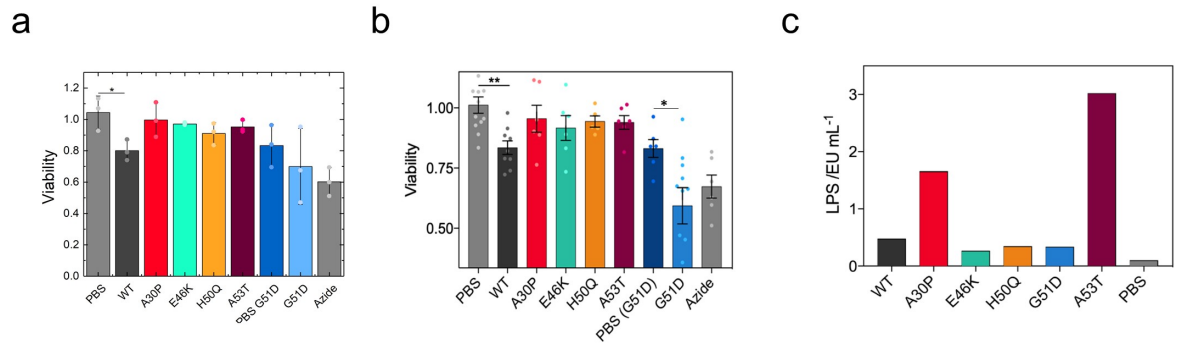

Figure 4.5: Cellular toxicity of the different oligomeric α-synuclein variants. (a) toxicity tested with MTT assay on SH-SY5Y cells of 3 preparations of each oligomer variant, with error bars shown for standard error and data for all individual replicates overlaid as points. (b) toxicity tested with MTT assay on SH-SY5Y cells of (n $\geq$ 5) preparations of each oligomer variants, with error bars shown for standard error and data for all individual replicates overlaid as points. (c) Quantification of LPS content in 1 μM monomer stocks of each variant, with PBS shown for comparison. Statistical analysis was run using one-way ANOVA (all variants except for G51D) or Student's t-test (G51D only) *($p < 0.05$) **($p < 0.001$).

variants. However, our MTT and ROS results point out towards another conclusion, being that the G51D oligomers are the most toxic within the variants, therefore, it is clear that other variables, apart of size and hydrophobicity, need to be considered in order to explain the toxic properties of the α-synuclein variants [123].

As the variability of the G51D readouts in both tests was significantly higher than for any of the other variants and the G51D preparations are the ones that show more structural diversity between them, the possibility that structural changes between G51D batches could be affecting its ability to induce cellular toxicity was next investigated. In order to explores this hypothesis we deconvoluted the far-UV CD spectra of the different variants and estimated the relative secondary structures of the different preparations of all the oligomers variants [134, 135]. Even though the fits obtained reproduced our experimental data with extremely low residuals, indicating that this is a robust method for comparatively analysing our spectra (Figure 4.8 a), the deconvolution analysis identified an 11 % of α-helical content in the WT oligomers, which was not observed in the solid state NMR structural data reported previously [36]. This suggest that the α-helical percentage reported here should only be used as a relative quantification between oligomer samples, but not as an absolute one. Since, as previously confirmed by FT-IR, G51D batches only differ structurally between them in α-helical content, the possibility of the relative amount of α-helical content present in each sample correlating with its cellular

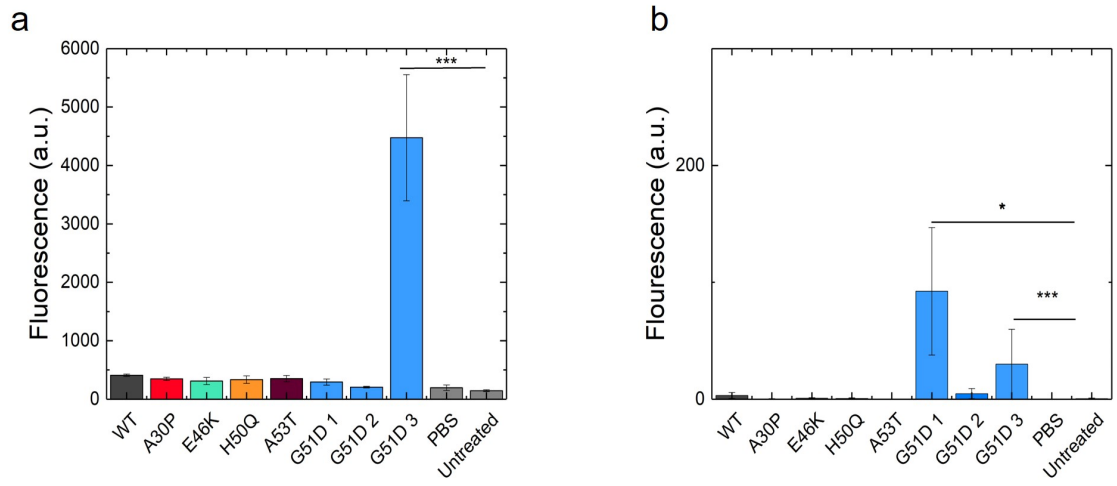

Figure 4.6: Intracellular ROS levels induce by different oligomeric α-synuclein variants. Example of two different experimental replicas (a) and (b) performed with different preparations of α-synuclein oligomers. SH-SH5Y were exposed to 0.6 μM oligomers variant and ROS levels were measure after 2 h using CellRox-Orange. Statistical analysis was run using one-way ANOVA (all variants except for G51D) or Student's t-test (G51D only) *($p < 0.05$) **($p < 0.001$).

toxicity was explored. In order to avoid the variability in toxicity associated with the differences in sample volumes, the relative value of MTT reduction was normalised here to its corresponding PBS controls instead of to untreated. Indeed, a clear correlation between increased α-helical content and decreased MTT values (Figure 4.8 b) was found. However, no correlation was observed between cell toxicity and β-sheet or random coil structures, suggesting that the effect on cellular dysfunction can be solely attributed to the α-helical content (Figure 4.8 c). This in agreement with previous reports that showed, using stabilised oligomers from several proteins, that the amount β-sheet content present in the sample did not correlate with cellular toxicity [136].

4.3 Discussion

In conclusion, our results suggest that together with size and hydrophobicity, the amount of α-helical content can be a determinant of the toxicity of diverse oligomeric structures. Indeed, α-synuclein acquires an α-helical structure upon binding lipids, which it is believed to be the first step towards triggering cell toxicity mediated by membrane disruption [36, 133]. Detailed work on the WT oligomers generated through this protocol has identified the mechanistic features by which α-synuclein oligomers induced membrane disruption: first the disordered N-terminal regions of the oligomers binds to the cellular membrane adopting an α-helical structure and acting as an anchor and allowing the β-

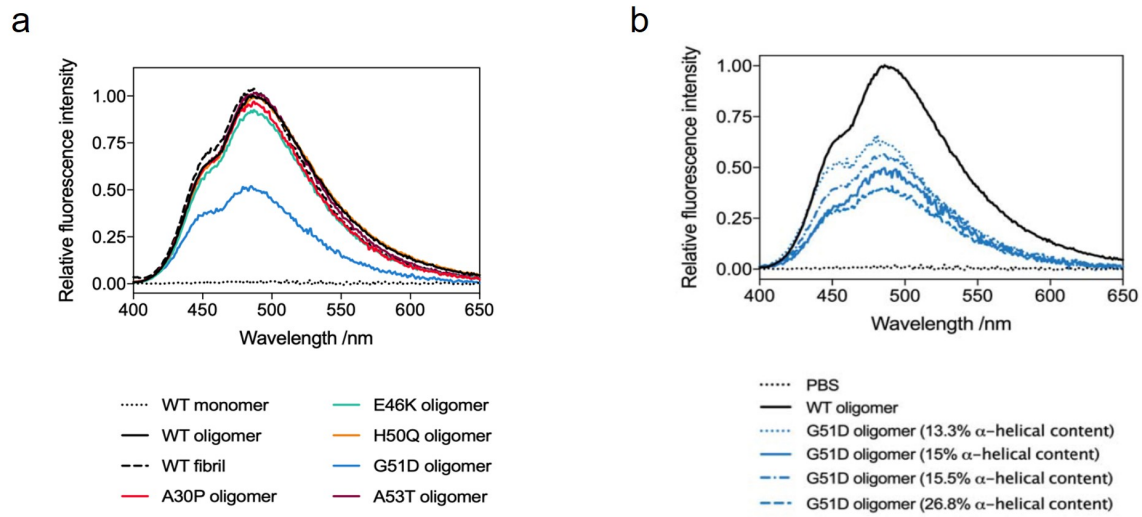

Figure 4.7: Hydrophobicity of the different oligomeric α-synuclein variants. (a) Representative ANS emission spectra of variant oligomers (n $\geq$ 3) (b) The surface hydrophobicity of G51D oligomers is markedly decreased compared to that of the WT oligomers, despite differences in α-helical content of the G51D oligomers.

sheet hydrophobic core to get closer to the membrane and insert itself into the interior of the lipid bilayer [36]. Furthermore, the impairment of the N-terminal binding to the membrane has been reported to abolish the oligomers associated toxicity [37, 36]. In our study, despite the lower hydrophobic nature of the G51D oligomers, we observe an enhanced cellular toxicity correlating with an increase in the content of α-helical structural. This may suggest that the existence of pre-formed α-helical structure in the G51D oligomers facilitates the anchoring to the plasma membrane, allowing a more efficient insertion of the hydrophobic core into the lipid bilayer, which in turn would induce membrane disruption and cellular dysfunction. One possible hypothesis to explain the higher propensity of G51D to form an α-helical structure is the introduction of a negative charge near the fourth imperfect KTKEGV repeat which could extend its length and, in turn, shortened the hydrophobic region between the fourth and fifth KTKEGV repeats. This increases the homogeneity in length of the hydrophobic motives and the periodicity of the KTKEGV repeats which could facilitate the acquisition of an α-helical configuration.

Although the intermediate content of β-sheet between a monomer and a fibril is one of the main structural characteristics of amyloid oligomers, it has recently been shown that the percentage of β-sheet structure present in the oligomers does not correlate with their toxicity; therefore, investigations of other factors that can dictate toxicity are necessary [136]. Interestingly, α-helical structure has previously been detected in the aggregation

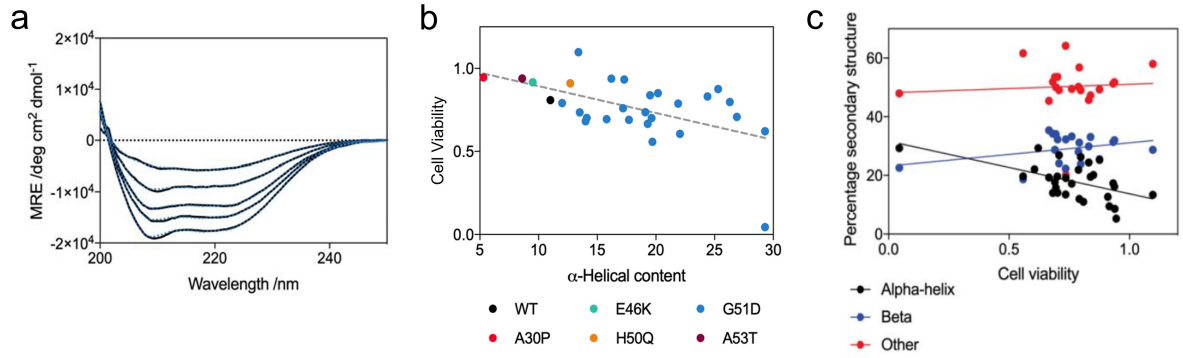

Figure 4.8: Relationship between the secondary structure of α-synuclein oligomeric variants and cellular toxicity. (a) Far-UV CD spectra of G51D oligomers displaying different degrees of α-helical structure (black solid), shown alongside the fitted spectra (blue dotted) (b) MTT reduction as a function of α-helical content of oligomers as estimated by far-UV CD spectra deconvolution. The data correlation (linear relationship visualized as a grey dashed line) obtained was: (fraction viability) = -0.016 * (percentage α-helical content) + 1.06, with an R^2 value of 0.29 and p value of 0.0026. (c) Liner fitting of the toxicity data versus the β-sheet and random coil content. However, the only fit with a statistically significant deviation from null correlation was α-helical content (0.0026), with values of 0.14 and 0.77 for β-sheet and random coil content, respectively.

cascade of several α-synuclein variants [137, 138]. Moreover, α-helical intermediates have been observed in multiple systems such as IAPP (islet amyloid precursor protein), the Aβ amyloid peptide associated with Alzheimer's disease, and the PSM3α peptide; together this suggests that the presence of α-helix configuration within amyloid structures may have broader implications [139, 140, 141, 142, 143, 144, 145]. In addiction an α-helical conformation of the PrP monomer have been shown to induce higher toxicity *in vitro* and *in vivo* than other configurations of PrP [146]. Furthermore, structural polymorphs of amyloid fibrils derived from the PSM3α peptide, implicated in Staphylococcus aureus pathogenicity, have previously been found to induce several degrees of cellular toxicity, with the α-helical form showing a higher toxicity towards eukaryotic cells [140, 127]. Moreover, studies on the PSM3α peptide showed that this increase toxicity shown by the α-helical variant may be mediated by interactions with lipid membranes, supporting our suggestion that the α-helical content within α-synuclein oligomers promotes toxicity by facilitating membrane insertion [141]. The observation of such effects in two unrelated systems implies that α-helical content may be a key determinant in a range of systems that exert their toxicity via interactions of oligomeric protein species with membranes.

Together with our results, this suggest that along with the size and hydrophobicity, the α-helical content may be a determinant of the oligomeric toxicity. In order to confirm

this hypothesis, more studies with amyloid conformers from different proteins containing varying degrees of α-helical content are needed. Such studies will allow the determination of the threshold of helical content that can modulate the toxicity predicted by models that take into account size and hydrophobicity [123] and further our knowledge about amyloid toxicity. One of the key factors that would determine the success of these studies is the ability to accurately deconvolute the CD spectra of different amyloid aggregates. In the present study the deconvolution software BESTSEL was used for this purpose, this software allowed the fitting of the different spectra (that range form β-sheet in shape to α-helical) with low residuals (Figure 4.8) and the estimation of the percentage of α-helical, β-sheet and random coil content of the different oligomeric variants. However, the deconvolution of the spectra cannot precisely determine the secondary structure of these aggregates [135, 134]. Because of this, it would be beneficial to incorporate the use of other markers of α-helical content, like the absorbance value at 208 nm or the ratio between the absorbance at 220 nm and at 208 nm [135], to further support this correlation between the degree of α-helical content and cellular toxicity in future studies.

Even though all the α-synuclein variants used in this chapter are related to early onset forms of PD, only the oligomers produced from the WT and G51D variants were able to significantly reduce cellular viability as shown in Figure (4.5). However this does not necessarily imply a lack of toxicity of on-pathway oligomeric species derived from A53T, E46K, H50Q and A30P α-synuclein variants. Although the WT α-synuclein kinetically trapped oligomers used in this study are considered to be structurally close to WT α-synuclein on-pathway form [34], this has yet to be proven for the rest of the α-synuclein variants. Moreover, the increased toxicity of the pathological mutations of α-synuclein may not be related to the structure of the oligomeric intermediaries. An increment in the number of these species during the aggregation process or a higher propensity to generate off-pathway oligomers during this process may also explain the higher toxicity attributed to these α-synuclein variants [124]. Furthermore, a recent study has detected the release of oligomers from WT α-synuclein fibrils upon its interaction with the cellular membrane [116]. A different propensity of different fibrillar variants of α-synuclein to realease oligomers could also affect the capability of this PD-associated forms of α-synuclein to induce cellular toxicity. In conclusion, the origin of oligomeric toxicity is sill poorly understood and more studies with both off-pathway and on-pathway species are necessary in order to fully elucidate its source.

Chapter 5

Assessing the seeding capabilities of different α-synuclein fibrillar conformers

This work was developed during a visit (September 2019 - December 2019) to the lab of Dr. Nunilo Cremades in Zaragoza, Spain. Although this study was based in previous results of José Camino, the protein and the different conformers of α-synuclein used in this project were produced by Marta Castellana Cruz.

5.1 Introduction

The secondary structure polymorphism within fibrils, at the end point of the aggregation process, has extensively been studied in the context of fibrillar polymorphs, or strains, and toxicity [56, 147, 148, 42, 55]. Different neurodegenerative diseases caused by the aggregation of α-synuclein have been shown to be related to slightly different fibrillar polymorphs [58] (Figure 5.1). Moreover the injection of different α-synuclein strains into mouse brains have been shown to produce different phenotypes [56]. In light of this, it is important to study the effects that different α-synuclein polymorphs may have upon cellular toxicity. Moreover fibrils encounter in the brain of Parkinson's disease (PD) patients have been proven to be different to the ones generated *in vitro* [59], since fibrillar polymorphism modulates cellular toxicity [42, 58] it is specially relevant to develop the ability of generating new α-synuclein polymorphs that could potentially be structurally closer to those generated *in vivo*.

José Camino, a PhD student in the Cremades lab has been working on characterising

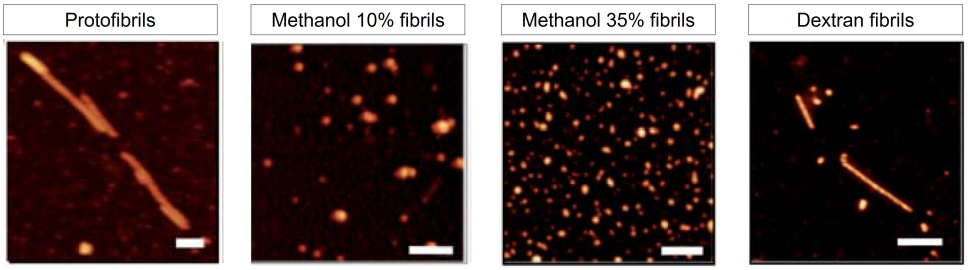

Figure 5.1: AFM images of the different polymorphs of α-synuclein fibrils used in this study. Scale bar corresponds to 200 nm. Figure adapted from [19]

a number of different α-synuclein polymorphs [19]. These different polymorphs (Table 5.1) have been produced in the presence of crowding agents such as dextran and polyethylene glycol (PEG) or in the presence of alcohols, such as methanol, under minimal shaking conditions. Most of the aggregates display a parallel β-sheet core, characteristic of amyloid fibrils but morphologically, they are more globular species closer in size to kinetically trapped oligomers. Through the incubation of α-synuclein in highly dehydrating conditions (i.e. the addition of 35 % methanol) it was possible to obtain antiparallel fibrils of α-synuclein, however these structures are not stable in more physiologically relevant buffers like PBS. Antiparallel intermolecular β-sheet structure is normally found in the kinetically trapped toxic oligomers but amyloid fibrils are always parallel in nature. This raises the question of if on-pathway oligomers will be parallel or anti-parallel in nature, as all the amyloid fibrils characterised have a parallel β-sheet structure the existence of anti-parallel on-pathway oligomers will imply a significant reorganisation of the β-sheet core before being able to progress into mature fibrils. Because of this, on-pathway anti-parallel oligomers are improbable to exist in nature. As the kinetically trapped oligomers used to model and study the structural and toxic properties of on-pathway oligomers are antiparallel in nature, it is necessary to determine if possessing an anti-parallel β-sheet core influences the cellular toxicity of these species. Since the isolation of on-pathway oligomers is extremely difficult, the possibility of producing antiparallel fibrils would allow us to further study the relationship between secondary structure and toxicity and to determine if intermolecular β-sheet arrangement plays a role in it.

Given that toxicity has generally been linked with antiparallel oligomeric species and to a lesser extent, parallel β-sheet fibrils, the array of polymorphs that can be generated allows us to compare different structural attributes in relationship with cellular toxicity, internalisation rate and seeding ability.

Aggregation conditions	β-sheet core	Morphology	Size (nm)		
			Heigh	Width	Length
300 mg/ml PEG 8000	Parallel	Globular	36 ± 0.4	70 ± 7	70 ± 7
300 mg/ml Dextran 70000	Parallel	Fibrillar	4.4 ± 0.7	59 ± 9	280 ± 5
		Globular	10 ± 2	80 ± 6	80 ± 6
10% Methanol	Parallel	Globular	8 ± 2	82 ± 3	82 ± 3
35% Methanol	Anti-parallel	Globular	4.8 ± 0.7	29 ± 5	29 ± 5
Stabilised oligomers	Anti-parallel	Globular	5.5 ± 0.5	54 ± 10	54 ± 10
F1 fibrils	Parallel	Fibrillar	13 ± 1	50 ± 10	1200 ± 600

Table 5.1: Structural and morphological characteristics of the different fibrillar α-synuclein aggregates.

5.2 Results

The alternative parallel fibrillar synculein polymorphs were generated by incubating 100 μM of human monomeric α-synuclein in PBS in the presence of the 300 mg/ml dextran or PEG or 10 % methanol at 37 °C in a 96 well plate for seven days. Initially, since the aggregation kinetics were acquired in a plate reader without shacking, this process was performed in a static 37 °C incubator. However this strategy proved unsuccessful as the aggregation yield after seven days was between 0 and 2 %, it was hypothesised that some minimal shaking (as the one produced by the plate reading process itself) was indeed necessary. Subsequent tries in which the plate was incubating inside the plate reader with or without it performing a read every 10 minutes confirmed this hypothesis. From this point onwards these aggregates were produced inside a plate reader programmed to read a single well every 10 minutes. Antiparallel fibrils were generated by incubating 100 μM of human monomeric α-synuclein in PBS in the presence 35 % methanol at 37 °C in an static incubator. Protofibrils were produced by the aggregation of 100 μM human α-synuclein in the presence of DMPS vesicles as describe in [27]. Finally F1 generation fibrils were generated as described in chapter 1.

Since protofibrils have been shown to be formed in the presence of lipid vesicles, to which they remain attached, it was necessary to isolate them before testing their effect on cells. With this objective in mind, protofibrils were incubated for 1.5 h at 37 °C

with 1 % sarkosyl in 20 mM sodium phosphate buffer, pH 6.5, afterwards the sample was ultracentrifugated at 20 °C, 120000 rpm for 1.5 h before resuspending it in PBS. In order to remove the lipids and detergent mixture completely this process was repeated three times. The parallel conformers produced in the presence of dextran, PEG or 10 % methanol were subjected to the same process in order to wash away any residual monomer from solution. As the antiparallel conformers are not stable in PBS (Figure 5.2), the 35 % methanol fibrils and a sample of F1 fibrils, as a control, were cross-linked by incubating with 0.25 % glutaraldehyde for two minutes at 37 °C. The excess of glutaraldehyde was washed away by centrifuging the samples at maximum speed for 10 minutes at room temperature. The concentration of all the conformers was determined by an aliquot with 4M GmdCl to solubilise the aggregates and measuring the absorbance at 275 nm.

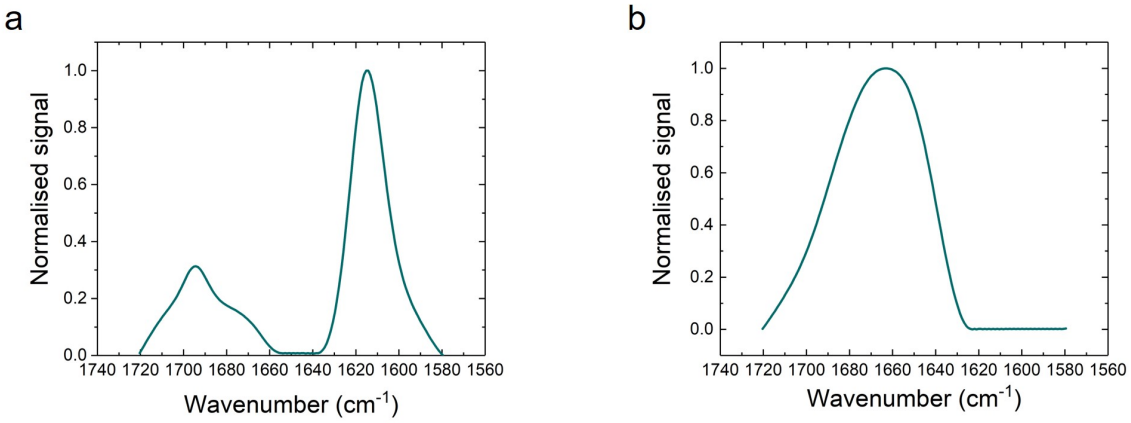

Figure 5.2: Fibrils made in the presence of 35% methanol (a) revert to a mostly monomeric conformation after incubation in PBS for 2 h (b). Representative FT-IR spectra are shown.

Since different polymorphs of fibrils have been shown to be related with different synucleinopathies the different fibrillar generated here were tested for their ability to seed α-synuclein inclusions. As the SH-SY5Y do not express endogenous α-synuclein, we used mouse hippocampal primary neurons, a more advanced model for PD, in this study. Since the objective of this study was to compare the toxicity of conformers of different size and morphology, only the F1 fibrils and the protofibrils were sonicated before applying them to the cells according to established protocols [101, 100] in order to allow their internalisation. As the rest of the α-synuclein conformers generated here (Table 5.1) are similar in size to sonicated fibrils (120nm, as established in chapter 3) no sonication step was applied to these conformers. Primary neurons were incubated with 0.3 μM of each conformer, and after 5 days the amount of aggregated α-synuclein was determined by the presence of S129-phosphorylated α-synuclein (Figure 5.3). α-Synuclein

inclusions have been reported to be widely phosphorylated at serine 129 [104], because of that S129-phosphorylation of α-synuclein has been extensively used as a maker for α-synuclein aggregation both *in vivo* and *in vitro*. Surprisingly, the protofibrils were able induce the aggregation of endogenous α-synuclein in a more efficient way than the F1 fibrils (Figure 5.3). Neither the fibrils produced in the presence of dextran nor PEG were able to induce the formation of α-synuclein inclusions, while the ones produced in the presence of 10 % methanol induced only low levels of aggregation (Figure 5.3). Neither set of cross-linked fibrils were able to seed endogenous α-synuclein, but as the standard F1 fibrils were seeding competent (Figure 5.4), this is possibly caused by the cross-linking itself. As most of the amines available to react with glutaraldehyde in α-synuclein are in the N-terminal region, which has been shown to mediate the anchoring of oligomers and monomers to the lipid membrane [36, 149], it is possible that the cross-linking with glutaraldehyde inhibits the internalisation of the conformers by impeding the N-terminal region from forming an α-helical structure.

As the ability to seed endogenous α-synuclein is directly related to the internalisation rate of these conformers, the ability of mouse hippocampal neurons were indeed to internalised these α-synuclein species at similar rates was assessed. In order to do this, we labelled a cysteine mutant of human α-synuclein N122C, chosen because the C-terminal localisation of the cysteine makes it less probable to the dye to interfere with the aggregation process, with alexa-488 and produced the different parallel aggregates as previously described. After 1 h incubation with 0.3 μM of each of the conformers the neurons were fixed and the membrane labelled with wheat germ agglutinin (WGA)-Alexa 647. Although, in agreement with previous reports [30, 102], a partial internalisation could be detected in the case of the F1 fibrils, protofibrils and monomer (Figure 5.5), the imaging of the aggregates produced with 10 % methanol, dextran and PEG revealed the presence of large clumps of protein (Figure 5.5). These clumps of protein are most likely formed during the ultracentrifugation process and since the majority of the sample protein is sequestered in them, they may be responsible for the poor seeding of these aggregates (Figure 5.3).

In order to address this issue the clumped samples were subjected to a gentle sonication before applying them to the neurons. After this, the internalisation and seeding experiments were repeated. No clumps of protein could be detected during the internalisation experiments and indeed, a partial internalisation of the aggregates was detected in all the cases (Figure 5.6). In agreement with the internalisation results, the aggregates formed in the presence of PEG were able to seed the aggregation of endogenous α-synuclein. Interestingly, the aggregates formed in the presence of 10 % methanol were

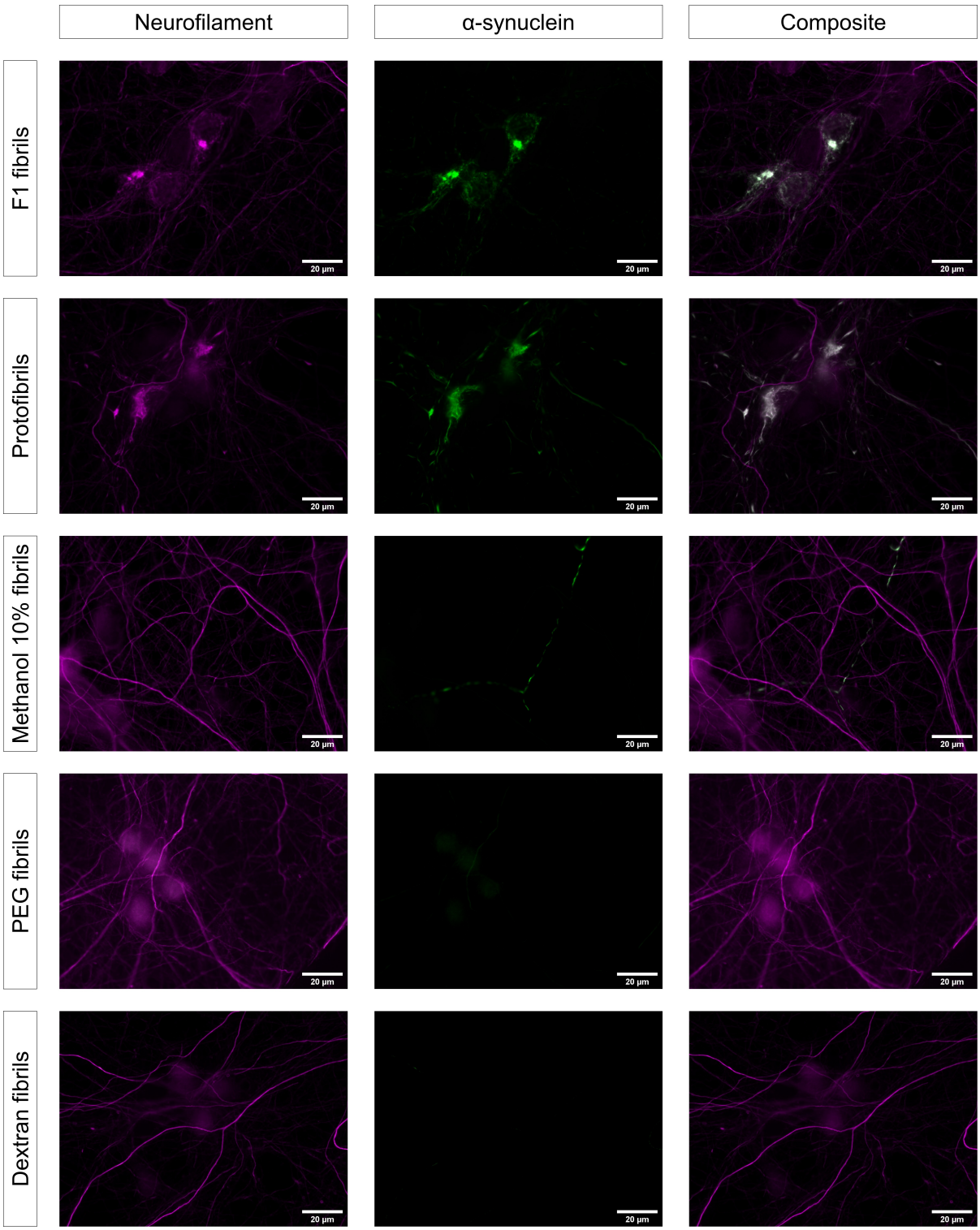

Figure 5.3: Seeding of α-synuclein aggregation in mouse primary neurons (I). Mouse hippocampal neurons were incubated with 0.3 μM α-synuclein aggregates. They were stained with p-129-α-syn (green) and neurofilament (magenta). Representative images of one set of experiments are shown, at least 5 images of 3 different coversilps treated with the same preparation of α-synuclein fibrillar variants were taken). Due to clumping issues (Figure 5.5), only the experiments using protofibrils and F1 fibrils were repeated twice using different neuronal cultures and fibrillar preparations.

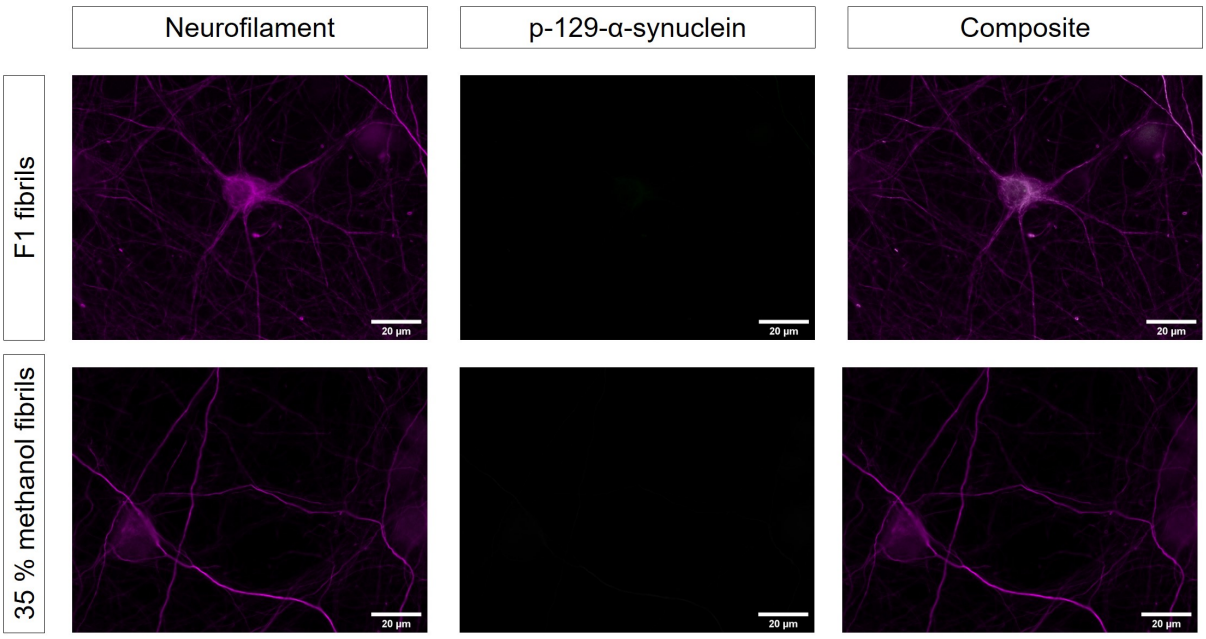

Figure 5.4: Seeding of α-synuclein aggregation in mouse primary neurons (II). Mouse hippocampal neurons were incubated with 0.3 μM cross-linked α-synuclein aggregates. They were stained with p-129-α-syn (green) and neurofilament (magenta). Representative images of 1 out of 2 sets of experiments (at least 5 images of 3 different coversilps were taken) are shown. Different preparations α-synuclein fibrillar aggregates were used in each experiment.

still able to induce just a fraction of the aggregation induced by F1 fibrils (Figure 5.7, Figure 5.3), this may indicated that these aggregated are seeding deficient or that they are only able to grow up to certain length (this is generally true for all amyloid fibrils, although usually mature amyloid fibrils can reach a length of microns). Due to a lack of protein, the seeding experiments with the aggregates produced in the presence of dextran could not be repeated. Although these results are very promising, further follow up is needed to obtain repeats of these experiments, as well as the experiments with the dextran produced aggregates, to confirm our findings.

5.3 Discussion

In conclusion, these preliminary results suggest that the different conformers of α-synuclein, previously characterised by José Camino, are able to seed the aggregation of endogenous α-synuclein in mouse primary neurons with different efficiencies. These results further support the theory that different α-synuclein polymorphs, or strains, are able to induce different synucleinopathies. While conformers produced in the presence of 10 % methanol, a type of globular fibrils with a similar size to stabilised oligomers, were barely

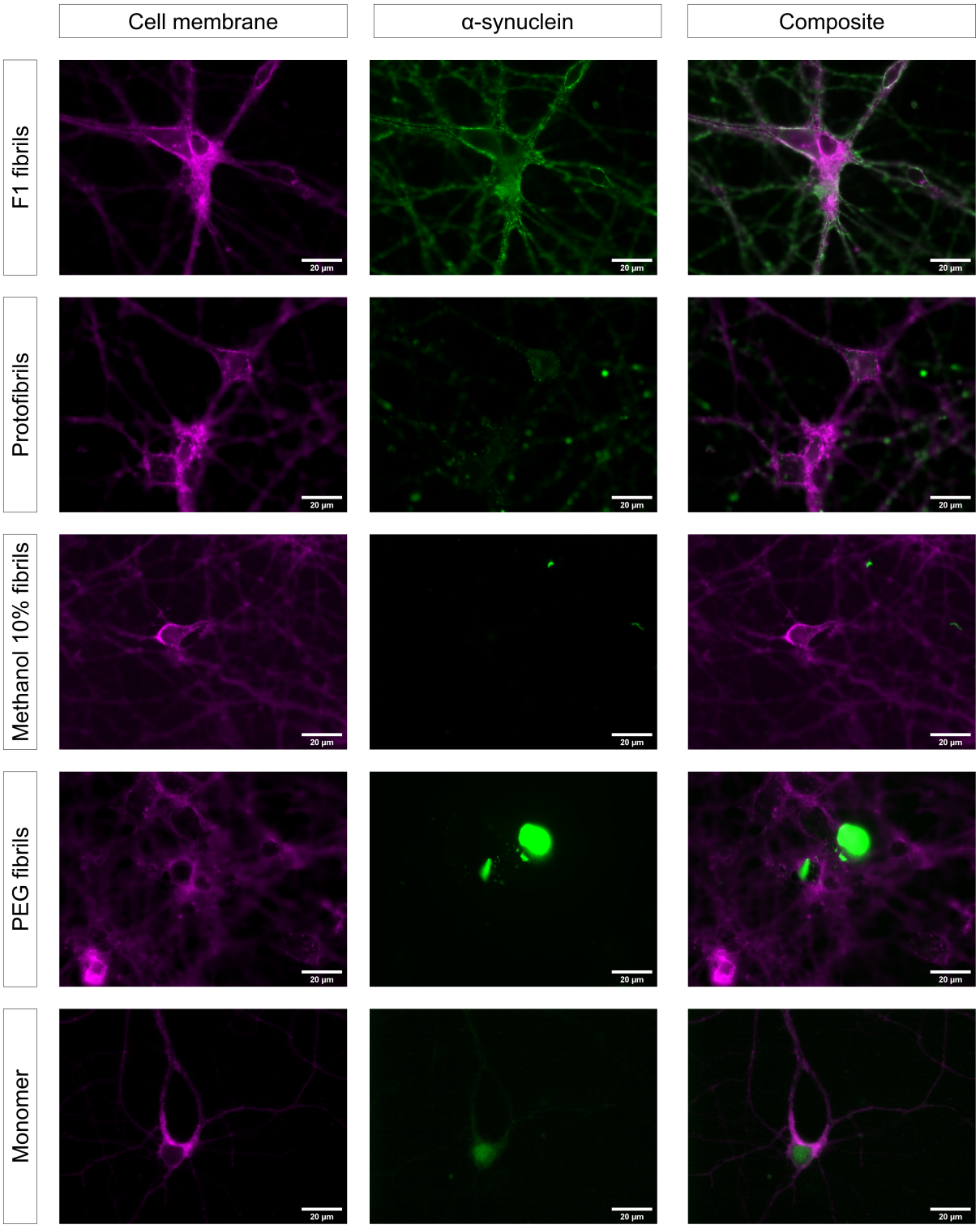

Figure 5.5: Internalisation of different α-synuclein aggregates (I). Mouse hippocampal neurons were incubated with 0.3 μM Alexa-488 labelled α-synuclein conformers for 1 hour. The cellular membrane was stained with WGA-647 (magenta). All the species were produced using Alexa-488 labelled α-synuclein. Representative images of an n=1 preparation of α-synuclein fibrillar aggregates (at least 5 images of 3 different coversilps were taken) are shown. This experiment was not repeated.

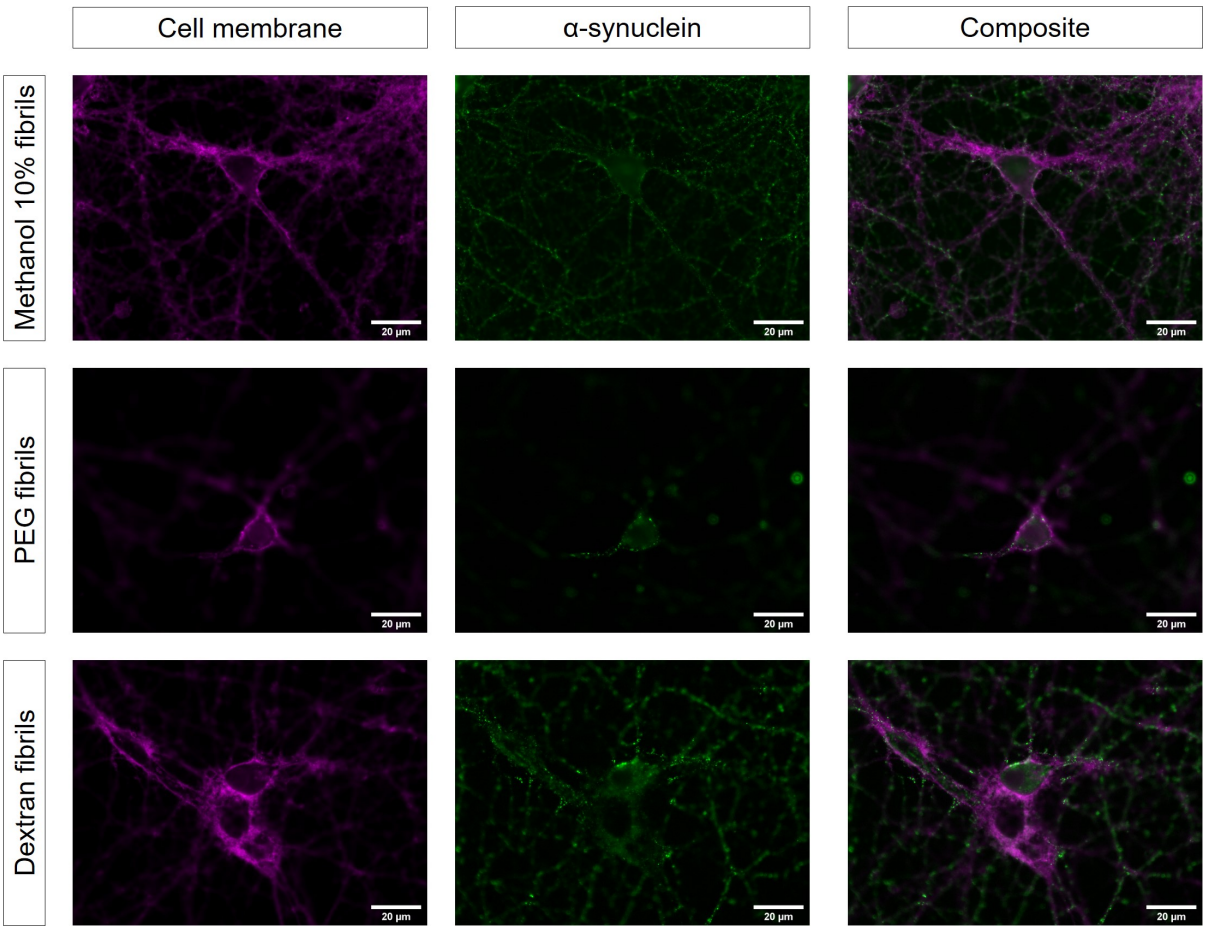

Figure 5.6: Internalisation of different α-synuclein aggregates (II). Mouse hippocampal neurons were incubated with 0.3 μM Alexa-488 labelled sonicated α-synuclein conformers for 1 hour. The cellular membrane was stained with WGA-647 (magenta). Representative images of an n=1 preparation of α-synuclein fibrillar aggregates (at least 5 images of 3 different coversilps were taken) are shown. Due to time constrains this experiment could only be performed once.

able to induce the formation of inclusions, protofibrils were able to trigger this process in a more efficient way than mature F1 fibrils. It is possible that longer incubation times would significantly increase the aggregation seeded by the 10 % methanol fibrils. As any residual clumping of the samples or fragmentation of the original α-synuclein aggregates could potentially affect the seeding properties of these conformers the sonication precess needs to be further optimised. As the objective of this project was to compare the toxicity profiles of α-synuclein aggregates with different morphologies, it is important to evaluate, by atomic force microscopy (AFM) or transmitted electron microscopy (TEM), how the sonication process affects their original conformation and selects those settings that allow for minimal clumping of the sample and minimal disruption of the original morphology.

In addition to the ability to seed, other toxicity readouts must be explored. α-

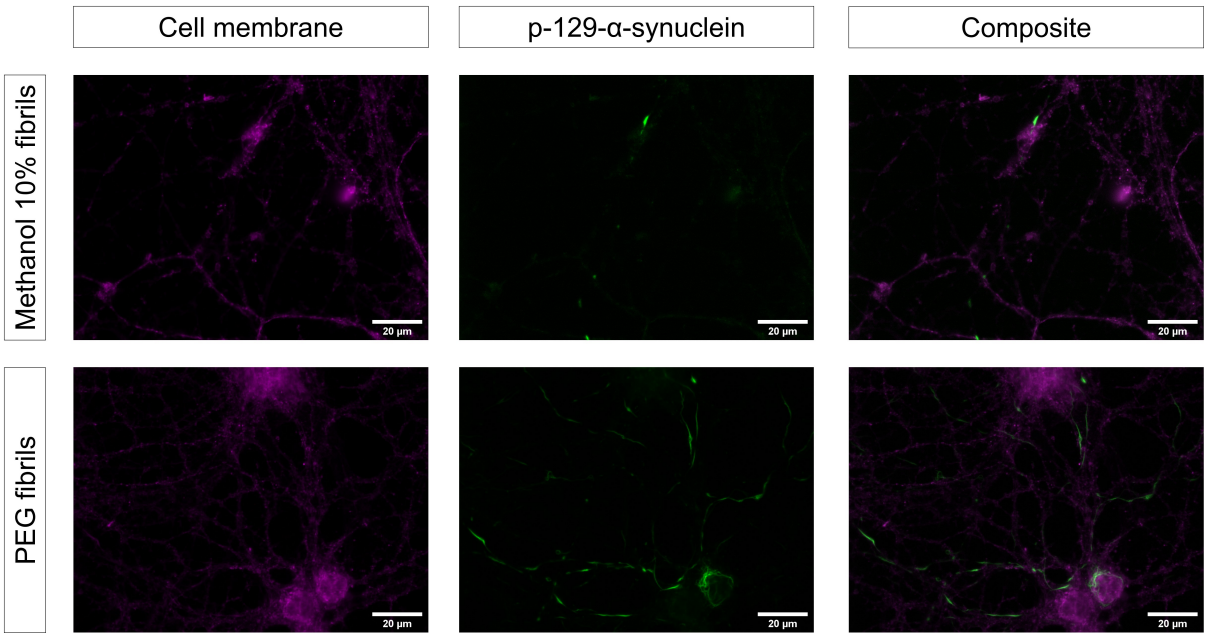

Figure 5.7: Seeding of α-synuclein aggregation in mouse primary neurons after sonication. Mouse hippocampal neurons were incubated with 0.3 μM of sonicated fibrils made with 10% methanol (a) or sonicated fibrils made in the presence of PEG (b) for 5 days. They were stained with p-129-α-syn (green) and WGA-647 (magenta). Representative images of an n=1 preparation of α-synuclein fibrillar aggregates (at least 5 images of 3 different coverslips were taken) are shown.Due to time constrains this experiment could only be performed once.

Synuclein fibrils have shown to mildly elevate the intracellular reactive oxygen species (ROS) production [34], to induce the disruption of the cellular membrane [36, 38] allowing an influx of calcium into the cytoplasm and to induce neuronal death dependent of parthanatos [150]. Since the smaller size of these aggregates may facilitate their binding to the membrane and consequently the internalisation as well as the binding to other membrane receptors like the sodium-potassium ATPase special attention to these alternative toxicity readouts must be paid. Moreover, a recent study [116] identified oligomers released from α-synuclein fibrils upon binding with the membrane as the species responsible from cellular toxicity induced by fibrils. If these polymorphs of fibrillar α-synuclein were to present different rates of oligomeric release or were not be affected by this phenomena, their ability to induce cellular toxicity could be affected, and in consequence a differential pattern of cellular toxicity could emerge.

Hopefully the study of the process by which these α-synuclein fibrillar aggregates interact with the neurons, are internalised, recruit endogenous α-synuclein monomers and induce cellular toxicity will advance the current understanding of how small differences in the fibrils structure, which create different fibrillar strains, modulates the origin and

spreading of different synucleinopathies.

Furthermore, the assessment of the ability of antiparallel fibrils to disrupt the cellular membrane will advance our knowledge of the possible differences between the toxicity triggered by the kinetically trapped oligomers used in chapter 3 and on-pathway oligomers. The determination of which percentage, if any, of the toxicity associated with kinetically trapped oligomers comes from the fact that they possess an antiparallel core, will help to further validate the use of the kinetically trapped oligomers to model the effects of the on-pathway ones, which are probably parallel in nature. As on-pathway oligomers are transient species present in the aggregation reaction at low concentrations, and hence difficult to isolate and study by traditionally techniques, the study of these anti parallel fibrils in comparison between the parallel fibrils may help to highlight any possible relevant difference between off-pathway and on-pathway oligomers. However, the instability of the antiparallel fibrils makes it necessary to cross-link these samples in order to study their effects in a physiological context. Most probably due to its mechanism of action, the cross-linking with glutaraldehyde, that suppressed ability of α-synuclein fibrillar aggregates to recruit monomeric α-synuclein, has proven to be unsuitable for this purpose. Alternative methods that could be explored are cross-linking via PICUP (Photo-Induced Cross-Linking of Unmodified Proteins) [151] or the introduction of cysteine residues in the α-synuclein amino acid sequence in order to direct the cross-linking via formation of malemide bonds.

Chapter 6

Effects of amyloid fibrils on the MTT test

This work has been done in collaboration with Katarina Pisani and Dr. Janet Kumita. Katarina Pisani purified the $A\beta_{40}$ monomer and generated the different conformers used in this chapter. Dr Janet Kumita prepared the fibrillar species of lysozyme.

6.1 Introduction

The 2-(4,5-dimethyl-2-thiazolyl)-3,5-diphenyl-2H-tetrazolium bromide (MTT) (Figure 6.1) assay is a wildly used test to measure the cellular metabolic rate and cellular viability. In its oxidised state MTT is positively charged which it has been hypothesised to facilitate its cellular uptake via the membrane potential [128]. Once inside the cytosol, MTT is reduced mainly by NAD(P)H-dependent oxidoreductases and dehydrogenases and partially (∼10 %) by succinate dehydrogenase in the mitochondria [128] (Figure 6.1). Once reduced MTT becomes insoluble forming a formazan salt, and accumulates in intracellular granules that with time are transported to the plasma membrane where they get extruded via exocytosis. The formazan salt is then exposed to the extracellular media where it crystallises [152]. Although these intracellular granules were initially thought to be endosomes and lysosomes [152], recent experiments have shown that they are lipid droplets [153, 154] which provide an intracellular hydrophobic environment for the water-insoluble formazan product. As the MTT reduction depends mainly of the available amount of NAD(P)H, it is a measure of the cellular metabolic rate, and hence indirectly of cell viability [128].

Early studies on the toxicity of Aβ revealed that the addition of Aβ_{25-35} and Aβ_{42} to the cytosol of cells was able to induce an enhancement of the formazan crystallisa-

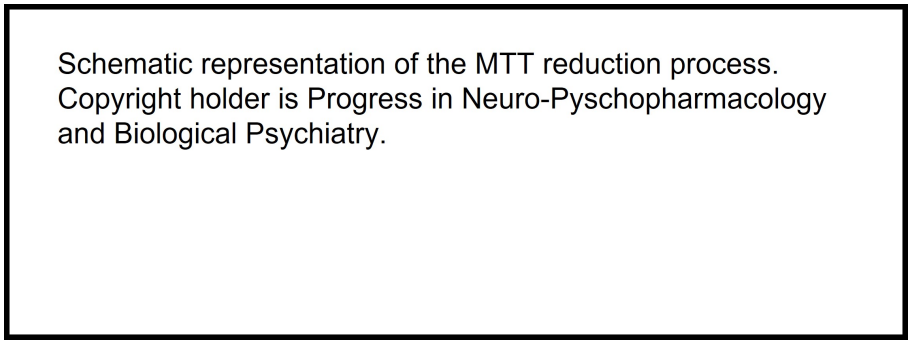

Figure 6.1: 2-(4,5-dimethyl-2-thiazolyl)-3,5-diphenyl-2H-tetrazolium bromide (MTT) and formazan salt structures. Figure taken from ([155])

tion rate in PC12, B12, rat cortical neurons and rat astrocytes cultures (Figure 6.2) [156, 157, 158, 159]. This effect was accompanied by a reduction in the total formazan levels [157]. The comparison with other viability test, like MTS ((3-(4,5-dimethylthiazol-2-yl)-5-(3-carboxymethoxyphenyl)-2-(4-sulfophenyl)-2H-tetrazolium)) and LDH (lactate dehydrogenase)) release, showed that these latter assays were not in agreement with the MTT test, pointing out that the result of the MTT reduction levels could be an artefact and not reflect any real change in cellular viability [156]. Although it could not be experimentally proven, it was hypothesised that this reduction in the formazan levels was a result of the blockage of the MTT endocytosis by the formazan crystals present at the plasma membrane [159]. Moreover, it was also hypothesised that the increased rate of formazan crystallisation was a consequence of an enhancement of exocytotic processes induced by the presence of Aβ species [157]. Additional experiments with human amylin allowed the authors to suggest that the responsible species behind this effect were probably amyloid fibrils, but they were not able to prove the existence of fibrils within the Aβ monomeric solution [159].

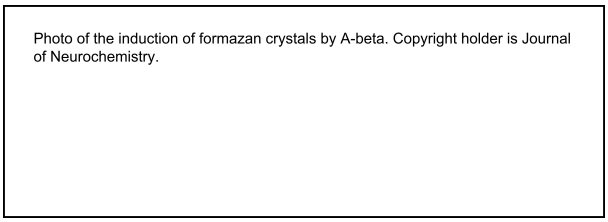

Figure 6.2: Aβ induce the formation of formazan crystals. B12 cells were treated with DMSO (a) or 10 μM Aβ_{25-35} (b) for 16 hours followed by 30 min of MTT reduction. Figure reproduced from [159]

Additional experiments revealed the that the presence of free cholesterol is crucial to the formation of formazan crystals in both, untreated and Aβ treated cells [160]. The

addition of cholesterol was able to induce the crystallisation of the formazan in untreated cells while the depletion of it abrogated this effect in both untreated and treated cells. In addition other compounds, like β-estradiol [161], genistecin or monesine [159], without apparent relation among each other were found to completely inhibit the crystallisation of the formazan.

Here, the effect of different amyloid species from three different proteins, α-synuclein, lysozyme and Aβ_{40} on the MTT test is explored. Pure monomeric, oligomeric and fibrillar species of different lengths were used in order to determined the conformers behind the alterations in the formazan salt crystallisation patterns. Furthermore, using an broad range of concentrations the specificity of this effect and the response time were defined. Moreover the possible mechanisms by which amyloid fibrils induce formation of formazan crystals were further investigated, exploring the possibility of an alteration in the exocytosis rate, the involvement of extracellular receptors, and the ability of amyloid fibrils to induce changes in the cholesterol cellular levels.

6.2 Results

6.2.1 Amyloids fibrils induce the formation of formazan crystals

After having studied how structural features are able to influence the toxic effect of α-synuclein oligomers and how the structural characteristics of different fibrillar aggregates are able to affect their seeding properties, our next aim was to compare the toxicity of these different fibrillar α-synuclein aggregates. With this objective in mind the MTT test, which have been extensively used in the field to study the toxicity associated to amyloid species [58, 162, 96, 42, 80, 136], was selected. Previous studies showed that in comparison to α-synuclein oligomers, α-synuclein fibrils present a milder toxicity in both reactive oxygen species (ROS) and membrane permeability tests [34, 30, 114, 38], and because of this reason, similar results in the MTT test were expected. Surprisingly, after 24h incubation α-fibrils consistently induce a higher reduction of cell viability (55 %) than the kinetically trapped oligomers (83 %) at the same concentration (Figure 6.4). Due to previous reports of Aβ species being able to induce artefacts in the MTT test, the possibility that α-synuclein species were able to produce the same effect was explored. Indeed, SH-SY5Y cells treated with α-synuclein fibrils for 24 hours and then incubated with MTT solution for 2 h displayed formazan crystals on their surface while in the untreated ones the formazan remained trapped inside the cytosol (Figure 6.3). Moreover, when performing the CellTiter-Glo test, which measures the amount of intracellular adenosine triphosphate (ATP), no indication of reduced cell viability was found using the

same experimental setup (Figure 6.4 f).

Due to the methodology available when previous studies were performed, the data generated were able to suggest but not to prove that this effect is caused specifically by the fibrillar form of Aβ [159]. Hence, it was decided to explore and characterise this phenomena in a greater detail. Different α-synuclein conformers (fibrils, sonicated fibrils [or short firbils], kinetically trapped oligomers and monomer) were prepared. SH-SY5Y cells were exposed for 24 h to different concentrations of these conformers (ranging from 0.03 nM to 3 μM), the cells were imaged 2 and 4 hours after the addition of MTT and the final levels of MTT reduction were determine using a plate reader measuring absorbance. The quantification of the amount of crystals present in the cells at a different timepoints revealed that only the fibrillar species were able to induce the formation of formazan crystals at earlier timepoints than the control cells (Figure 6.3 a-g). Interestingly, concentration as low as 0.3 nM of short fibrils were enough to induce a statistically significant difference respect to controls in both number cells presenting formazan crystals and final MTT reduction absorbance levels (Figure 6.4). Moreover, long fibrils were only able to induce similar effects at higher concentrations (3 nM) (Figure 6.3 f-n) indicating that this effect is dependent not only on the concentration of the fibrillar species but also on their size. Both types of fibrils reached saturation, meaning the point where all the cells showed the presence of crystals, at 0.03 μM (Figure 6.4 a and b). In the case of the long fibrils it is possible to detect the presence of the protein itself in the microscope pictures at the higher concentration (3 μM) in the form of clumps (Figure 6.3 i and o), which could easily be confused with cellular debris. The results after 4 h closely resembled the 2h ones, with the untreated cells and the ones treated with unsaturating concentrations of fibrils presenting a higher number of crystals as a result of the natural exocytosis of the formazan salt (Figure 6.4 a and b). In addition, the same trend observed at the microscope can be identified in the final absorbance readout of the MTT test, with the cells presenting a higher number of crystals having reduced a lower amount of MTT (Figure 6.4 c, d). Since long fibrils have been reported to be internalise more slowly that shorter ones [102], this may indicate that this effect is dependent on fibrils internalisation. Alternatively, it is also possible that differences in the number of fibrillar fragments binding to the membrane could explain this effect: at the same concentration, there will be a major number of fibrillar fragments present in the short fibrillar samples than in the long ones, as the concentration is calculated as monomer equivalent resulting in higher number of fibrillar conformers binding to the cellular membrane. Moreover, experiments using the N-terminal acetylated form of α-synuclein, a more physiological variant since α-synuclein have been reported to be 100 % N-acetylated *in vivo* [163], confirmed the ability of α-synuclein fibrils to trigger the formazan crystallisation (Figure 6.5).

Furthermore, neither monomeric nor oligomeric species af α-synuclein were able to induce early formation of formazan crystals (Figure 6.6) at any of the concentrations tested. Moreover, in agreement with previous results [80], the addition of 0.3 μM kinetically trapped oligomer did produce a decreased of around 17 % in MTT reduction at the endpoint of the reaction, indicating that the toxicity observed in previous studies for the different α-synuclein oligomeric variants (including those described in chapter 4), is not the result of an artefact of the MTT test. The fact that higher concentration of stabilised oligomers are unable to trigger a reduction of cell viability may be explained by the crowding and clumping of the aggregates induced by the presence of high amounts of protein [164, 162].

Since the previous results indicated that this effect on the MTT test seems to be related to the presence of amyloid fibrils we then decided to explore if amyloid aggregates of different proteins were able to induce the same phenomenon as the α-synuclein ones. Indeed, it was found that lysozyme amyloid fibrils but not lysozyme monomer, were able to induce the early crystallisation of the formazan inducing a false readout of reduced cell viability (figure 6.7). The fact that lysozyme fibrils were not able to induce cellular death in SH-SY5Y cells was further confirmed by the CellTiterGlo, which showed no decreased in the ATP levels of treated respect to the untreated ones (Figure 6.4 g). However, the lysozyme fibrils seemed to induce the formation of formazan crystals less efficiently than its α-synuclein counterparts as illustrated by the fact that at 0.003 μM and after 2h of MTT incubation only 25.6 % of the cells presented crystals in contrast with the 65.9 % in the case of the long α-synuclein fibrils and the 78.5 % for the short ones (Figure 6.4 a and b). Following this experiments with lysozyme fibrils, the ability of Zn^{+2} stabilised Aβ_{40} oligomers [96] to induce the crystallisation of the formazan was tested. These oligomers have been reported to induce cellular death by several tests (MTT test; resazurin assay, which also measures the metabolic activity of the cells; and trypan blue, which is only able to stain cells whose membrane has been disrupted), an increment of ROS and membrane disruption [96]. As previously observed in the case of α-synuclein, after 24h incubation there was not appreciable induction of the early formation of formazan crystals respect to control cells in the concentration range previously tested (Figure 6.8). However, at high oligomeric concentration, 10 μM, a small percentage of cells (25.7 %) presented formazan crystals after 2h of MTT incubation (Figure 6.4 a and b). This may be indicative of a residual amount of amyloid fibrils present within the oligomeric population or of these oligomers, which have a β-sheet core, being able to trigger this phenomenon at high concentrations. Preliminary data showed that, in agreement with our previous results, Aβ_{40} amyloid fibrils but not monomers were able to induce the crystallisation of the formazan salt after 24 h incubation and 2 h of MTT reduction (Figure 6.8). These

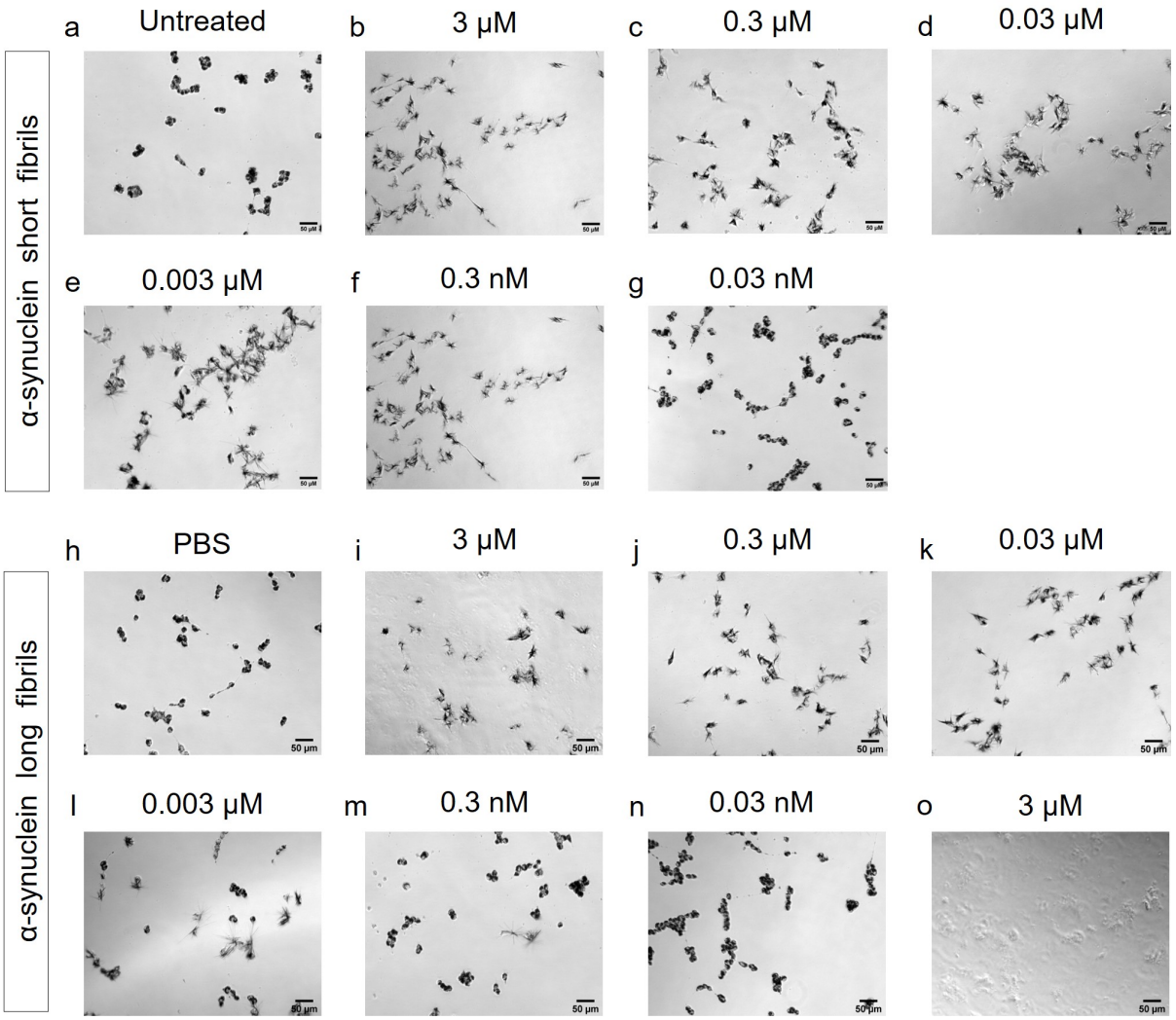

Figure 6.3: α-Synuclein fibrillar species induce formazan crystallisation. (a-g) SH-SY5Y cells were incubated for 24 h with increasing concentrations of short α-synuclein fibrils following by incubation in the MTT solution for 2 h. It is possible to observe the presence of formazan crystals with concentrations as low as 0.3 nM. (h-n) SH-SY5Y cells were incubated for 24 h with increasing concentrations of long α-synuclein fibrils following by incubation in the MTT solution for 2 h. It is possible to observe the presence of formazan crystals with concentrations as low as 3 nM. (o) 3 μM long α-synuclein fibrils were incubated in cellular media for 24 h and then imaged. Representative images taken from 1 experiment out of 3 (at least 5 pictures per condition in each of these experiments were taken) are shown. Each of these three experiments were performed using independent 96 well plates and different batches of α-synuclein fibrils. The results of these experiments were consistent between replicates.

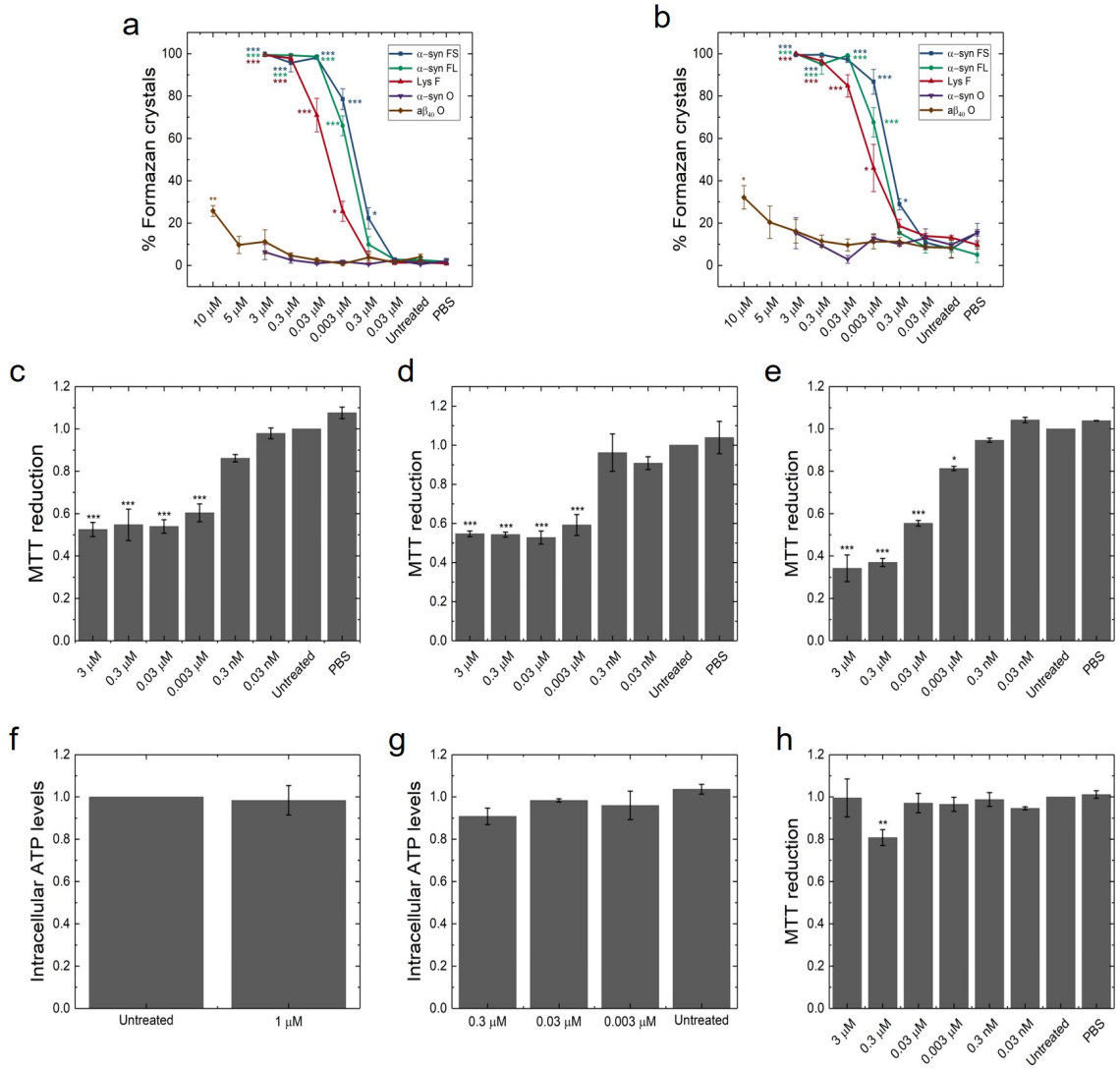

Figure 6.4: Formazan crystallisation correlated with lower levels of MTT reduction but does not affect cellular viability. Quantification of the number of SH-SY5Y cells presenting formazan crystals at 2 h (a) and 4 h (b) at different concentrations of short α-synuclein fibrils, long α-synuclein fibrils, lysozyme fibrils, α-synuclein oligomers and Aβ_{40} oligomer after 24 h incubation. At least 15 images from 3 different experiments were quantified. Final levels of MTT reduction normalised to untreated after 24 h treatment with short α-synuclein fibrils (c), long α-synuclein fibrils (d), lysozyme fibrils (e) or α-synuclein oligomers (h). Intracellular levels of ATP were measured with the CellTiter-Glo kit using SH-SY5Y cells treated with (f) 1 μM α-synuclein short fibrils or (g) 0.3, 0.03 and 0.003 μM of lysozyme fibrils. In all the cases, data from 3 different experiments performed with 3 different preparations of α-synuclein fibrillar aggregates were averaged together. In all the cases the data is represented as average $\pm$ SEM and was analyse by one-way ANOVA, *p $\leq$ 0.05, **p $\leq$ 0.001, ***p $\leq$ 0.0001.

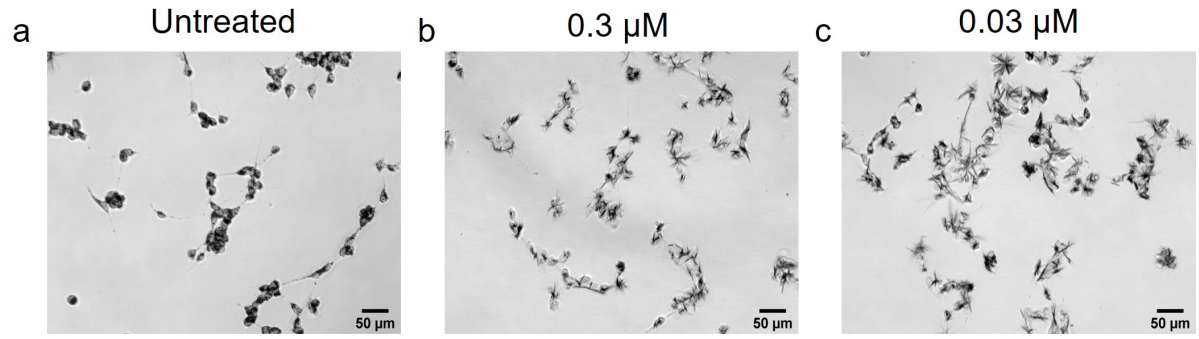

Figure 6.5: Acetylated α-synuclein fibrillar species induce formazan crystallisation. SH-SY5Y cells were incubated for 24 h with vehicle, 0.3 μM and 0.03 μM of short acetylated α-synuclein fibrils. After 2 h of MTT reduction crystals could be detected in the treated cells. Representative images of 3 different experiments performed with 3 different preparations of α-synuclein fibrillar aggregates (at least 5 pictures were taken per condition in each of these experiments) are shown. The results of these experiments were consistent between replicates.

results further confirm the hypothesis that only amyloid fibrils, but no other species, are able to induce early formation of formazan crystals and thus generate a false readout of reduce cell viability. Furthermore, these results suggests that this is a characteristic shared between all the amyloid fibrils, with independence of by which protein are they composed of.

Since SH-SY5Y cells incubated for 24 h with concentrations equal or superior to 0.03 μM of short α-synuclein fibrils presented ubiquitous formazan crystals after 2 h incubation with MTT, the time course of the formation of these crystals was studied next. With this aim we incubated SH-SY5Y with 0.3 μM short α-synuclein fibrils for 24 h and after adding the MTT pictures were acquired every 5 minutes. Formazan crystals can be detected only 10 minutes after the beginning of the incubation, and at 20 minutes all the cells treated with the α-synuclein fibrils showed these crystals (Figure 6.9).

Following this observation, and as the formation of formazan crystals seems to be extremely sensitive to the presence of amyloid fibrils, the incubation time in the presence of short α-synuclein fibrils necessary to trigger this effect in the cells was determined. With this aim cells were incubated in either, the presence of α-synuclein fibrils for 2 h before removing the media and adding the MTT or in the presence of media containing both MTT and different concentrations of α-synuclein short fibrils. The incubation of SH-SY5Y cells with fibrils directly in the presence of MTT resulted in a significant amount of crystals being present after 2h of MTT reduction at fibrillar concentrations of 0.3 μM (17 %) or higher while, in agreement with previous results, the percentage of cells presenting crystals at this same concentration had increased (37.2 %) at 4 h (Figure

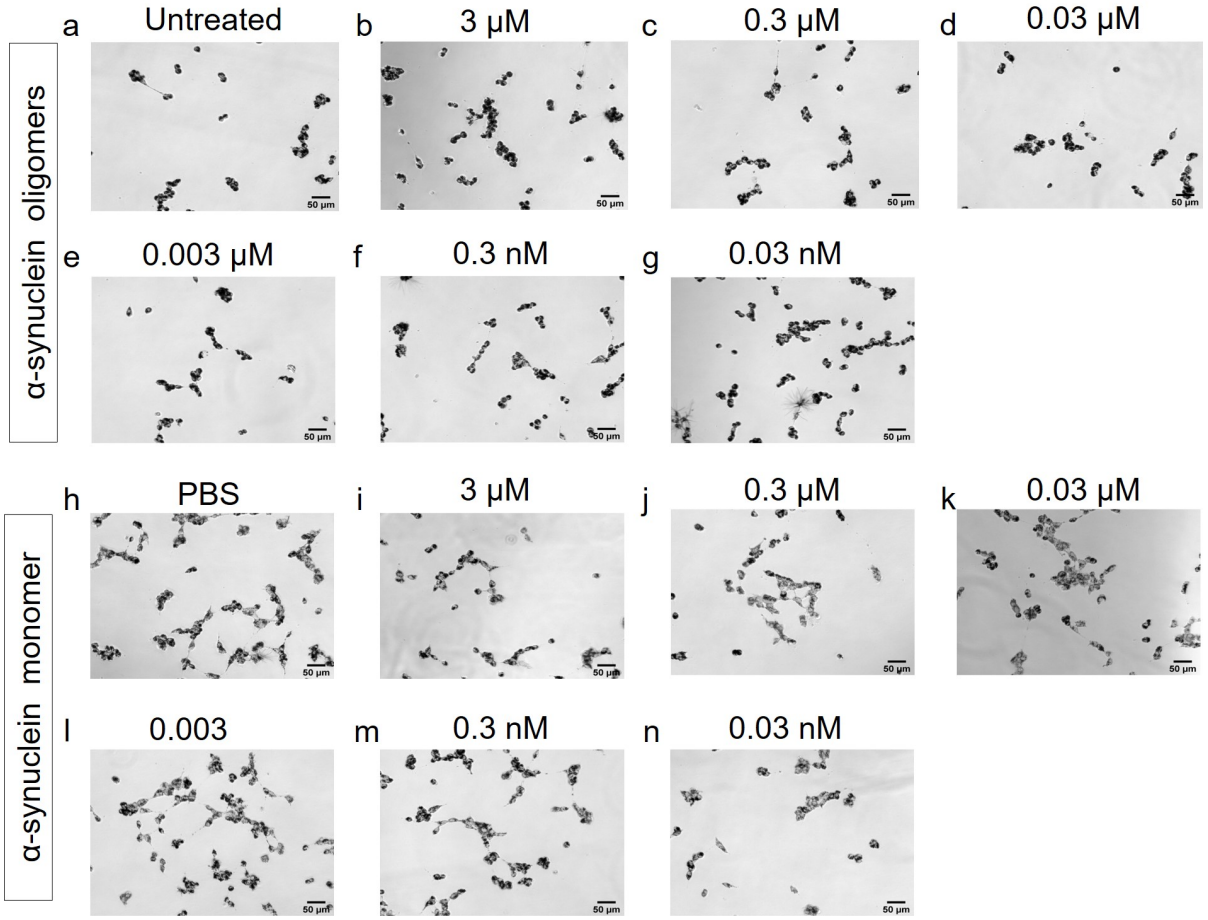

Figure 6.6: α-Synuclein monomeric and oligomeric species are unable to induce formazan crystallisation. (a-g) SH-SY5Y cells were incubated for 24 h with increasing concentrations of α-synuclein oligomers following by 2 h of MTT reduction. It is not possible to observe the presence of formazan crystals at any of the concentrations tested. (h-n) SH-SY5Y cells were incubated for 24 h with increasing concentrations of α-synuclein monomers following by 2 h of MTT reduction. It is not possible to observe the presence of formazan crystals at any of the concentrations tested. Representative images of 3 different experiments performed with 3 different preparations of α-synuclein species (at least 5 pictures were taken per condition in each of these experiments) are shown. The results of these experiments were consistent between replicates.

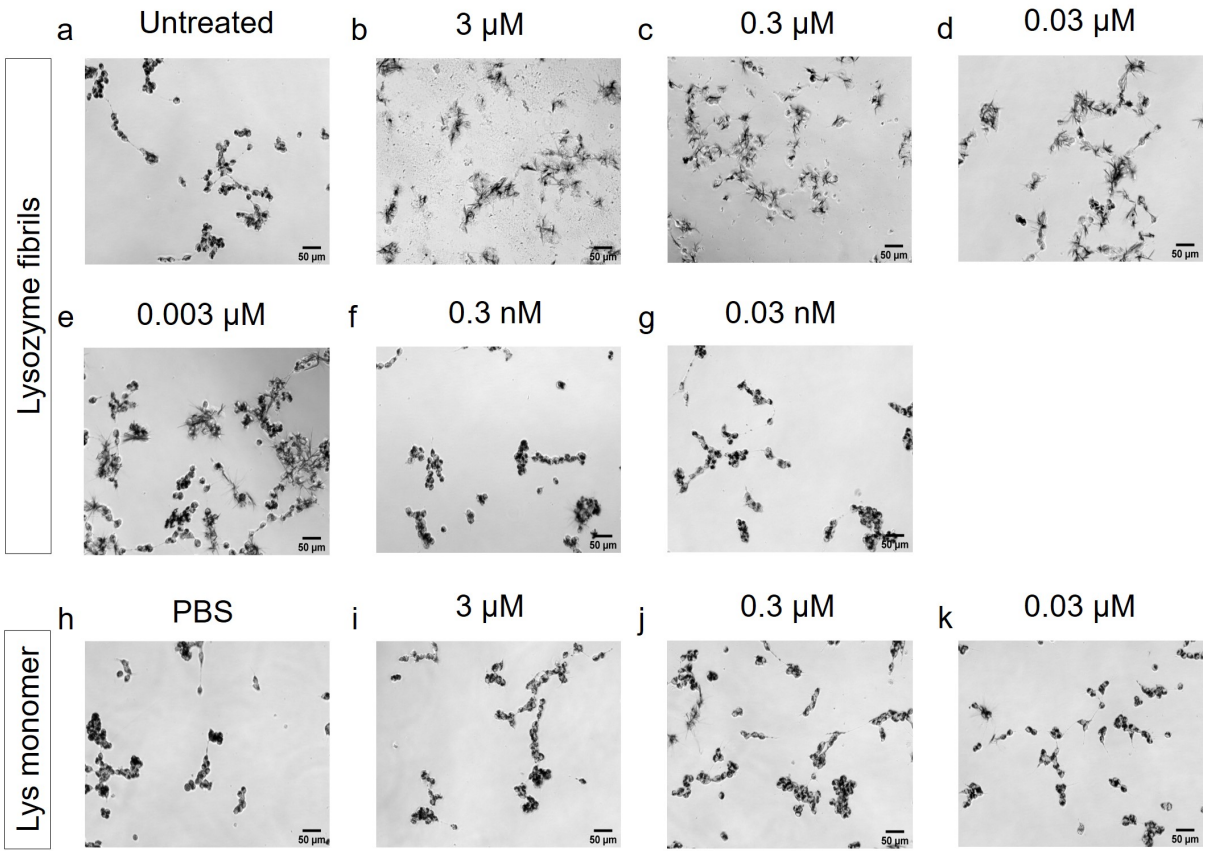

Figure 6.7: Lysozyme fibrils but not monomers induce formazan crystallisation. (a-g) SH-SY5Y cells were incubated for 24 h with increasing concentrations of lysozyme fibrils following by MTT reduction for 2 h. It is possible to observe the presence of formazan crystals with concentrations as low as 3 nM. (h-n) SH-SY5Y cells were incubated for 24 h with vehicle, 3, 0.3 or 0.03 μM of lysozyme monomers following by 2 h MTT reduction. It is not possible to observe the presence of formazan crystals at any of the concentrations tested. Representative images of 3 different experiments performed with 3 different preparations of lysozyme conformers (at least 5 pictures were taken per condition in each of these experiments) are shown. The results of these experiments were consistent between replicates.

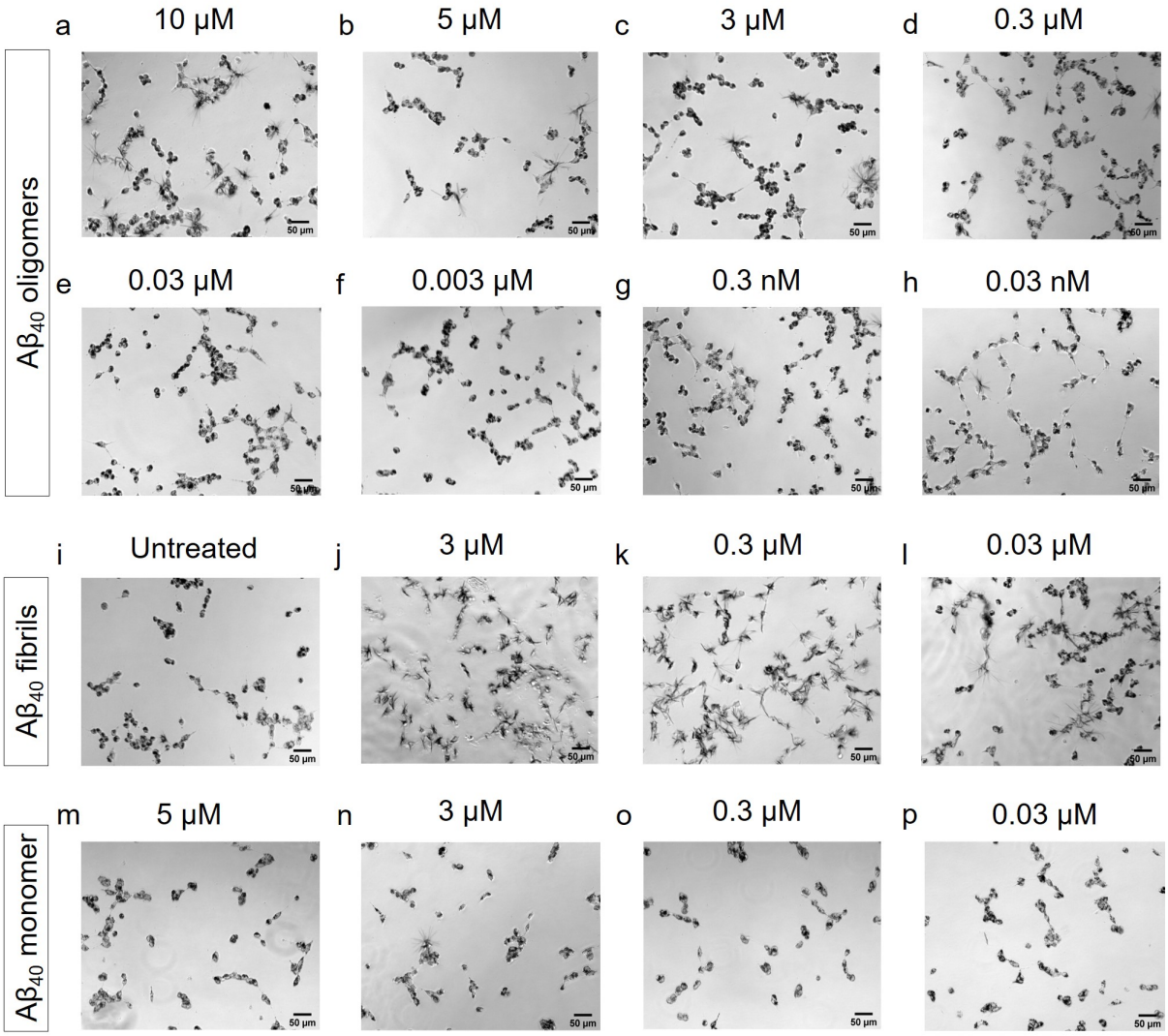

Figure 6.8: Aβ_{40} fibrils but not oligomers or monomers induce formazan crystallisation. (a-h) SH-SY5Y cells were incubated for 24 h with increasing concentrations of β_{40} oligomers following by 2 h of MTT reduction. The presence of formazan crystals could only be observed at 10 μM β_{40} oligomers. Representative images of 3 different experiments performed with 3 different preparations of Aβ_{40} oligomeric species (at least 5 pictures were taken per condition in each of these experiments) are shown. (i-l) SH-SY5Y cells were incubated for 24 h with vehicle, 3, 0.3 or 0.03 μM of Aβ_{40} fibrils. After 2 h of MTT reduction crystals could be detected in the treated cells. Representative images of one experiments performed with one preparations of Aβ_{40} fibrils (at least 5 pictures per condition were taken) are shown. Due to time constrains this experiment could only be performed once. (m-p) SH-SY5Y cells were incubated for 24 h with vehicle, 3, 0.3 or 0.03 μM of β_{40} monomers following by 2 h of MTT reduction. It is not possible to observe the presence of formazan crystals at any of the concentrations tested. Representative images of one experiment performed with one preparation of Aβ_{40} monomer (at least 5 pictures were taken per condition) are shown. Due to time constrains this experiment could only be performed once.

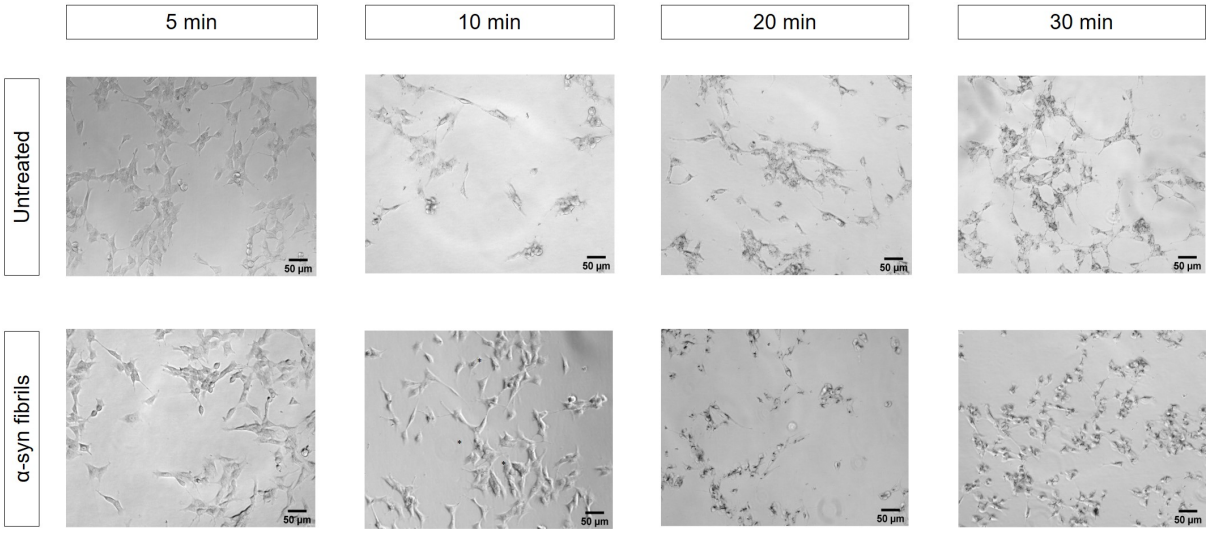

Figure 6.9: Timeline of the crystallisation of formazan. SH-SY5Y cells were incubated for 24 h with 0.3 μM short α-synuclein fibrils and images at 5, 10, 20 and 30 minutes after the the incubation in the presence of the MTT solution were taken. After 10 minutes formazan crystals (here marked with an *) can be appreciated in the treated cells. Representative images of 3 different experiments performed with 3 different preparations of α-synuclein fibrillar aggregates are shown. The results of these experiments were consistent between replicates.

6.10). Cells incubated with short fibrillar aggregates for 2 h before the addition of MTT, presented an increment in the number of cells with crystals after 2 h of MTT reduction at concentrations of 0.003 μM (14.9 %) (Figure 6.10). This result indicated that this effect on the MTT test is not only dependent on fibrillar concentration but also on incubation time, needing only hours to induce the maximum effect. The internalisation of the α-synuclein fibrils has been detected after just 1 h incubation [102, 30] which is consistent with the current time frame observed in this experiment, indicating that the effect of the α-synuclein fibrils on MTT test may be related in its internalisation.

6.2.2 Elucidating the mechanism behind amyloid-induced formazan crystallisation

In the past, studies with different Aβ peptides suggested that the induction of early crystallisation of formazan was due to an increased exocytosis of the intracellular vesicles containing reduced MTT [159]. As short fibrils have been reported to induce a certain degree of membrane disruption, allowing an influx of Ca^{2+} inside the cells [38, 36] which in turn may trigger exocytotic processes with the aim of resealing the disrupting membrane [165, 166, 167, 168], it was first hypothesised that this crystallisation phenomenon

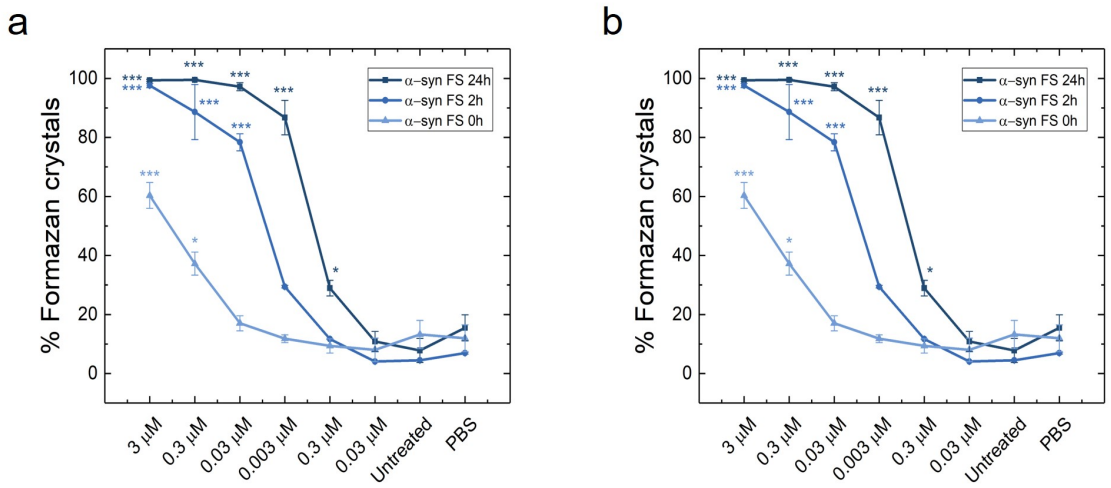

Figure 6.10: Time dependence of the crystallisation of formazan. Quantification of the number of SH-SY5Y cells presenting formazan crystals at 2 h (a) and 4 h (b) at different concentrations of short α-synuclein fibrils after 24 h, 2 h or 0 h incubation. 15 or more images from 3 different experiments each one performed with a different preparation of aggregates were quantified. The data is represented as average ± SEM and was analyse by one-way ANOVA, *p $\leq$ 0.05, **p $\leq$ 0.001, ***p $\leq$ 0.0001.

is a consequence of an exocytosis process triggered by the binding of the α-synuclein fibrils to the cellular membrane. With this aim, SH-SY5Y cells were incibated with 3 μM α-synuclein short fibrils in the absence of calcium. After 1 h incubation with MTT, cells treated with α-synuclein fibrils for 2 h already presented formazan crystals while untreated cells remained undisturbed (Figure 6.11). Together with the fact that oligomers, a more potent disrupting agent for the lipid membranes, were unable to trigger this effect these data suggest that this process is independent of membrane disruption and calcium signalling. Thus, toxicity data from previous studies [34, 38, 30, 36] comparing the ability of different α-synuclein species to induce membrane disruption are still valid and the conclusions of these studies are unaffected by the artificial decrease in MTT reduction induced by amyloid fibrils.

Since the enhancement of exocytosis as the mechanism underlying the crystallisation of formazan at earlier time points have not been experimentally observed, a series of experiments with the objective of validating this theory were performed. After 4 h of MTT reduction it was possible to observe the exocytosis and crystallisation on the formazan in untreated cells (Figure 6.12) using an optical microscope. This supports the theory that formazan crystals are formed after being exocytated once the reduced MTT comes in contact with the extracellular media. This suggests that the crystallisation of the formazan happens in a short period of time, indeed, upon 24 h treatment with α-synuclein short fibrils, crystals of formazan were detected in cells after only 10 minutes of the

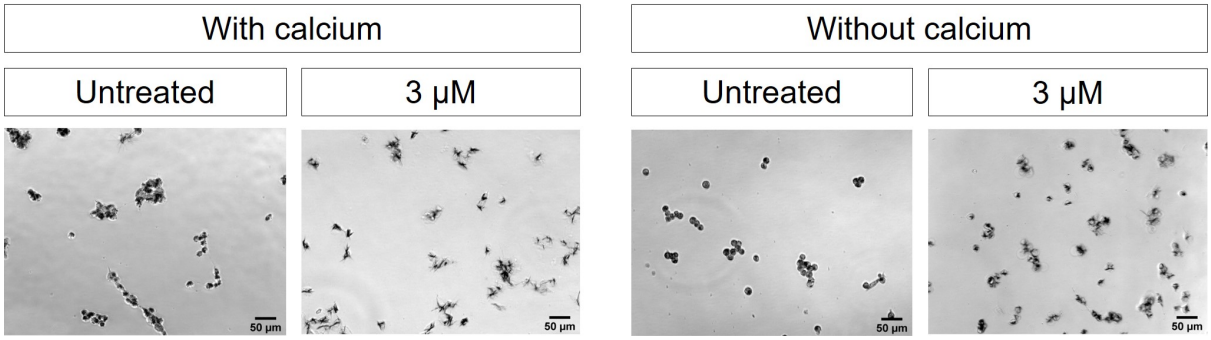

Figure 6.11: Formazan crystallisation is independent of Ca^{2+}. SH-SY5Y cells were treated in the presence or absence of Ca^{2+} for 2 h with 3 μM short α-synuclein fibrils. After 1 hour of MTT reduction formazan crystals could be observed in boths sets of treated cells. Representative images of 3 different experiments performed with 3 different preparations of α-synuclein fibrillar aggregates (at least 5 pictures were taken per condition in each of these experiments) are shown. The results of these experiments were consistent between replicates.

addition of the MTT solution. Therefore, the enhancement of the exocytosis should be an early event and exocytotic vesicles should be quickly translocated to the cellular membrane. To explore this hypothesis, cells incubated with 0.3 μM α-synuclein fibrils for 24 h immediately after the addition of the MTT were imaged every two minutes. It was possible to observe the formation of blue positive vesicles after 2 minutes, indicating the beginning of the MTT reduction. However, these vesicles appeared to remain inside the cells over time and the formation of the formazan crystals occurred near the original position observed for each dot (Figure 6.12). These results indicate that α-synuclein short fibrils are able to induce the crystallisation of the formazan inside the cytoplasm of the cells rather than on the membrane surface. Moreover it is possible to observe the retraction of the cellular membrane after the formation of the formazan crystals, suggesting that these crystals damage the cell membrane as they grow in size with the result of effectively killing the cells and stopping the reduction of the MTT. Here it is important to highlight that, if this were to be proven, the MTT readouts would be faithfully reporting on the viability of the cells, but the observed cellular death would be a consequence of the interaction between the fibrillar aggregates of α-synuclein and the fromazan and not of the toxicity induced by this conformers.

To further investigate this possibility, the integrity of the cellular membrane after the induction of the formazan crystallisation by α-synuclein short fibrils was assessed. In order to achieve this, SH-SY5Y cells treated for 24 h with 0.3 μM short α-synuclein fibrils were incubated in the presence of 2 μM Calcein-AM, a cell permeant dye that gets converted into its fluorescent membrane impermeable form by cellular esterases. After

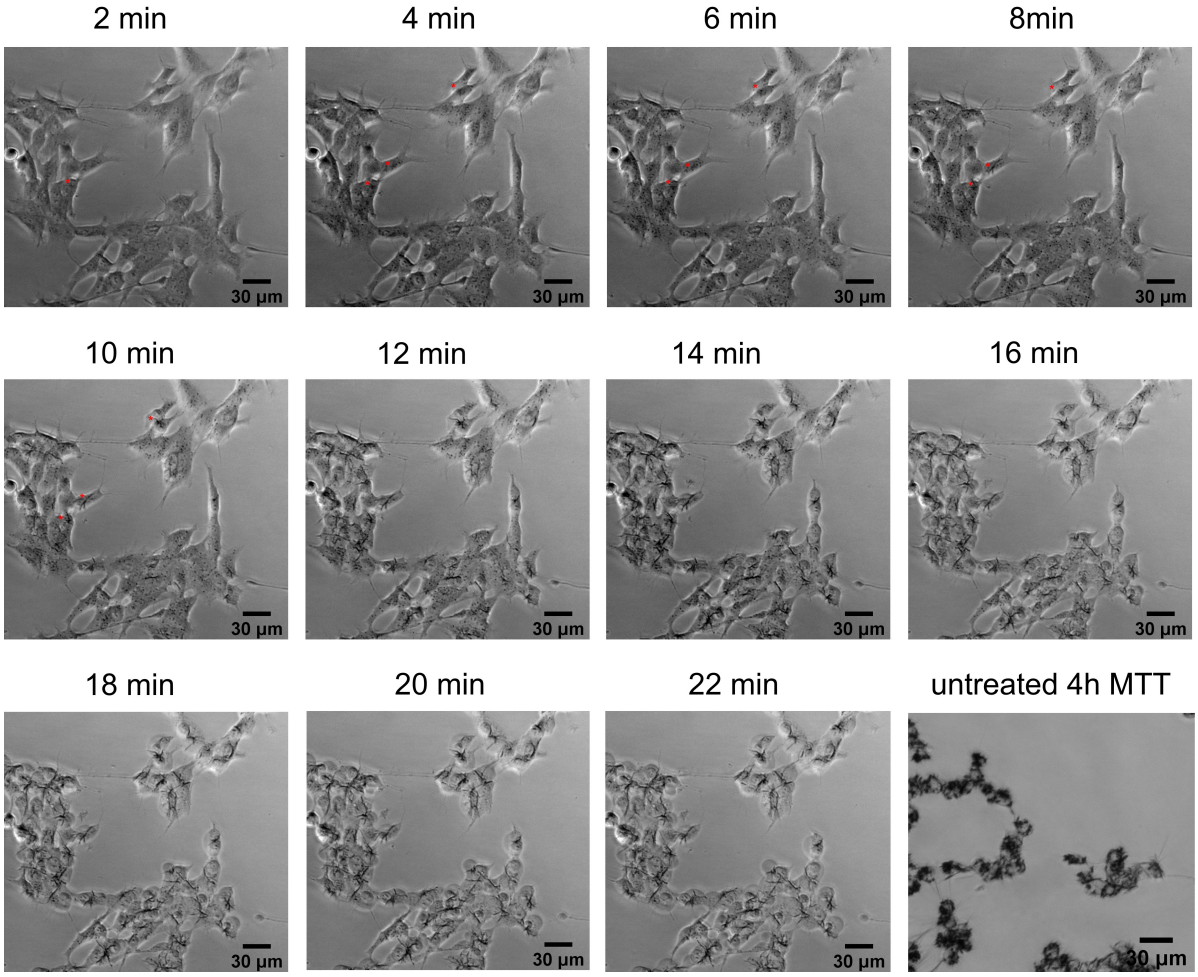

Figure 6.12: α-Synuclein fibrils do not enhance the exocytosis of formazan. SH-S5Y5 cells were treated with 0.3 μM short α-synuclein fibrils for 24 h after which the media was replaced with an MTT solution and pictures were acquired every 2 minutes. After 4 minutes the formazan granules are already visible and at 8-10 minutes the first crystals appear. During this process the formazan granules remain static inside the cells. The cellular membrane retracts after the formazan crystals have formed. After 4 h of MTT reduction it is possible to observe the formazan exocytosis in the untreated cells. Representative images of 3 different experiments performed with 3 different preparations of α-synuclein fibrillar aggregates are shown. The results of these experiments were consistent between replicates.

30 minutes at 37 °C of incubation, the Calcein-AM dye was replaced by a solution of MTT and the cells are imaged at 30 minutes and 2.5h, for this last time point 4 μM of ethidium homodimer (a marker of cellular death) was added to the mixture 30 min in advance. Due to the possible cytotoxic effect of ethidium homodimer, this marker could not be co-incubated with Calcenin-AM for the complete duration of the experiment. The images acquired 30 minutes after the addition of the MTT showed that cells presenting larger formazan crystals had lost the Calcein-AM stain whereas, cell containing smaller crystals still retained the Calcein-AM derived florescence to a certain extend, indicating that the cellular membrane is less affected by the presence of the formazan crystals (Figure 6.13). This trend could also be appreciated at a second time point, where most of the cells showing formazan crystals had lost the Calcenin-AM stain and where instead positive for ethidium homodimer (Figure 6.13). These data corroborate the hypothesis that large formazan crystals are able to disrupt the cellular membrane, inducing the loss of membrane integrity and eventually leading to cell death. This is in agreement with previous reports showing that the formation of these crystals in untreated cells induced cellular death through apoptotis mediated by the activation of caspase-3 [169]

Taken together these results do not support the hypothesis of the formazan crystallisation being a direct consequence of an enhance exocytosis of the formazan-positive intracellular granules. Instead the data obtained in this study are consistent with the formzan crystals forming inside the cellular cytoplasm from where they would be able to pierce the cellular membrane, compromising the membrane integrity and ultimately triggering cellular death.

Once the possibility of an enhancement of exocytosis being responsible for the formation of the formazan crystals was discarded alternative possibilities had to be considered. One of these possibilities is the formazan crystallisation being triggered by a downstream signalisation pathway activated upon binding of the fibrillar conformers to the cellular membrane. Previously, several amyloid conformers have been reported to bind and inhibit the activity of the Na^{2+}/K^{+} ATPasa (NKA) [45, 170, 171], which in turn, activated a signallisation pathway via Src kinase (involved in the regulation of cellular proliferation, differentiation, motility, and adhesion). Indeed, the inhibition of the NKA by ouabain has been reported to inhibit the reduction of MTT producing a false readout of reduced cell viability [172] in HUVEC cells dependent on the activation of Src. In order to investigate if this interaction is responsible for the effects on the MTT test previously described in this study SH-SY5Y cells were incubated with 200 nM ouabain for 24 h before replacing the media with a solution of MTT, imaged at 2 h and 4 h, and the final levels of reduced MTT were quantified in a platereader. Surprisingly, no difference in the amount of cells

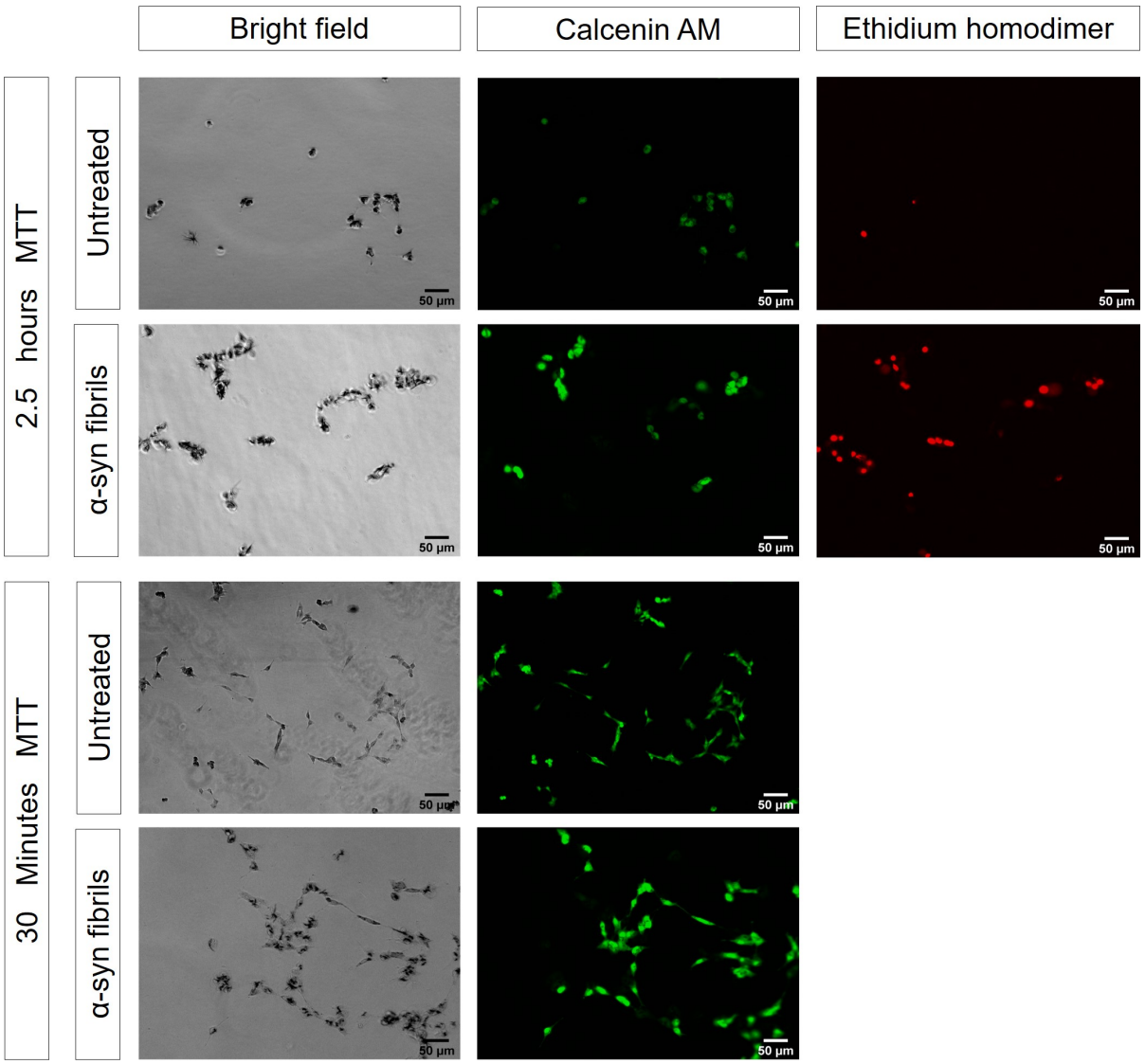

Figure 6.13: Formazan crystals disrupt the cellular membrane upon formation. SH-S5Y5 cells were treated with vehicle or 0.3 μM short α-synuclein fibrils for 24 h after which they were incubated with 2 μM Calcein-AM. After 30 min the Calcein-AM was replaced with an MTT solution. 30 min and 2.5 h into the reaction and pictures were taken. Cells presenting large formazan crystals had lost the Calcein-AM fluorescence were untreated and cells with smaller crystals retained it. Before the 2.5 h timepoint 4 μM of ethidium homodimer was added for 30 min, cells with formazan crystals had lost the Calcein-AM signal and were stained by ethidium homodimer. Representative images of 3 different experiments performed with 3 different preparations of α-synuclein fibrillar aggregates are shown. The results of these experiments were consistent between replicates.

presenting formazan crystals or the final levels of reduced product were found between treated and controls cells (Figure 6.14 a-d). Thus, this indicates that the amyloid fibrils induce the crystallisation of formazan in SH-SH5Y cells by an alternative mechanism to the one reported in HUVEC cells.

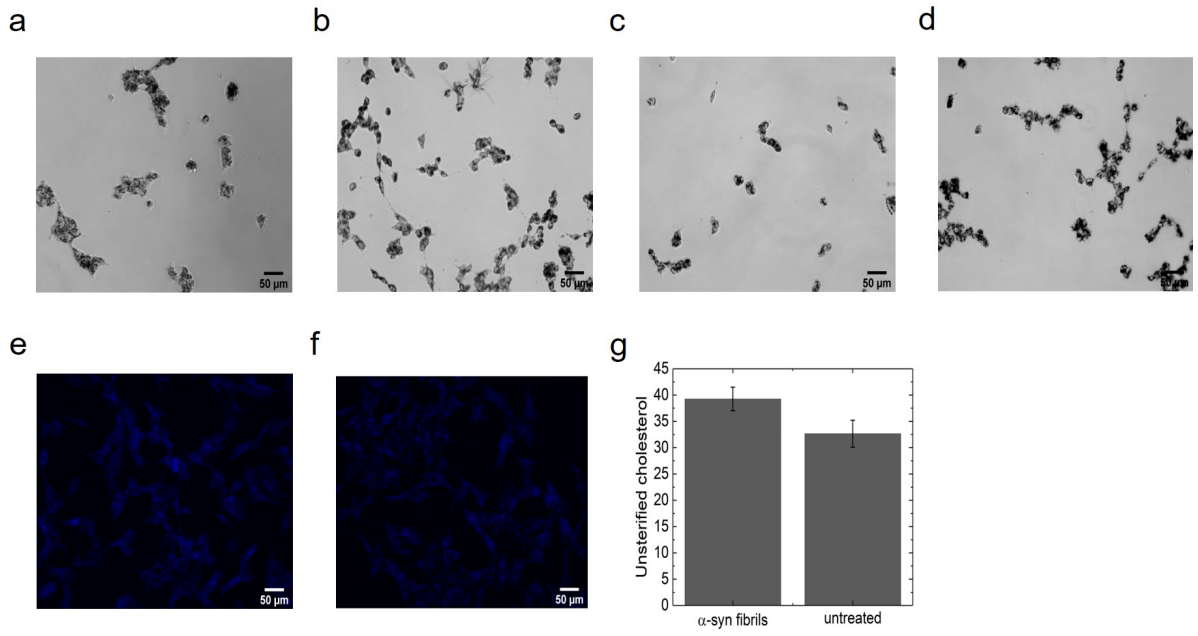

Figure 6.14: Insights into the mechanism of formazan crystallisation. (a-d) Inhibition of the NKA does not cause the crystallisation of the formazan. After 2h of MTT reduction neither cells treated with 200 nM ouabain for 24 h (a) nor untreated ones (b) showed formazan crystals. The same results could be observed after 4 h of MTT reduction (c, cells treated with 200 nm oubain), (d, untreated cells). Representative images of 3 different experiments performed with 3 different preparations of α-synuclein fibrillar aggregates (at least 5 pictures were taken per condition in each of these experiments) are shown. The results of these experiments were consistent between replicates. (e-g) The presence of α-synuclein fibrils does not alter the intracellular levels of cholesterol. SH-SY5Y were treated with 0.3 μM short α-synuclein fibrils (e) or vehicle (f) and the unsterified cellular cholesterol was stained with Flipin III. Representative images of 2 different experiments performed with 2 different preparations of α-synuclein fibrillar aggregates (at least 5 pictures were taken per condition in each of these experiments) are shown. The quantification of the Flipin III fluorescence (g), represented as the average $\pm$ SEM, showed no significant difference between the two populations. Data were analysed via a Student t-test.

Another possible explanation for this phenomenon involves the alteration of cellular levels of cholesterol induced by the presence of amyloid fibrils. The levels of unsterified cholesterol present in the cells has been identified as an important determinant for the formation of fromazan crystals [160, 154]. The addition of external cholesterol has been

shown to induce the early crystallisation of the formazan in untreated cells while its depletion completely abrogates this reaction in both untreated and Aβ-treated cells [160]. Moreover, Aβ has been shown to increase the amount free cholesterol present inside the cells which could in turn affect the formazan crystallisation rate [160]. In order to test if this was also true in the case of α-synuclein, SH-SY5Y cells were incubated in the presence of 0.3 μM short fibrils for 24 h afterwards free cholesterol staining by filipin III was performed. Filipin III is an antibiotic that upon interaction with unsterified cholesterol undergoes a conformation change and becomes fluorescent. Interestingly no difference between the cholesterol content of the treated and untreated cells was detected (Figure 6.14 e-g). Since the data acquired in this study suggest that the acceleration of the formazan crystallisation is a feature common to abroad spectra of amyloid fibrils, there is a low probability of an increment in the intracellular levels of unsterified cholesterol being behind the reported enhancement of formazan crystallisation.

Finally, as reduced MTT has been recently shown to accumulate inside lipid droplets [153, 154], the possibility of α-synuclein fibrils inducing changes in the lipid droplet population was explored. With this aim, untreated and cells incubated with short α-synuclein fibrils, were fixed and stained with Nile Red, a fluorescence probe that binds neutral lipids. Image analysis revealed no differences between the lipid droplets population of the untreated and treated cells (Figure 6.15 a and b). Interestingly the co-treatment of short α-synuclein fibrils and 2.5 μM U-18666A, which induces the sequestration of cholesterol in late endosomes, for 24 h inhibited the enhanced formation of formazan crystals, returning the crystallisation rate to untreated levels (figure 6.15 c-f). This suggest that the presence of cholesterol inside the lipid droplets is indeed necessary for the amyloid fibrils to induce this characteristic effect. As both, the fact that the concentration of α-synuclein fibrils necessary to induce this effect changes with fibrillar size and the time necessary to first observe this process points toward the induction of the formazan crystallisation being related to fibrillar internalisation the possibility of a direct interaction between the amyloid fibrils and the lipid droplets needs to be considered. Although amyloid fibrils are internalised by endocytosis, they are able to disrupt the endocytotic vesicles effectively escaping the proteolytic pathway [47, 173], which could allow them to interact with the lipid droplets once in the cytoplasm. Preliminary results (Figure 6.16), in which co-staining with Nile Red and fibrillar (OC) or oligomeric (A11) specific antibodies was carry out, shows that this is indeed a possibility worth exploring.

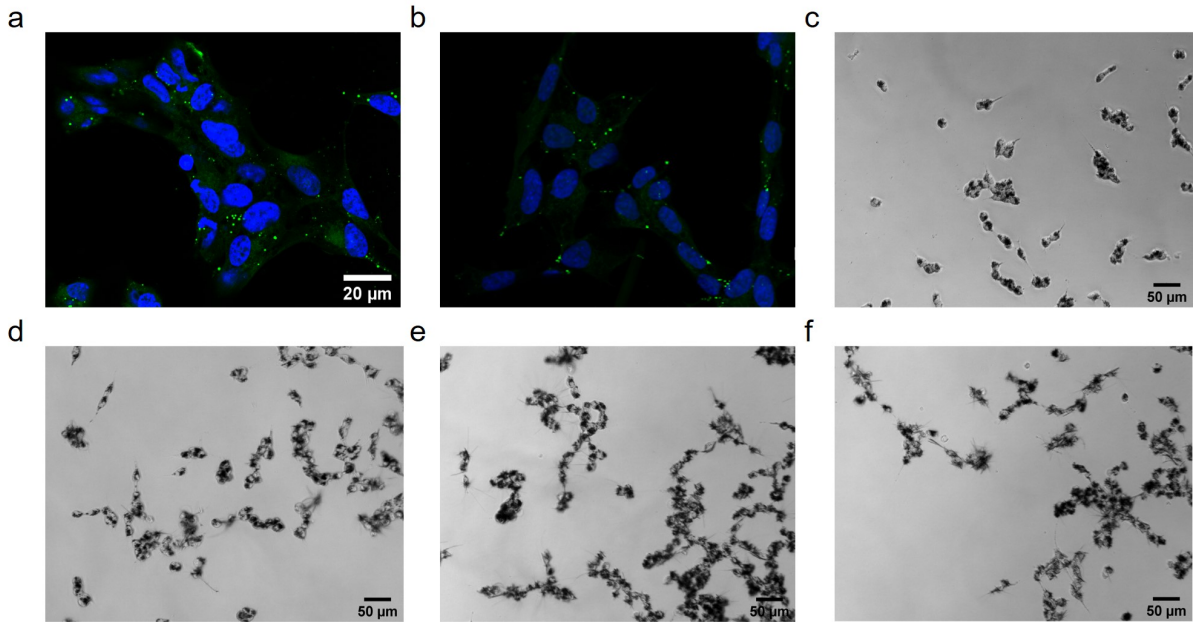

Figure 6.15: Relationship between formazan crystallisation and lipid droplets. SH-SY5Y cells untreated (a) and treated (b) with 0.3 μM α-synuclein short fibrils were stained with Nile Red and imaged in a confocal microscope. No difference could be observed between the lipid droplets population of both conditions. (c-f) SH-SY5Y cells were treated with 2.5 μM U-18666A for 24 h in the presence (d,f) or absence (c,e) of 0.3 μM short α-synuclein fibrils. 2 hours after the addition of MTT nor untreated (c) nor fibrillar treated cells (d) displayed formazan crystals. After 4 h incubation with MTT, both untreated (e) and treated (f) cells showed a similar number of cells presenting crystals. Representative images of 3 different experiments performed with 3 different preparations of α-synuclein fibrillar aggregates are shown.

6.3 Discussion

In conclusion these results showed that amyloid fibrils induce the crystallisation of the formazan in a time and concentration dependence manner. Once formed, these crystals pierce the plasmatic membrane inducing cellular death and effectively stopping the MTT reduction. As this happens as early as 10 minutes of incubation of the cells in the MTT solution the final readout of the test, performed in a platereader, detects significantly less formazan in the fibril-treated cells compared to the untreated ones leading towards to the artifact of a reduced cell metabolic activity and viability. The fact that the addition of amyloid fibrils does not indeed induce cellular death has been proved with the help of an alternative cellular viability test that measures the amount of ATP present inside the cells. Moreover, this phenomenon have been proven to be extremely sensitive to the presence of amyloid fibrils, with concentration as low as 300 pm triggering a significant effect. The ability of producing and isolating different species (monomer, oligomers and fibrils) in the

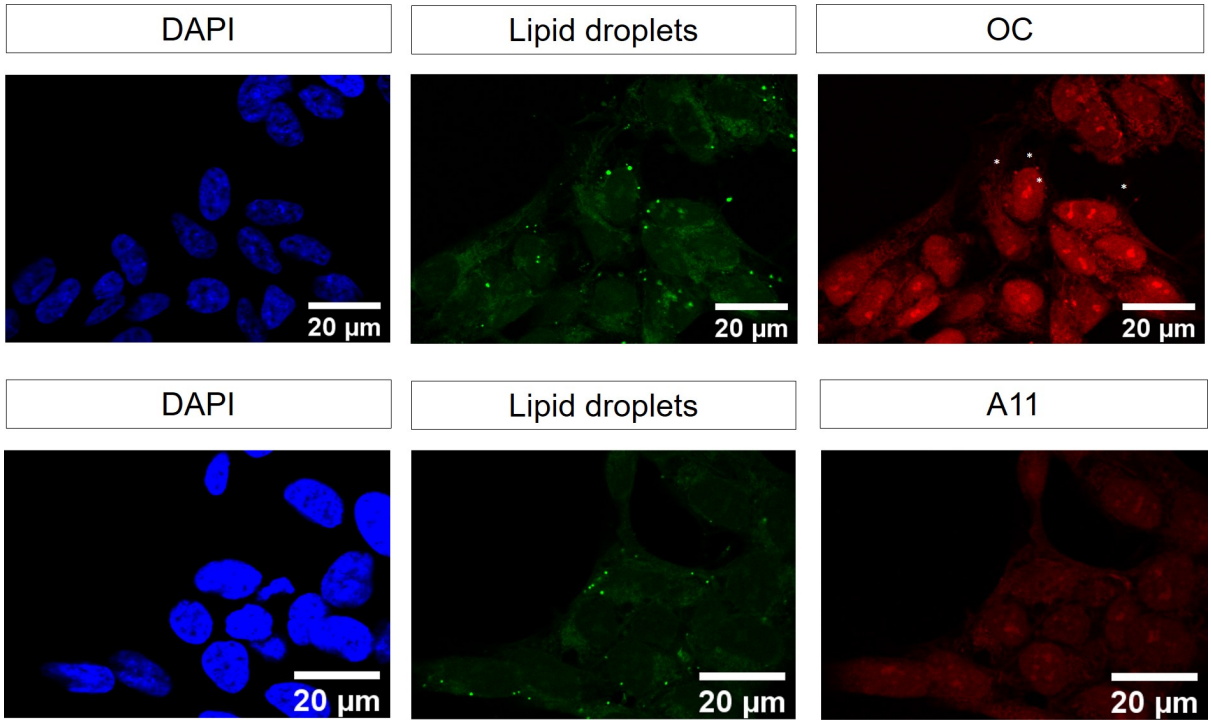

Figure 6.16: Co-localisation between α-synuclein fibrils and lipid droplets. SH-SY5Y cells were incubated in the presence of 0.3 μM α-synuclein short fibrils for 24 h. After fixation cells were stained with Nile Red and OC (anti-fibrillar antibody) or A11 (anti-oligomeric antibody). Partial co-localisation between the Nile Red positive vesicles and the OC antibody could be detected. Representative images of one experiment performed with one preparation of α-synuclein fibrillar aggregates are shown. Due to time constrains this experiment could not be repeated.

aggregation pathway of amyloidogenic proteins have allowed us to undoubtedly identify amyloid fibrils as the species responsible for triggering this effect in the case of both, α-synuclein and Aβ. Although oligomeric species do not trigger this effect and hence it is possible to use the MTT with the objective of evaluate their effect upon cellular viability, the high sensitivity of the test means that the presence of any residual fibrillar aggregate will trigger the formazan crystallisation, and thus potentially result in a false positive. Furthermore, the inability of the oligomeric species to induce the crystallisation of the formazan salt have been determined here using off-pathway oligomers. Despite the fact that they share similar toxicity properties with on-pathway oligomers [34], it is probable that their structure differs from one another. Since the induction of the early crystallisation of the formazan seems to be highly dependant on structural features of the amyloid aggregates and the on-pathway oligomers are the precursors of amyloid fibrils it is possible that they have a different effect upon the formazan crystallisation than their stabilised counterparts. Although the transient nature of the oligomeric on-pathway species make them extremely difficult to isolate, further efforts on this matter need to be

carried out in order to achieve a clearer picture of the species able to trigger this effect. Moreover, if on-pathway oligomers are proven to be unable to induce this effect, the high sensitivity of the test could be used to discriminate among different species forming during the aggregation reaction, and it could allow the correlation between their structure and activity. Taking into account all these considerations we encourage complementing the MTT test with other cell viability tests like LDH release, ATP content or resazurin.

Both, the fact that long α-synuclein fibrils induce this effect at a higher concentration (3 nm) than short ones (0.3 nm) and that the this effect is triggered in the timescale of hours after the addition of the α-synuclein fibrils are consistent with the internalisation of the fibrils being determinant for the triggering of the formazan crystallisation. Preliminary results exposed in this study pointing towards a possible direct interaction between the α-synuclein fibrils and the lipid droplets further supports this hypothesis (Figure 6.17). If additional experiments confirm this hypothesis, differences in internalisation, binding rate to the lipid membrane or ability to escape the endocytotic pathway may explain the differences in the ability to induce the crystallisation of the formazan observed in this study between different amyloid fibrils at the same concentrations (Figure 6.4). In this context, the use of fluorescently labelled α-synuclein species could have allowed us to evaluate some of this aspects, as it would be possible to easily determine their internalisation rate and once internalised, to follow their journey through the endosomal pathway and potentially into lipid droplets. Moreover, the repeat of these experiments in HEK293T cells, which have been recently reported to present an impairment internalisation of the α-synuclein fibrils [174], might support our efforts in confirming this hypothesis. If a difference in the ability of α-synuclein fibrils to induce the formation of formazan crystals were to be detected, this could be indicate that this process is dependent on cellular subtype. This could offer a potential explanation to the difference between the reduction in MTT reduction previously reported in the literature (10 %) [34, 30, 114, 38, 116] and the one observed in this study (50 %). Even though, SH-Y5Y cells have routinely being used both, here and in previous studies [34, 30, 114, 38, 116], differences in the differentiation protocol used to obtain neuron-like SH-Y5Y in each lab could potentially affect the metabolism of these cells and consequently explain the observed differences.

In addition, the fact that the crystallisation of formazan is also triggered by N-acetylated α-synuclein is specially relevant. It has been reported that *in vivo* α-synuclein is constitutively acetylated in the N-terminal region [163] and the presence of this post-translational modification is able to influence the interaction between α-synuclein fibrils and cells. For example, N-terminal acetylated synuclein fibrils have been shown to be

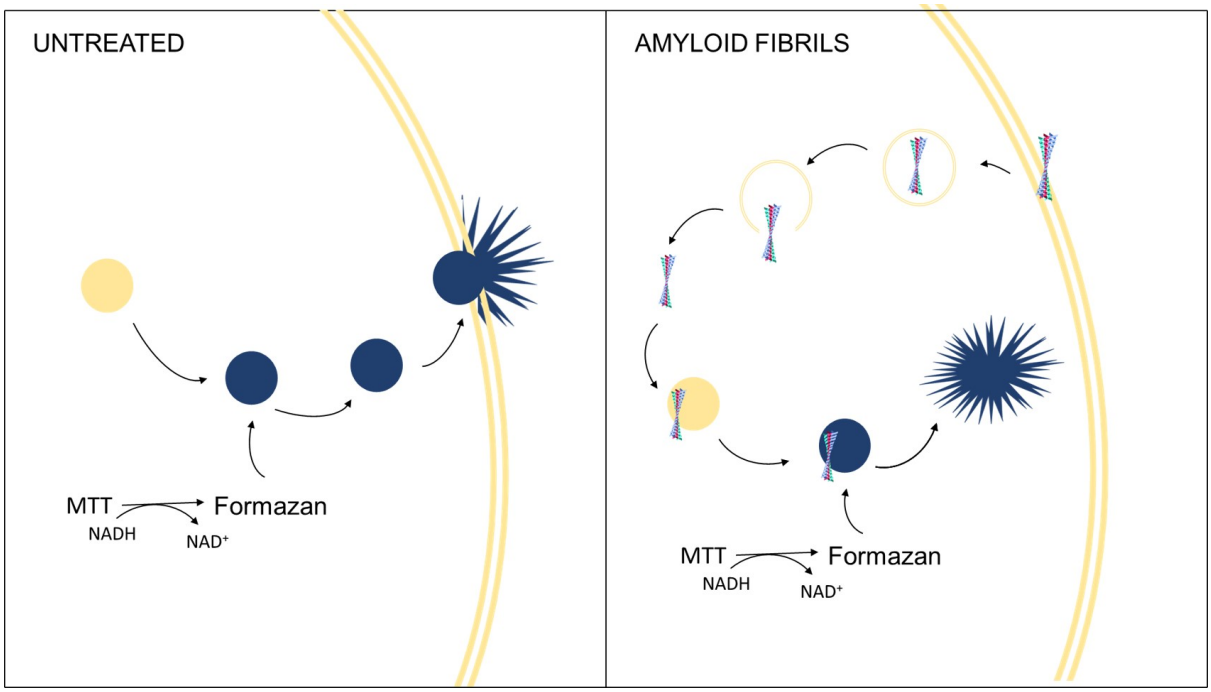

Figure 6.17: Proposed mechanism of MTT crystallisation.

internalised at a faster rate than the WT form [174] via specific interactions with the cellular membrane. Here, the fact that N-acetylated α-synuclein and WT fibrils were able to induce the same response indicated that the underlying cellular processes responsible for triggering the crystallisation of the formazan may be happening *in vivo*. Even though the acetylation of α-synuclein is physiologically relevant, N-acetylated variants of α-synuclein have not been used in other chapters of these thesis due to different reasons. The purification of N-acetylated α-synuclein involves the co-transfection of *E. Coli* with two plasmids, the α-synuclein one and the NatB (N-terminal acetyltransferase), as we did not had access to the NatB plasmid at the moment N-acetylated mouse α-synuclein could not be purified. With respect to the production of the different oligomers variants used in chapter 4, N-acetylated kinetically trapped oligomers have been shown to present the same structure and toxic properties than the WT form [36]. This fact allowed the used the unacetylated version of α-synuclein, with its ease of purification, to prepare the different oligomeric variants used in this study. Finally, since the N-terminal acetylation of α-synuclein has been shown to affect the interaction between the cellular membrane and α-synuclein fibrils the generation of the different fibrillar conformers used in chapter 5 with N-acetylated α-synuclein could have been specially relevant. However, since these conformers had been kinetically and structurally characterised using the unacetylated variant of α-synuclein [19] and one of the objectives of the study was to establish a link between different structural fibrillar polymorphs and different seeding capabilities in

primary neurons, the use of the unacetylated variant of α-synuclein was preferred. If in the future the N-acetylated version of α-synuclein were to be used to generate these fibrillar conformers, their full biophysical characterisation will be required before performing the cellular experiments.

The MTT test is still widely used in the field to monitor cellular toxicity of amyloid aggregates, particularly in the case of α-synuclein [42, 58, 80], which in light of these results need to be revisited. Moreover, based on the assumption that Aβ is able to trigger an enhancement of the exocytosis, the formation of formazan crystals has been used as a tool to monitor Aβ-induced changes in synapsis plasticity [175, 176]. In addition, these results highlight the importance of using different experimental approaches in order to validate a working hypothesis, as when using a single method unknown factors may influence the final results leading the scientists to draw conclusion based on an artefact of the test in question. In conclusion, the results presented here revealed that the formation of formazan crystals is not directly linked to the enhancement of the exocytosis rate, meaning that the conclusions of these assays should be revisited when amyloid aggregates are tested.

Chapter 7

Conclusions

In this PhD thesis I have extensively explored and characterised how the structure of different amyloids α-synuclein conformers is able to modulate cellular toxicity. Since different polymorphs of α-synuclein are able to induce different synucleinopathies [57, 58, 59], the understanding of how apparently small structural changes can modulate not only cellular toxicity but also the spreading of the α-synuclein aggregates *in vivo*, is specilly important not only to understand the mechanism behind the onset and progress of Parkinson's disease (PD) but also of other synucleinopathies.

First, we aimed to improve the reproducibility of the PFF mouse model of Parkinson's disease by biophysically characterising and isolating the different α-synuclein conformers present in the injected samples. This allowed us to identify two potential sources of variability: the storing method of the samples and their composition. We first observed that the storage under cryogenic conditions lead to the fragmentation of the samples, which could potentially affect the reproducibility of the results obtained. This is especially relevant in the light of our next results, which showed that shorter fibrillar fragments are able to induce the pathology and the spreading of the disease more efficiently than other α-synuclein conformers both, *in vitro* and *in vivo*. Moreover, by comparing the ability to induce a PD-like phenotype of these small fibrillar fragments and kinetically trapped oligomers, which have been shown to induce higher levels of cellular toxicity than the fibrils [34], we were able to determine that the ability to recruit endogenous α-synuclein is key to successfully induce the spreading of α-synuclein aggregates in the brain. Hence the seeding ability of different α-synuclein conformers *in vitro* could potentially be an marker for enhanced toxicity *in vivo*.

Secondly, the different properties of kinetically trapped oligomers produced from pathological variants of α-synuclein and their ability to affect cellular toxicity were stud-

ied. Surprisingly, it was found that G51D oligomers presented a higher structural polymorphism than any of the other variants, although the presence of an antiparallel β-sheet core was conserved between preparations, they presented different degrees of α-helical content. Moreover, the amount of α-helix present in the preparation proved to be a key determinant of cellular toxicity, being more toxic those preparation with higher degrees of α-helical content. This indicates that more parameters beside size and hydrophobicity content [123] need to be taken into account when predicting the toxic properties of amyloids conformers.

The next step was to investigate the relationship between different fibrillar polymorphs of α-synuclein and cellular toxicity. We found that different α-synuclein fibrillar conformers were able to seed the aggregation of endogenous α-synuclein with different efficiencies. While protofibrils were able to induce a higher degree of aggregation than F1 fibrils, oligomeric-size aggregates formed in the presence of 10 % methanol presented a reduced ability to seed the formation of endogenous α-synuclein inclusions. Since different α-synuclein fibrillar polymorphs have been linked to different synucleinopathies, the understanding of how these modulate cell toxicity could further our knowledge of the origin of these diseases. As these α-synuclein aggregates have been shown to seed endogenous α-synuclein at different rates *in vitro*, once injected into the brains of mice they could trigger the formation of aggregates at different speeds and in consequence model different synucleinopathies or different stages of the disease. Because of this, the injection of these aggregates into brains of mice could improve our understanding of the relationship between fibrillar structure and pathology.

Finally, we studied the effect of different amyloid aggregates on the MTT test. Our experiments show that amyloid fibrils are able to induce the crystallisation of the formazan salt in a time and concentration dependent manner. Once formed, these crystals pierce the plasmatic membrane inducing cellular death and effectively stopping the MTT reduction. As this happens early in the MTT reduction reaction, the formazan levels are significantly decreased respect to the control cells at the end of the reaction, leading towards a false conclusion of amyloid aggregates inducing cellular death. The high sensitivity of this test means that, although it should not be used to asses cellular variability, it could be repurposed as a method of detection of amyloid fibrils in solution. As the MTT test is still widely used in the field to asses the toxicity of amyloids aggregates, this is especially relevant and highlights the importance of using different experimental approaches in order to validate a working hypothesis.

In conclusion, this PhD thesis highlights the importance of integrating knowledge from different fields in order to solve complex problems. Here, we have successfully applied our

understanding of the biophysical properties of different amyloids aggregates to explain the different effects that these have upon cellular toxicity.

Bibliography

[1] Fabrizio Chiti and Christopher M Dobson. Amyloid formation, protein homeostasis, and human disease: a summary of progress over the last decade. *Annual Review of Biochemistry*, 86(1):1–42, 2017.

[2] Tuomas P J Knowles, Michele Vendruscolo, and Christopher M Dobson. The amyloid state and its association with protein misfolding diseases. *Nature Reviews Molecular Cell Biology*, 15(7):496, 2014.

[3] Pu Chun Ke, Ruhong Zhou, Louise C. Serpell, Roland Riek, Tuomas P. J. Knowles, Hilal A. Lashuel, Ehud Gazit, Ian W. Hamley, Thomas P. Davis, Marcus Fa, Matthew R. Chapman, Daniel Erik Otzen, Christopher M. Dobson, David S. Eisenberg, and Raffaele Mezzenga. Half a century of amyloids: past, present and future. *Chemical Society Reviews*, 49:5473–5509, 2020.

[4] Christopher M. Dobson. Protein misfolding, evolution and disease. *Trends in Biochemical Sciences*, 24:329–332, 1999.

[5] Matthew Biancalana and Shohei Koide. Molecular mechanism of Thioflavin-T binding to amyloid fibrils, 2010.

[6] Alexander K. Buell, Céline Galvagnion, Ricardo Gaspar, Emma Sparr, Michele Vendruscolo, Tuomas P.J. Knowles, Sara Linse, and Christopher M. Dobson. Solution conditions determine the relative importance of nucleation and growth processes in α-synuclein aggregation. *Proceedings of the National Academy of Sciences of the United States of America*, 111(21):7671–7676, 2014.

[7] Mattias Tornquist, Thomas C. T. Michaels, Kalyani Sanagavarapu, Xiaoting Yang, George Meisl, Samuel I. A. Cohen, Toumas P. J. Knowles, and Sara Linse. Secondary nucleation in amyloid formation. *Chemical Communications*, 54:8667–8684, 2018.

[8] Alexander J. Dear, Thomas C.T. Michaels, Georg Meisl, David Klenerman, Si Wu, Sarah Perrett, Sara Linse, Christopher M. Dobson, and Tuomas P.J. Knowles. Kinetic diversity of amyloid oligomers. *Proceedings of the National Academy of Sciences of the United States of America*, 117(22):28–31, 2020.

[9] Thomas C.T. Michaels, Andela Šarić, Samo Curk, Katja Bernfur, Paolo Arosio, Georg Meisl, Alexander J. Dear, Samuel I.A. Cohen, Christopher M. Dobson, Michele Vendruscolo, Sara Linse, and Tuomas P.J. Knowles. Dynamics of oligomer populations formed during the aggregation of Alzheimer's Aβ42 peptide. *Nature Chemistry*, 12(5):445–451, 2020.

[10] Alessandra Recchia, Patrizia Debetto, Alessandro Negro, Guido Guidolin, Skaper Stephen D., and Pietro Giusti. α-Synuclein and Parkinson's disease. *The FASEB Journal*, 18(6):617–626, 2004.

[11] Koichi Wakabayashi, Kunikazu Tanji, Fumiaki Mori, and Hitoshi Takahashi. The Lewy body in Parkinson's disease: Molecules implicated in the formation and degradation of α-synuclein aggregates. *Neuropathology*, 27(5):494–506, 2007.

[12] Heiko Braak, Kelly Del Tredici, Udo Rüb, Rob A I De Vos, Ernst N H Jansen Steur, and Eva Braak. Staging of brain pathology related to sporadic Parkinson's disease. *Neurobiology of Aging*, 24(2):197–211, 2003.

[13] Christina M. Lill. Genetics of Parkinson's disease. *Molecular and Cellular Probes*, 30(6):386–396, 2016.

[14] Zhentao Zhang, Seong Su Kang, Xia Liu, Eun Hee Ahn, Zhaohui Zhang, Li He, P. Michael Iuvone, Duc M. Duong, Nicholas T. Seyfried, Matthew J. Benskey, Fredric P. Manfredsson, Lingjing Jin, Yi E. Sun, Jian Zhi Wang, and Keqiang Ye. Asparagine endopeptidase cleaves α-synuclein and mediates pathologic activities in Parkinson's disease. *Nature Structural and Molecular Biology*, 24(8):632–642, 2017.

[15] Julia M. George, Hui Jin, Wendy S. Woods, and David F. Clayton. Characterization of a novel protein regulated during the critical period for song learning in the zebra finch. *Neuron*, 15(2):361–372, 1995.

[16] Benoit I. Giasson, Ian V. J. Murray, John Q. Trojanowski, and Virginia M. Y. Lee. A hydrophobic stretch of 12 amino acid aesidues in the middle of α-synuclein is essential for filament assembly. *Journal of Biological Chemistry*, 276(4):2380–2386, 2001.

[17] Matthew M. Dedmon, Kresten Lindorff-Larsen, John Christodoulou, Michele Vendruscolo, and Christopher M. Dobson. Mapping long-range interactions in α-synuclein using spin-label NMR and ensemble molecular dynamics simulations. *Journal of the American Chemical Society*, 127(2):476–477, 2005.

[18] Jacqueline Burré, Manu Sharma, and Thomas C. Südhof. Cell biology and pathophysiology of α-synuclein. *Cold Spring Harbor Perspectives in Medicine*, 8(3):1–28, 2018.

[19] José D. Camino, Pablo Gracia, Serene W. Chen, Jesús Sot, Igor De La Arada, Víctor Sebastián, José L.R. Arrondo, Félix M. Goñi, Christopher M. Dobson, and Nunilo Cremades. The extent of protein hydration dictates the preference for heterogeneous or homogeneous nucleation generating either parallel or antiparallel β-sheet α-synuclein aggregates. *Chemical Science*, 11(43):11902–11914, 2020.

[20] Kelly A. Conway, Seung-Jae Lee, Jean-Christopher Rochet, Tomas T. Ding, Robin E. Williamson, and Peter T. Lansbury. Acceleration of oligomerization, not fibrillization, is a shared property of both α -synuclein mutations linked to early-onset Parkinson's disease: Implications for pathogenesis and therapy. *Proceedings of the National Academy of Sciences*, 97(2):571–576, 2000.

[21] Ross A. Fredenburg, Carla Rospigliosi, Robin K. Meray, Jeffrey C. Kessler, Hilal A. Lashuel, David Eliezer, and Peter T. Lansbury. The impact of the E46K mutation on the properties of α-synuclein in its monomelic and oligomeric states. *Biochemistry*, 46(24):7107–7118, 2007.

[22] Dhiman Ghosh, Mrityunjoy Mondal, Ganesh M. Mohite, Pradeep K. Singh, Priyatosh Ranjan, A. Anoop, Saikat Ghosh, Narendra Nath Jha, Ashutosh Kumar, and Samir K. Maji. The parkinson's disease-associated H50Q mutation accelerates α-synuclein aggregation in vitro. *Biochemistry*, 52(40):6925–6927, 2013.

[23] Katerina Levitan, David Chereau, Samuel I A Cohen, Tuomas P J Knowles, Christopher M Dobson, Anthony L Fink, John P Anderson, Jason M Goldstein, and Glenn L Millhauser. Conserved C-terminal Charge Exerts a Profound Influence on the Aggregation Rate of α-Synuclein. *Journal of Biological Chemistry*, 411(2):329–333, 2012.

[24] Wolfgang Hoyer, Dmitry Cherny, Vinod Subramaniam, and Thomas M. Jovin. Impact of the acidic C-terminal region comprising amino acids 109-140 on α-synuclein aggregation in vitro. *Biochemistry*, 43(51):16233–16242, 2004.

[25] Ian V.J. Murray, Benoit I. Giasson, Shawn M. Quinn, Vishwanath Koppaka, Paul H. Axelsen, Harry Ischiropoulos, John Q. Trojanowski, and Virginia M.Y. Lee. Role of α-synuclein carboxy-terminus on fibril formation in vitro. *Biochemistry*, 42(28):8530–8540, 2003.

[26] Mohamed Bilal Fares, Nadine Ait-Bouziad, Igor Dikiy, Martial K. Mbefo, Ana Jovičić, Aoife Kiely, Janice L. Holton, Seung Jae Lee, Aaron D. Gitler, David Eliezer, and Hilal A. Lashuel. The novel Parkinson's disease linked mutation G51D attenuates in vitro aggregation and membrane binding of α-synuclein, and enhances its secretion and nuclear localization in cells. *Human Molecular Genetics*, 23(17):4491–4509, 2014.

[27] Céline Galvagnion, Alexander K. Buell, Georg Meisl, Thomas C.T. Michaels, Michele Vendruscolo, Tuomas P.J. Knowles, and Christopher M. Dobson. Lipid vesicles trigger α-synuclein aggregation by stimulating primary nucleation. *Nature Chemical Biology*, 11(3):229–234, 2015.

[28] Patrick Flagmeier, Georg Meisl, Michele Vendruscolo, Tuomas P.J. Knowles, Christopher M. Dobson, Alexander K. Buell, and Céline Galvagnion. Mutations associated with familial Parkinson's disease alter the initiation and amplification steps of α-synuclein aggregation. *Proceedings of the National Academy of Sciences of the United States of America*, 113(37):10328–10333, 2016.

[29] Ingrid M. Van Der Wateren, Tuomas P.J. Knowles, Alexander K. Buell, Christopher M. Dobson, and Céline Galvagnion. C-terminal truncation of α-synuclein promotes amyloid fibril amplification at physiological pH. *Chemical Science*, 9(25):5506–5516, 2018.

[30] Nunilo Cremades, Samuel I A Cohen, Emma Deas, Andrey Y. Abramov, Allen Y. Chen, Angel Orte, Massimo Sandal, Richard W. Clarke, Paul Dunne, Francesco A. Aprile, Carlos W. Bertoncini, Nicholas W. Wood, Tuomas P J Knowles, Christopher M. Dobson, and David Klenerman. Direct observation of the interconversion of normal and toxic forms of α-synuclein. *Cell*, 149(5):1048–1059, 2012.

[31] K. M. Danzer, D. Haasen, A. R. Karow, S. Moussaud, M. Habeck, A. Giese, H. Kretzschmar, B. Hengerer, and M. Kostka. Different Species of alpha-Synuclein Oligomers Induce Calcium Influx and Seeding. *Journal of Neuroscience*, 27(34):9220–9232, 2007.

[32] Laura Pieri, Karine Madiona, and Ronald Melki. Structural and functional properties of prefibrillar α-synuclein oligomers. *Scientific Reports*, 6:24526, 2016.

[33] Laura Pieri, Philippe Chafey, Morgane Le Gall, Guilhem Clary, Ronald Melki, and Virginie Redeker. Cellular response of human neuroblastoma cells to α-synuclein fibrils, the main constituent of Lewy bodies. *Biochimica et Biophysica Acta - General Subjects*, 1860(1):8–19, 2016.

[34] Serene W. Chen, Srdja Drakulic, Emma Deas, Myriam Ouberai, Francesco A. Aprile, Rocío Arranz, Samuel Ness, Cintia Roodveldt, Tim Guilliams, Erwin J. De-Genst, David Klenerman, Nicholas W. Wood, Tuomas P J Knowles, Carlos Alfonso, Germán Rivas, Andrey Y. Abramov, José María Valpuesta, Christopher M. Dobson, and Nunilo Cremades. Structural characterization of toxic oligomers that are kinetically trapped during α-synuclein fibril formation. *Proceedings of the National Academy of Sciences of the United States of America*, 112(16):1994–2003, 2015.

[35] Dagmar E. Ehrnhoefer, Jan Bieschke, Annett Boeddrich, Martin Herbst, Laura Masino, Rudi Lurz, Sabine Engemann, Annalisa Pastore, and Erich E. Wanker. EGCG redirects amyloidogenic polypeptides into unstructured, off-pathway oligomers. *Nature Structural and Molecular Biology*, 15(6):558–566, 2008.

[36] Giuliana Fusco, Serene W. Chen, Philip T. F. Williamson, Roberta Cascella, Michele Perni, James A. Jarvis, Cristina Cecchi, Michele Vendruscolo, Fabrizio Chiti, Nunilo Cremades, Liming Ying, Christopher M. Dobson, and Alfonso De Simone. Structural basis of membrane disruption and cellular toxicity by α-synuclein oligomers. *Science*, 358(6369):1440–1443, 2017.

[37] Roberta Cascella, Michele Perni, Serene W. Chen, Giuliana Fusco, Cristina Cecchi, Michele Vendruscolo, Fabrizio Chiti, Christopher M. Dobson, and Alfonso De Simone. Probing the Origin of the Toxicity of Oligomeric Aggregates of α-Synuclein with Antibodies. *ACS Chemical Biology*, 14(6):1352–1362, 2019.

[38] Plamena R Angelova, Marthe H R Ludtmann, Mathew H Horrocks, Alexander Negoda, Nunilo Cremades, David Klenerman, Christopher M Dobson, Nicholas W Wood, Evgeny V Pavlov, Sonia Gandhi, and Andrey Y Abramov. Ca2+ is a key factor in alpha-synuclein-induced neurotoxicity. *Journal of cell science*, 129(9):1792–1801, 2016.

[39] Jeppe T. Pedersen, Serene W. Chen, Christian B. Borg, Samuel Ness, Justyna M. Bahl, Niels H H Heegaard, Christopher M. Dobson, Lars Hemmingsen, Nunilo Cremades, and Kaare Teilum. Amyloid-β and α-Synuclein Decrease the Level of Metal-Catalyzed Reactive Oxygen Species by Radical Scavenging and Redox Silencing. *Journal of the American Chemical Society*, 138(12):3966–3969, 2016.

[40] Marçal Vilar, Hui-Ting Chou, Thorsten Lührs, Samir K Maji, Dominique Riek-Loher, Rene Verel, Gerard Manning, Henning Stahlberg, and Roland Riek. The

fold of alpha-synuclein fibrils. *Proceedings of the National Academy of Sciences of the United States of America*, 105(25):8637–42, 2008.

[41] Nunilo Cremades, Serene W. Chen, and Christopher M. Dobson. Structural characteristics of α -synuclein oligomers. *Early Stage Protein Misfolding and Amyloid Aggregation*, pages 1–65, 2016.

[42] Luc Bousset, Laura Pieri, Gemma Ruiz-Arlandis, Julia Gath, Poul Henning Jensen, Birgit Habenstein, Karine Madiona, Vincent Olieric, Anja Böckmann, Beat H Meier, and Ronald Melki. Structural and functional characterization of two alpha-synuclein strains. *Nature communications*, 4:2575, 2013.

[43] Brandon B. Holmes, Sarah L. DeVos, Najla Kfoury, Mei Li, Rachel Jacks, Kiran Yanamandra, Mohand O. Ouidja, Frances M. Brodsky, Jayne Marasa, Devika P. Bagchi, Paul T. Kotzbauer, Timothy M. Miller, Dulce Papy-Garcia, and Marc I. Diamond. Heparan sulfate proteoglycans mediate internalization and propagation of specific proteopathic seeds. *Proceedings of the National Academy of Sciences of the United States of America*, 110(33), 2013.

[44] Elisabet Ihse, Hodaka Yamakado, Xander M. Van Wijk, Roger Lawrence, Jeffrey D. Esko, and Eliezer Masliah. Cellular internalization of alpha-synuclein aggregates by cell surface heparan sulfate depends on aggregate conformation and cell type. *Scientific Reports*, 7(1):1–10, 2017.

[45] Amulya Nidhi Shrivastava, Virginie Redeker, Nicolas Fritz, Laura Pieri, Leandro G Almeida, Maria Spolidoro, Thomas Liebmann, Luc Bousset, Marianne Renner, Clément Léna, Anita Aperia, Ronald Melki, and Antoine Triller. alpha-synuclein assemblies sequester neuronal α3-Na/ K -ATPase and impair Na+ gradient Amulya. *The EMBO Journal*, 34(19):2408–2423, 2015.

[46] Xiaobo Mao, Xiling Yin, Yulan Xiong, Preston Ge, George Essien Umanah, Rafaella Araújo Gonçalves, Yu Liang, Shu Zhang, Chen Qi, Sharon Lam, Creg J Workman, Dario A A Vignali, Valina L Dawson, and Han Seok. Pathological α-synuclein transmission initiated by binding lymphocyte-activation gene 3. *Science*, 353(6307):1–33, 2017.

[47] William P. Flavin, Luc Bousset, Zachary C. Green, Yaping Chu, Stratos Skarpathiotis, Michael J. Chaney, Jeffrey H. Kordower, Ronald Melki, and Edward M. Campbell. Endocytic vesicle rupture is a conserved mechanism of cellular invasion by amyloid proteins. *Acta Neuropathologica*, 134(4):629–653, 2017.

[48] Laura A. Volpicelli-Daley, Kelvin C. Luk, Tapan P. Patel, Selcuk A. Tanik, Dawn M. Riddle, Anna Stieber, David F. Meaney, John Q. Trojanowski, and Virginia M.Y. Lee. Exogenous α-Synuclein Fibrils Induce Lewy Body Pathology Leading to Synaptic Dysfunction and Neuron Death. *Neuron*, 72(1):57–71, 2011.

[49] Kelvin C. Luk, Dustin J. Covell, Victoria M. Kehm, Bin Zhang, Insung Y. Song, Matthew D. Byrne, Rose M. Pitkin, Samantha C. Decker, John Q. Trojanowski, and Virginia M.-Y. Lee. Molecular and Biological Compatibility with Host Alpha-Synuclein Influences Fibril Pathogenicity. *Cell Reports*, 16(12):3373–3387, 2016.

[50] Patrik Brundin, Ronald Melki, and Ron Kopito. Prion'like transmission of protein aggregates inneurodegenerative diseases. *Nature Reviews Molecular Cell Biology*, 11(April):301–307, 2010.

[51] Airi Tarutani, Genjiro Suzuki, Aki Shimozawa, Takashi Nonaka, Haruhiko Akiyama, Shin Ichi Hisanaga, and Masato Hasegawa. The effect of fragmented pathogenic α-synuclein seeds on prion-like propagation. *Journal of Biological Chemistry*, 291(36):18675–18688, 2016.

[52] Simona Gribaudo, Philippe Tixador, Luc Bousset, Alexis Fenyi, Patricia Lino, Ronald Melki, Jean Michel Peyrin, and Anselme L. Perrier. Propagation of α-Synuclein Strains within Human Reconstructed Neuronal Network. *Stem Cell Reports*, 12(2):230–244, 2019.

[53] Katrina L. Paumier, Kelvin C. Luk, Fredric P. Manfredsson, Nicholas M. Kanaan, Jack W. Lipton, Timothy J. Collier, Kathy Steece-Collier, Christopher J. Kemp, Stephanie Celano, Emily Schulz, Ivette M. Sandoval, Sheila Fleming, Elliott Dirr, Nicole K. Polinski, John Q. Trojanowski, Virginia M. Lee, and Caryl E. Sortwell. Intrastriatal injection of pre-formed mouse α-synuclein fibrils into rats triggers α-synuclein pathology and bilateral nigrostriatal degeneration. *Neurobiology of Disease*, 82:185–199, 2015.

[54] Pablo Gracia, José D. Camino, Laura Volpicelli-Daley, and Nunilo Cremades. Multiplicity of α-synuclein aggregated species and their possible roles in disease. *International Journal of Molecular Sciences*, 21(21):1–27, 2020.

[55] Francesco Simone Ruggeri, Patrick Flagmeier, Janet R. Kumita, Georg Meisl, Dimitri Y. Chirgadze, Marie N. Bongiovanni, Tuomas P.J. Knowles, and Christopher M. Dobson. The Influence of Pathogenic Mutations in α-Synuclein on Biophysical and Structural Characteristics of Amyloid Fibrils. *ACS Nano*, 14(5):5213–5222, 2020.

[56] Wouter Peelaerts, Luc Bousset, Anke Van Der Perren, A. Moskalyuk, R. Pulizzi, M. Giugliano, Chris Van Den Haute, Ronald Melki, and Veerle Baekelandt. α-Synuclein strains cause distinct synucleinopathies after local and systemic administration. *Nature*, 522(7556):340–344, 2015.

[57] Anke Van der Perren, Géraldine Gelders, Alexis Fenyi, Luc Bousset, Filipa Brito, Wouter Peelaerts, Chris Van den Haute, Steve Gentleman, Ronald Melki, and Veerle Baekelandt. The structural differences between patient-derived α-synuclein strains dictate characteristics of Parkinson's disease, multiple system atrophy and dementia with Lewy bodies. *Acta Neuropathologica*, 139(6):977–1000, 2020.

[58] Mohammad Shahnawaz, Abhisek Mukherjee, Sandra Pritzkow, Nicolas Mendez, Prakruti Rabadia, Xiangan Liu, Bo Hu, Ann Schmeichel, Wolfgang Singer, Gang Wu, Ah Lim Tsai, Hamid Shirani, K. Peter R. Nilsson, Phillip A. Low, and Claudio Soto. Discriminating α-synuclein strains in Parkinson's disease and multiple system atrophy. *Nature*, 578(7794):273–277, 2020.

[59] Timo Strohäker, Byung Chul Jung, Shu Hao Liou, Claudio O. Fernandez, Dietmar Riedel, Stefan Becker, Glenda M. Halliday, Marina Bennati, Woojin S. Kim, Seung Jae Lee, and Markus Zweckstetter. Structural heterogeneity of α-synuclein fibrils amplified from patient brain extracts. *Nature Communications*, 10(1):1–12, 2019.

[60] Amanda L. Woerman, Jan Stöhr, Atsushi Aoyagi, Ryan Rampersaud, Zuzana Krejciova, Joel C. Watts, Takao Ohyama, Smita Patel, Kartika Widjaja, Abby Oehler, David W. Sanders, Marc I. Diamond, William W. Seeley, Lefkos T. Middleton, Steve M. Gentleman, Daniel A. Mordes, Thomas C. Südhof, Kurt Giles, and Stanley B. Prusiner. Propagation of prions causing synucleinopathies in cultured cells. *Proceedings of the National Academy of Sciences of the United States of America*, 112(35):4949–4958, 2015.

[61] Manuel Schweighauser, Yang Shi, Airi Tarutani, Fuyuki Kametani, and Alexey G Murzin. Structures of α -Synuclein Filaments from Multiple System Atrophy. *Nature*, 585(7825):464–469, 2020.

[62] Bjorn H Falkenburger, Theodora Saridaki, and Elisabeth Dinter. Cellular models for Parkinson's disease. *Journal of Neurochemistry*, pages 121–130, 2016.

[63] Bjorn H. Falkenburger and Jörg B. Schulz. Limitations of cellular models in Parkinson's disease research. *Journal of neural transmission. Supplementum*, (70):261–268, 2006.

[64] Silvia Campioni, Benedetta Mannini, Mariagioia Zampagni, Anna Pensalfini, Claudia Parrini, Elisa Evangelisti, Annalisa Relini, Massimo Stefani, Christopher M. Dobson, Cristina Cecchi, and Fabrizio Chiti. A causative link between the structure of aberrant protein oligomers and their toxicity. *Nature Chemical Biology*, 6(2):140–147, 2010.

[65] Janin Lautenschläger, Sara Wagner-Valladolid, Amberley D. Stephens, Ana Fernández-Villegas, Colin Hockings, Ajay Mishra, James D. Manton, Marcus J. Fantham, Meng Lu, Eric J. Rees, Clemens F. Kaminski, and Gabriele S. Kaminski Schierle. Intramitochondrial proteostasis is directly coupled to α-synuclein and amyloid β1-42 pathologies. *The Journal of biological chemistry*, 295(30):10138–10152, 2020.

[66] Xuping Li, Yunlan Du, Xiaolan Fan, Dehua Yang, Guangrui Luo, and Weidong Le. C-Jun N-Terminal kinase mediates lactacystin-induced dopamine neuron degeneration. *Journal of Neuropathology and Experimental Neurology*, 67(10):933–944, 2008.

[67] Laura A. Volpicelli-Daley, Kelvin C. Luk, and Virginia M-Y. Lee. Addition of exogenous α-synuclein preformed fibrils to primary neuronal cultures to seed recruitment of endogenous α-synuclein to Lewy body and Lewy neuriteâ€“like aggregates. *Nature Protocols*, 9(9):2135–2146, 2014.

[68] Qihui Wu, Hajime Takano, Dawn M. Riddle, John Q. Trojanowski, Douglas A. Coulter, and Virginia M.Y. Lee. α-Synuclein (αsyn) preformed fibrils induce endogenous αsyn aggregation, compromise synaptic activity and enhance synapse loss in cultured excitatory hippocampal neurons. *Journal of Neuroscience*, 39(26):5080–5094, 2019.

[69] Diego Grassi, Shannon Howard, Minghai Zhou, Natalia Diaz-Perez, Nicolai T. Urban, Debbie Guerrero-Given, Naomi Kamasawa, Laura A. Volpicelli-Daley, Philip LoGrasso, and Corinne Ida Lasmézas. Identification of a highly neurotoxic α-synuclein species inducing mitochondrial damage and mitophagy in Parkinson's disease. *Proceedings of the National Academy of Sciences of the United States of America*, 115(11):2634–2643, 2018.

[70] Kazutoshi Takahashi and Shinya Yamanaka. Induction of Pluripotent Stem Cells from Mouse Embryonic and Adult Fibroblast Cultures by Defined Factors. *Cell*, 126(4):663–676, 2006.

[71] Elizabeth M. Hartfield, Michiko Yamasaki-Mann, Hugo J. Ribeiro Fernandes, Jane Vowles, William S. James, Sally A. Cowley, and Richard Wade-Martins. Physiological characterisation of human iPS-derived dopaminergic neurons. *PLoS ONE*, 9(2), 2014.

[72] Federico Zambon, Marta Cherubini, Hugo J.R. Fernandes, Charmaine Lang, Brent J. Ryan, Viola Volpato, Nora Bengoa-Vergniory, Siv Vingill, Moustafa Attar, Heather D.E. Booth, Walther Haenseler, Jane Vowles, Rory Bowden, Caleb Webber, Sally A. Cowley, and Richard Wade-Martins. Cellular α-synuclein pathology is associated with bioenergetic dysfunction in Parkinson's iPSC-derived dopamine neurons. *Human Molecular Genetics*, 28(12):2001–2013, 2019.

[73] Laura A. Volpicelli-Daley, Deniz Kirik, Lindsay E. Stoyka, David G. Standaert, and Ashley S. Harms. How can rAAV-alpha-synuclein and the fibril alpha-synuclein models advance our understanding of Parkinson's disease? *Journal of Neurochemistry*, 139:131–155, 2016.

[74] Marie-François Chesselet, Sheila Fleming, and Farzad Mortazavi. Strengths and limitations of genetic mouse models of Parkinson's disease. *Parkinsonism & related*, 14(Suppl 2):1–5, 2008.

[75] C. Equence Sequencing Consortium. Genome sequence of the nematode C. elegans: A platform for investigating biology. *Science*, 282(5396):2012–2018, 1998.

[76] J. G. White, E Southgate, J.N. Thomson, and S. Brenner. The structure of the nervous system of the nematode Caenorhabitis elegans. *Philosophical Transactions of the Royal Society of London*, 314:1–340, 1986.

[77] Ludivine S. Breger and Marie T. Fuzzati Armentero. Genetically engineered animal models of Parkinson's disease: From worm to rodent. *European Journal of Neuroscience*, 49(4):533–560, 2019.

[78] Merja Lakso, Suvi Vartiainen, Anu Maarit Moilanen, Jouni Sirviö, James H. Thomas, Richard Nass, Randy D. Blakely, and Garry Wong. Dopaminergic neuronal loss and motor deficits in Caenorhabditis elegans overexpressing human α-synuclein. *Journal of Neurochemistry*, 86(1):165–172, 2003.

[79] Tjakko J. Van Ham, Karen L. Thijssen, Rainer Breitling, Robert M.W. Hofstra, Ronald H.A. Plasterk, and Ellen A.A. Nollen. C. elegans model identifies genetic modifiers of α-synuclein inclusion formation during aging. *PLoS Genetics*, 4(3), 2008.

[80] Michele Perni, Céline Galvagnion, Alexander Maltsev, Georg Meisl, Martin B.D. Müller, Pavan K. Challa, Julius B. Kirkegaard, Patrick Flagmeier, Samuel I.A. Cohen, Roberta Cascella, Serene W. Chen, Ryan Limboker, Pietro Sormanni, Gabriella T. Heller, Francesco A. Aprile, Nunilo Cremades, Cristina Cecchi, Fabrizio Chiti, Ellen A.A. Nollen, Tuomas P.J. Knowles, Michele Vendruscolo, Adriaan Bax, Michael Zasloff, and Christopher M. Dobson. A natural product inhibits the initiation of α-synuclein aggregation & suppresses its toxicity. *Proceedings of the National Academy of Sciences of the United States of America*, 114(6):E1009–E1017, 2017.

[81] Zhiyin Xun, Renã A. Sowell, Thomas C. Kaufman, and David E. Clemmer. A Drosophila Model of Parkinson's Disease. *Nature Reviews Neurology*, 404(March):47405, 2000.

[82] Wolfdieter Springer and Philipp J. Kahle. Mechanisms and models of α-synuclein-related neurodegeneration. *Current Neurology and Neuroscience Reports*, 6(5):432–436, 2006.

[83] Robert G. Pendleton, Feroz Parvez, Marwa Sayed, and Ralph Hillman. Effects of pharmacological agents upon a transgenic model of Parkinson's disease in Drosophila melanogaster. *Journal of Pharmacology and Experimental Therapeutics*, 300(1):91–96, 2002.

[84] Kyohei Kin, Takao Yasuhara, Masahiro Kameda, and Isao Date. Animal models for Parkinson's disease research: Trends in the 2000s. *International Journal of Molecular Sciences*, 20(21), 2019.

[85] Philipp J. Kahle. α-Synucleinopathy models and human neuropathology: Similarities and differences. *Acta Neuropathologica*, 115(1):87–95, 2008.

[86] Marie-Francoise Chesselet. In vivo alpha-synuclein overexpression in rodents: A useful model of Parkinson's disease? *Experimental Neurology*, 209(1):22–27, 2008.

[87] Naomi P. Visanji, Jonathan M. Brotchie, Lorraine V. Kalia, James B. Koprich, Anurag Tandon, Joel C. Watts, and Anthony E. Lang. α-Synuclein-Based Animal Models of Parkinson's Disease: Challenges and Opportunities in a New Era. *Trends in Neurosciences*, 39(11):750–762, 2016.

[88] Hodaka Yamakado, Yasuhiro Moriwaki, Nobuyuki Yamasaki, Tsuyoshi Miyakawa, Junko Kurisu, Kengo Uemura, Haruhisa Inoue, Makio Takahashi, and Ryosuke Takahashi. α-Synuclein BAC transgenic mice as a model for Parkinson's disease

manifested decreased anxiety-like behavior and hyperlocomotion. *Neuroscience Research*, 73(2):173–177, 2012.

[89] Diana M. Hendrickx, Pierre Garcia, Amer Ashrafi, Alessia Sciortino, Kristopher J. Schmit, Heike Kollmus, Nathalie Nicot, Tony Kaoma, Laurent Vallar, Manuel Buttini, and Enrico Glaab. A New Synuclein-Transgenic Mouse Model for Early Parkinson's Reveals Molecular Features of Preclinical Disease. *Molecular Neurobiology*, 58(2):576–602, 2021.

[90] Nicola J. Rutherford, Amanda N. Sacino, Mieu Brooks, Carolina Ceballos-Diaz, Thomas B. Ladd, Jasie K. Howard, Todd E. Golde, and Benoit I. Giasson. Studies of lipopolysaccharide effects on the induction of α-synuclein pathology by exogenous fibrils in transgenic mice. *Molecular neurodegeneration*, 10:32, 2015.

[91] Lijuan Kang, Kuen Phon Wu, Michele Vendruscolo, and Jean Baum. The A53T mutation is key in defining the differences in the aggregation kinetics of human and mouse α-synuclein. *Journal of the American Chemical Society*, 133(34):13465–13470, 2011.

[92] Mohamed-Bilal Fares, Bohumil Maco, Abid Oueslati, Edward Rockenstein, Natalia Ninkina, Vladimir L. Buchman, Eliezer Masliah, and Hilal A. Lashuel. Induction of de novo α-synuclein fibrillization in a neuronal model for Parkinson's disease. *Proceedings of the National Academy of Sciences of the United States of America*, 113(7):912–933, 2016.

[93] Pérola O. Magalhães, André M. Lopes, Priscila G. Mazzola, Carlota Rangel-yagui, and Thereza C. V. Penna. Methods of endotoxin removal from biological preparations : a review. *Journal of Pharmacy and Pharmaceutical Sciences*, 10(3):388–404, 2007.

[94] Hui Ming Gao, Feng Zhang, Hui Zhou, Wayneho Kam, Belinda Wilson, and Jau Shyong Hong. Neuroinflammation and α-synuclein dysfunction potentiate each other, driving chronic progression of neurodegeneration in a mouse model of Parkinson's disease. *Environmental Health Perspectives*, 119(6):807–814, 2011.

[95] Hui-ming Gao, Paul T Kotzbauer, Kunihiro Uryu, Susan Leight, Q John, and Virginia M Lee. Neuroinflamation and oxidation/nitration of α-synuclein linked to dopaminergic neurodegeneration. *Journal of Neuroscience*, 28(30):7687–7698, 2008.

[96] Benedetta Mannini, Johnny Habchi, Sean Chia, Francesco S. Ruggeri, Michele Perni, Tuomas P.J. Knowles, Christopher M. Dobson, and Michele Vendruscolo. Stabilization and Characterization of Cytotoxic Aβ 40 Oligomers Isolated from an Aggregation Reaction in the Presence of Zinc Ions. *ACS Chemical Neuroscience*, 9(12):2959–2971, 2018.

[97] Christine L. Hagan, Russell J.K. Johnson, Anne Dhulesia, Mireille Dumoulin, Janice Dumont, Erwin De Genst, John Christodoulou, Carol V. Robinson, Christopher M. Dobson, and Janet R. Kumita. A non-natural variant of human lysozyme (I59T) mimics the in vitro behaviour of the I56T variant that is responsible for a form of familial amyloidosis. *Protein Engineering, Design and Selection*, 23(7):499–506, 2010.

[98] Richard J. Karpowicz, Conor M. Haney, Tiberiu S. Mihaila, Raizel M. Sandler, E. James Petersson, and Virginia M.Y. Lee. Selective imaging of internalized proteopathic α-synuclein seeds in primary neurons reveals mechanistic insight into transmission of synucleinopathies. *Journal of Biological Chemistry*, 292(32):13482–13497, 2017.

[99] Tatsuya Ikenoue, Young Ho Lee, Jõzsef Kardos, Miyu Saiki, Hisashi Yagi, Yasushi Kawata, and Yuji Goto. Cold denaturation of α-synuclein amyloid fibrils. *Angewandte Chemie - International Edition*, 53(30):7799–7804, 2014.

[100] Nicole K. Polinski, Laura A. Volpicelli-Daley, Caryl E. Sortwell, Kelvin C. Luk, Nunilo Cremades, Lindsey M. Gottler, Jessica Froula, Megan F. Duffy, Virginia M.Y. Lee, Terina N. Martinez, and Kuldip D. Dave. Best practices for generating and using alpha-synuclein pre-formed fibrils to model Parkinson's disease in rodents. *Journal of Parkinson's Disease*, 8(2):303–322, 2018.

[101] Serene W. Chen and Nunilo Cremades. Preparation of α-synuclein amyloid assemblies for toxicity experiments. *Methods in Molecular Biology*, 1779:45–60, 2018.

[102] Jessica M. Froula, Marta Castellana-Cruz, Nadia M. Anabtawi, José D. Camino, Serene W. Chen, Drake R. Thrasher, Jennifer Freire, Allen A. Yazdi, Sheila Fleming, Christopher M. Dobson, Janet R. Kumita, Nunilo Cremades, and Laura A. Volpicelli-Daley. Defining α-synuclein species responsible for Parkinson's disease phenotypes in mice. *Journal of Biological Chemistry*, 294(27):10392–10406, 2019.

[103] Senthil T. Kumar, Somanath Jagannath, Cindy Francois, Hugo Vanderstichele, Erik Stoops, and Hilal A. Lashuel. How specific are the conformation-specific α-synuclein antibodies? Characterization and validation of 16 α-

synuclein conformation-specific antibodies using well-characterized preparations of α-synuclein monomers, fibrils and oligomers with distinct structures and morphology. *Neurobiology of Disease*, 146:105086, 2020.

[104] Hideo Fujiwara, Masato Hasegawa, Naoshi Dohmae, Akiko Kawashima, Eliezer Masliah, Matthew S Goldberg, Jie Shen, Koji Takio, and Takeshi Iwatsubo. α-Synuclein is phosphorylated in synucleinopathy lesions. *Nature Cell Biology*, 4(2):160–164, 2002.

[105] William E. Arter, Catherine K. Xu, Marta Castellana-Cruz, Therese W. Herling, Georg Krainer, Kadi L. Saar, Janet R. Kumita, Christopher M. Dobson, and Tuomas P. J. Knowles. Rapid Structural, Kinetic, and Immunochemical Analysis of Alpha- Synuclein Oligomers in Solution. *ACS Nano Letters*, 20(11):8163–8169, 2020.

[106] Emily R. Dirr, Osunde R. Ekhator, Rachel Blackwood, John G. Holden, Eliezer Masliah, Patrick J. Schultheis, and Sheila M. Fleming. Exacerbation of sensorimotor dysfunction in mice deficient in Atp13a2 and overexpressing human wildtype alpha-synuclein. *Behavioural Brain Research*, 343:41–49, 2018.

[107] Joseph R. Patterson, Nicole K. Polinski, Megan F. Duffy, Christopher J. Kemp, Kelvin C. Luk, Laura A. Volpicelli-Daley, Nicholas M. Kanaan, and Caryl E. Sortwell. Generation of alpha-synuclein preformed fibrils from monomers and use in vivo. *Journal of Visualized Experiments*, 2019(148):1–10, 2019.

[108] Vedad Delic, Sidhanth Chandra, Hisham Abdelmotilib, Tyler Maltbie, Shijie Wang, Danielle Kem, Hunter J. Scott, Rachel N. Underwood, Zhiyong Liu, Laura A. Volpicelli-Daley, and Andrew B. West. Sensitivity and specificity of phospho-Ser129 α-synuclein monoclonal antibodies. *Journal of Comparative Neurology*, 526(12):1978–1990, 2018.

[109] Nicola J. Rutherford, Mieu Brooks, and Benoit I. Giasson. Novel antibodies to phosphorylated α-synuclein serine 129 and NFL serine 473 demonstrate the close molecular homology of these epitopes. *Acta neuropathologica communications*, 4(1):80, 2016.

[110] Weixing X. Pan, Tianyi Mao, and Joshua T. Dudman. Inputs to the dorsal striatum of the mouse reflect the parallel circuit architecture of the forebrain. *Frontiers in Neuroanatomy*, 4(DEC):1–14, 2010.

[111] Karina J. Vargas, Nikolas Schrod, Taylor Davis, Ruben Fernandez-Busnadiego, Yumiko V. Taguchi, Ulrike Laugks, Vladan Lucic, and Sreeganga S. Chandra. Synucleins Have Multiple Effects on Presynaptic Architecture. *Cell Reports*, 18(1):161–173, 2017.

[112] Kelvin C. Luk, Victoria Kehm, Jenna Carroll, Bin Zhang, Patrick O. Brien, John Q. Trojanowski, and Virginia M. Lee. Pathological in Nontransgenic MicePathological α -Synuclein Transmission Initiates Parkinson-like Neurodegeneration in Nontransgenic Mice. *Science*, 338:949–954, 2012.

[113] N Ogawa, Y Hirose, S Ohara, T Ono, and Y Watanabe. A simple quantitative bradykinesia test in MPTP-treated mice. *Research communications in chemical pathology and pharmacology*, 50(3):435–441, dec 1985.

[114] Emma Deas, Nunilo Cremades, Plamena R. Angelova, Marthe H. R. Ludtmann, Zhi Yao, Serene Chen, Mathew H. Horrocks, Blerida Banushi, Daniel Little, Michael J. Devine, Paul Gissen, David Klenerman, Christopher M. Dobson, Nicholas W. Wood, Sonia Gandhi, and Andrey Y. Abramov. Alpha-Synuclein Oligomers Interact with Metal Ions to Induce Oxidative Stress and Neuronal Death in Parkinson's Disease. *Antioxidants & redox signaling*, 24(7):376–391, 2016.

[115] Beate Winner, Roberto Jappelli, Samir K. Maji, Paula A. Desplats, Leah Boyer, Stefan Aigner, Claudia Hetzer, Thomas Loher, Marçal Vilar, Silvia Campioni, Christos Tzitzilonis, Alice Soragni, Sebastian Jessberger, Helena Mira, Antonella Consiglio, Emiley Pham, Eliezer Masliah, Fred H. Gage, and Roland Riek. In vivo demonstration that α-synuclein oligomers are toxic. *Proceedings of the National Academy of Sciences of the United States of America*, 108(10):4194–4199, 2011.

[116] Roberta Cascella, Serene W. Chen, Alessandra Bigi, José D. Camino, Catherine K. Xu, Christopher M. Dobson, Fabrizio Chiti, Nunilo Cremades, and Cristina Cecchi. The release of toxic oligomers from α-synuclein fibrils induces dysfunction in neuronal cells. *Nature Communications*, 12(1):1–16, 2021.

[117] Asa Abeliovich, Yvonne Schmitz, Isabel Fariñ, Derek Choi-Lundberg, Wei-Hsien Ho, Pablo E. Castillo, Natasha Shinsky, Jose Manuel, Garcia Verdugo, Mark Armanini, Anne Ryan, Mary Hynes, and Heidi Phillips. Mice Lacking α-Synuclein Display Functional Deficits in the Nigrostriatal Dopamine System. *Neuron*, 25:239–252, 2000.

[118] Alevtina D. Zharikov, Jason R. Cannon, Victor Tapias, Qing Bai, Max P. Horowitz, Vipul Shah, Amina El Ayadi, Teresa G. Hastings, J. Timothy Greenamyre, and

Edward A. Burton. ShRNA targeting α-synuclein prevents neurodegeneration in a Parkinson's disease model. *Journal of Clinical Investigation*, 125(7):2721–2735, 2015.

[119] Andreas Weihofen, Yu Ting Liu, Joseph W. Arndt, Christian Huy, Chao Quan, Benjamin A. Smith, Jean Luc Baeriswyl, Nicole Cavegn, Luzia Senn, Lihe Su, Galina Marsh, Pavan K. Auluck, Fabio Montrasio, Roger M. Nitsch, Warren D. Hirst, Jesse M. Cedarbaum, R. Blake Pepinsky, Jan Grimm, and Paul H. Weinreb. Development of an aggregate-selective, human-derived α-synuclein antibody BIIB054 that ameliorates disease phenotypes in Parkinson's disease models. *Neurobiology of Disease*, 124:276–288, 2019.

[120] Giuliana Fusco, Alfonso De Simone, Tata Gopinath, Vitaly Vostrikov, Michele Vendruscolo, Christopher M. Dobson, and Gianluigi Veglia. Direct observation of the three regions in α-synuclein that determine its membrane-bound behaviour. *Nature Communications*, 5:1–8, 2014.

[121] David Snead and David Eliezer. Alpha-Synuclein Function and Dysfunction on Cellular Membranes. *Experimental Neurobiology*, 23(4):292–313, 2014.

[122] Pavan K. Auluck, Gabriela Caraveo, and Susan Lindquist. α-Synuclein: Membrane interactions and toxicity in parkinson's disease. *Annual Review of Cell and Developmental Biology*, 26:211–233, 2010.

[123] Benedetta Mannini, Estefania Mulvihill, Caterina Sgromo, Roberta Cascella, Reza Khodarahmi, Matteo Ramazzotti, Christopher M. Dobson, Cristina Cecchi, and Fabrizio Chiti. Toxicity of protein oligomers is rationalized by a function combining size and surface hydrophobicity. *ACS Chemical Biology*, 9(10):2309–2317, 2014.

[124] Laura Tosatto, Mathew H Horrocks, Alexander J Dear, Tuomas P J Knowles, Mauro Dalla Serra, Nunilo Cremades, Christopher M Dobson, and David Klenerman. Single-molecule FRET studies on alpha-synuclein oligomerization of Parkinson's disease genetically related mutants. *Scientific reports*, 5:16696, 2015.

[125] Nikolai Lorenzen, Søren Bang Nielsen, Alexander K. Buell, Jørn Døvling Kaspersen, Paolo Arosio, Brian Stougaard Vad, Wojciech Paslawski, Gunna Christiansen, Zuzana Valnickova-Hansen, Maria Andreasen, Jan J. Enghild, Jan Skov Pedersen, Christopher M. Dobson, Tuomas P.J. Knowles, and Daniel Erik Otzen. The role of stable α-synuclein oligomers in the molecular events underlying amyloid formation. *Journal of the American Chemical Society*, 136(10):3859–3868, 2014.

[126] Wojciech Paslawski, Simon Mysling, Karen Thomsen, Thomas J.D. Jørgensen, and Daniel E. Otzen. Co-existence of two different α-synuclein oligomers with different core structures determined by hydrogen/deuterium exchange mass spectrometry. *Angewandte Chemie - International Edition*, 53(29):7560–7563, 2014.

[127] Ciarán Manus Maguire, Matthias Rösslein, Peter Wick, and Adriele Prina-Mello. Characterisation of particles in solution a perspective on light scattering and comparative technologies. *Science and Technology of Advanced Materials*, 19(1):732–745, 2018.

[128] Michael V. Berridge, Patries M. Herst, and An S. Tan. Tetrazolium dyes as tools in cell biology: New insights into their cellular reduction. *Biotechnology Annual Review*, 11(SUPPL.):127–152, 2005.

[129] Rakez Kayed and Cristian A. Lasagna-Reeves. Molecular mechanisms of amyloid oligomers toxicity. *Journal of Alzheimer's Disease*, 33(SUPPL. 1), 2013.

[130] Benedetta Mannini, Roberta Cascella, Mariagioia Zampagni, Maria Van Waarde-Verhagen, Sarah Meehan, Cintia Roodveldt, Silvia Campioni, Matilde Boninsegna, Amanda Penco, Annalisa Relini, Harm H. Kampinga, Christopher M. Dobson, Mark R. Wilson, Cristina Cecchi, and Fabrizio Chiti. Molecular mechanisms used by chaperones to reduce the toxicity of aberrant protein oligomers. *Proceedings of the National Academy of Sciences of the United States of America*, 109(31):12479–12484, 2012.

[131] Yoko Oma, Yoshihiro Kino, Noboru Sasagawa, and Shoichi Ishiura. Comparative analysis of the cytotoxicity of homopolymeric amino acids. *Biochimica et Biophysica Acta - Proteins and Proteomics*, 1748(2):174–179, 2005.

[132] Benedetta Bolognesi, Janet R. Kumita, Teresa P. Barros, Elin K. Esbjorner, Leila M. Luheshi, Damian C. Crowther, Mark R. Wilson, Christopher M. Dobson, Giorgio Favrin, and Justin J. Yerbury. ANS binding reveals common features of cytotoxic amyloid species. *ACS Chemical Biology*, 5(8):735–740, 2010.

[133] Anja N.D. Stefanovic, Saskia Lindhoud, Slav A. Semerdzhiev, Mireille M.A.E. Claessens, and Vinod Subramaniam. Oligomers of Parkinson's disease-related α-synuclein mutants have similar structures but distinctive membrane permeabilization properties. *Biochemistry*, 54(20):3142–3150, 2015.

[134] András Micsonai, Frank Wien, Éva Bulyáki, Judit Kun, Éva Moussong, Young Ho Lee, Yuji Goto, Matthieu Réfrégiers, and József Kardos. BeStSel: A web server

for accurate protein secondary structure prediction and fold recognition from the circular dichroism spectra. *Nucleic Acids Research*, 46(W1):315–322, 2018.

[135] András Micsonai, Frank Wien, Linda Kernya, Young Ho Lee, Yuji Goto, Matthieu Réfrégiers, and József Kardos. Accurate secondary structure prediction and fold recognition for circular dichroism spectroscopy. *Proceedings of the National Academy of Sciences of the United States of America*, 112(24):3095–3103, 2015.

[136] Mirella Vivoli Vega, Roberta Cascella, Serene W. Chen, Giuliana Fusco, Alfonso De Simone, Christopher M. Dobson, Cristina Cecchi, and Fabrizio Chiti. The Toxicity of Misfolded Protein Oligomers Is Independent of Their Secondary Structure. *ACS Chemical Biology*, 14(7):1593–1600, 2019.

[137] Dhiman Ghosh, Pradeep K. Singh, Shruti Sahay, Narendra Nath Jha, Reeba S. Jacob, Shamik Sen, Ashutosh Kumar, Roland Riek, and Samir K. Maji. Structure based aggregation studies reveal the presence of helix-rich intermediate during α-Synuclein aggregation. *Scientific Reports*, 5:1–15, 2015.

[138] Mihaela M. Apetri, Nakul C. Maiti, Michael G. Zagorski, Paul R. Carey, and Vernon E. Anderson. Secondary structure of α-synuclein oligomers: Characterization by Raman and atomic force microscopy. *Journal of Molecular Biology*, 355(1):63–71, 2006.

[139] Nir Salinas, Jacques Philippe Colletier, Asher Moshe, and Meytal Landau. Extreme amyloid polymorphism in Staphylococcus aureus virulent PSMα peptides. *Nature Communications*, 9(1), 2018.

[140] Eniav Tayeb-Fligeman, Orly Tabachnikov, Asher Moshe, Orit Goldsmidt-Tran, Michael R. Sawaya, Nicolas Coquelle, Jacques-Philippe Colletier, and Maytal Landau. The cytotoxic Staphylococcus aureus PSMα3 reveals a cross-α amyloid-like fibril. *Science*, 176(3):139–148, 2017.

[141] Ravit Malishev, Einav Tayeb-Fligelman, Shimrit David, Michael M. Meijler, Meytal Landau, and Raz Jelinek. Reciprocal Interactions between Membrane Bilayers and S. aureus PSMα3 Cross-α Amyloid Fibrils Account for Species-Specific Cytotoxicity. *Journal of Molecular Biology*, 430(10):1431–1441, 2018.

[142] Marina D. Kirkitadze, Margaret M. Condron, and David B. Teplow. Identification and characterization of key kinetic intermediates in amyloid β-protein fibrillogenesis. *Journal of Molecular Biology*, 312(5):1103–1119, 2001.

[143] Carole Anne De Carufel, Noé Quittot, Phuong Trang Nguyen, and Steve Bourgault. Delineating the Role of Helical Intermediates in Natively Unfolded Polypeptide Amyloid Assembly and Cytotoxicity. *Angewandte Chemie - International Edition*, 54(48):14383–14387, 2015.

[144] Andisheh Abedini and Daniel P. Raleigh. A Role For Helical Intermediates in Amyloid Formation By Natively Unfolded Polypeptides? *Phisical Biology*, 23(1):1–7, 2008.

[145] Ruxi Qi, Yin Luo, Ruth Nissinov, and Gunghong Wei. Conformational Distribution and α-Helix to β-Sheet Transition of Human Amylin Fragment Dimer. *Biomacromolecules*, 176(3):139–148, 2014.

[146] Minghai Zhou, Gregory Ottenberg, Gian Franco Sferrazza, and Corinne Ida Lasmeźas. Highly neurotoxic monomeric α-helical prion protein. *Proceedings of the National Academy of Sciences of the United States of America*, 109(8):3113–3118, 2012.

[147] David R. Boyer, Binsen Li, Chuanqui Sun, Weija Fan, Michael R. Sawaya, Lin Jiang, and David S Eisenberg. Structures of fibrils formed by α-synuclein hereditary disease mutant H50Q reveal new polymorphs. *Nature*, 26(11):1044–1052, 2019.

[148] Roland Riek and David S. Eisenberg. The activities of amyloids from a structural perspective. *Nature*, 539(7628):227–235, 2016.

[149] Nikolai Lorenzen, Lasse Lemminger, Jannik Nedergaard Pedersen, Søren Bang Nielsen, and Daniel Erik Otzen. The N-terminus of α-synuclein is essential for both monomeric and oligomeric interactions with membranes. *FEBS Letters*, 588(3):497–502, 2014.

[150] Tae In Kam, Xiaobo Mao, Hyejin Park, Shih Ching Chou, Senthilkumar S. Karuppagounder, George Essien Umanah, Seung Pil Yun, Saurav Brahmachari, Nikhil Panicker, Rong Chen, Shaida A. Andrabi, Chen Qi, Guy G. Poirier, Olga Pletnikova, Juan C. Troncoso, Lynn M. Bekris, James B. Leverenz, Alexander Pantelyat, Han Seok Ko, Liana S. Rosenthal, Ted M. Dawson, and Valina L. Dawson. Poly(ADP-ribose) drives pathologic a-synuclein neurodegeneration in Parkinson's disease. *Science*, 362(6414), 2018.

[151] Farid Rahimi, Panchanan Maiti, and Gal Bitan. Photo-induced cross-linking of unmodified proteins (PICUP) applied to amyloidogenic peptides. *Journal of Visualized Experiments*, (23):10–12, 2009.

[152] Yuanbin Liu and Daniel A. Peterson. Mechanism of cellular 3-(4,5-dimethylthiazol-2-yl)-2,5-diphenyltetrazolium bromide (MTT) reduction. *Journal of Neurochemistry*, 69(2):581–93, 1997.

[153] Juan C. Stockert, Alfonso Blázquez-Castro, Magdalena Cañete, Richard W. Horobin, and Ángeles Villanueva. MTT assay for cell viability: Intracellular localization of the formazan product is in lipid droplets. *Acta Histochemica*, 114(8):785–796, 2012.

[154] Giacomo Diaz, M. Melis, A. Musinu, M. Piludu, M. Piras, and A. M. Falchi. Localization of MTT formazan in lipid droplets. An alternative hypothesis about the nature of formazan granules and aggregates. *European Journal of Histochemistry*, 51(3):213–218, 2007.

[155] Yuanbin Liu. Understanding the biological activity of amyloid proteins in vitro: From inhibited cellular MTT reduction to altered cellular cholesterol homeostatis. *Progress in Neuro-Psychopharmacology and Biological Psychiatry*, 23(3):377–395, 1999.

[156] C. Hertel, N. Hauser, R. Schubenel, B. Seilheimer, and J. A. Kemp. β-Amyloid-induced cell toxicity: Enhancement of 3-(4,5-dimethylthiazol-2-yl)-2,5-diphenyltetrazolium bromide-dependent cell death. *Journal of Neurochemistry*, 67(1):272–276, 1996.

[157] Kazuho Abe and Hiroshi Saito. Amyloid β protein inhibits cellular MTT reduction not by suppression of mitochondrial succinate dehydrogenase but by acceleration of MTT formazan exocytosis in cultured rat cortical astrocytes. *Neuroscience Research*, 31(4):295–305, 1998.

[158] Ichiro Isobe, Makoto Michikawa, and Katsuhiko Yanagisawa. Enhancement of MTT, a tetrazolium salt, exocytosis by amyloid β- protein and chloroquine in cultured rat astrocytes. *Neuroscience Letters*, 266(2):129–132, 1999.

[159] Yuanbin Liu and David Schubert. Cytotoxic amyloid peptides inhibit cellular 3-(4,5-dimethylthiazol-2-yl)-2,5-diphenyltetrazolium bromide (MTT) reduction by enhancing MTT formazan exocytosis. *Journal of Neurochemistry*, 69(6):2285–2293, 1997.

[160] Yuanbin Liu, Daniel A. Peterson, and David Schubert. Amyloid β peptide alters intracellular vesicle trafficking and cholesterol homeostasis. *Proceedings of the National Academy of Sciences of the United States of America*, 95(22):13266–13271, 1998.

[161] Yuanbin Liu and David Schubert. Steroid hormones block amyloid fibril-induced 3-(4,5-dimethylthiazol-2- yl)-2,5-diphenyltetrazolium bromide (MTT) formazan exocytosis: Relationship to neurotoxicity. *Journal of Neurochemistry*, 71(6):2322–2329, 1998.

[162] Ryan Limbocker, Benedetta Mannini, Rodrigo Cataldi, Shianne Chhangur, Aidan K. Wright, Ryan P. Kreiser, J. Alex Albright, Sean Chia, Johnny Habchi, Pietro Sormanni, Janet R. Kumita, Francesco S. Ruggeri, Christopher M. Dobson, Fabrizio Chiti, Francesco A. Aprile, and Michele Vendruscolo. Rationally designed antibodies as research tools to study the structure toxicity relationship of amyloid-β oligomers. *International Journal of Molecular Sciences*, 21(12):1–18, 2020.

[163] John P. Anderson, Donald E. Walker, Jason M. Goldstein, Rian De Laat, Kelly Banducci, Russell J. Caccavello, Robin Barbour, Jiping Huang, Kristin Kling, Michael Lee, Linnea Diep, Pamela S. Keim, Xiaofeng Shen, Tim Chataway, Michael G. Schlossmacher, Peter Seubert, Dale Schenk, Sukanto Sinha, Wei Ping Gai, and Tamie J. Chilcote. Phosphorylation of Ser-129 is the dominant pathological modification of α-synuclein in familial and sporadic lewy body disease. *Journal of Biological Chemistry*, 281(40):29739–29752, 2006.

[164] Shawn C. Owen, Allison K. Doak, Ahil N. Ganesh, Lyudmila Nedyalkova, Christopher K. McLaughlin, Brian K. Shoichet, and Molly S. Shoichet. Colloidal drug formulations can explain "bell-shaped" concentration-response curves. *ACS Chemical Biology*, 9(3):777–784, 2014.

[165] Richard A. Steinhardt, Guoqiang Bi, and Janet M. Alderton. Cell membrane resealing by a vesicular mechanism similar to neurotransmitter release. *Science*, 263(5145):390–393, 1994.

[166] Katsuya Miyake and Paul L. McNeil. Vesicle accumulation and exocytosis at sites of plasma membrane disruption. *Journal of Cell Biology*, 131(6 II):1737–1745, 1995.

[167] Tatsuru Togo. Disruption of the plasma membrane stimulates rearrangement of microtubules and lipid traffic toward the wound site. *Journal of Cell Science*, 119(13):2780–2786, 2006.

[168] Alisa D. Blazek, Brian J. Paleo, and Noah Weisleder. Plasma membrane repair: A central process for maintaining cellular homeostasis. *Physiology*, 30(6):438–448, 2015.

[169] Lanhai Lü, Lihong Zhang, Maria Sen Mun Wai, David Tai Wai Yew, and Jie Xu. Exocytosis of MTT formazan could exacerbate cell injury. *Toxicology in Vitro*, 26(4):636–644, 2012.

[170] Amulya Nidhi Shrivastava, Virginie Redeker, Laura Pieri, Luc Bousset, Marianne Renner, Karine Madiona, Caroline Mailhes Hamon, Audrey Coens, Luc Buée, Philippe Hantraye, Antoine Triller, and Ronald Melki. Clustering of Tau fibrils impairs the synaptic composition of α3-Na/K - ATPase and AMPA receptors. *The EMBO Journal*, 38(3):1–22, 2019.

[171] Irina Y. Petrushanko, Vladimir A. Mitkevich, Anastasia A. Anashkina, Alexei A. Adzhubei, Ksenia M. Burnysheva, Valentina A. Lakunina, Yulia V. Kamanina, Elena A. Dergousova, Olga D. Lopina, Omolara O. Ogunshola, Anna Y. Bogdanova, and Alexander A. Makarov. Direct interaction of beta-amyloid with Na,K-ATPase as a putative regulator of the enzyme function. *Scientific Reports*, 6:1–10, 2016.

[172] Lucia Trevisi, Isabella Pighin, Sara Bazzan, and Sisto Luciani. Inhibition of 3-(4,5-dimethylthiazol-2-yl)-2,5-diphenyltetrazolium bromide (MTT) endocytosis by ouabain in human endothelial cells. *FEBS Letters*, 580(11):2769–2773, 2006.

[173] Mihaela M. Apetri, Rolf Harkes, Vinod Subramaniam, Gerard W. Canters, Thomas Schmidt, and Thijs J. Aartsma. Direct observation of α-synuclein amyloid aggregates in endocytic vesicles of neuroblastoma cells. *PLoS ONE*, 11(4):1–13, 2016.

[174] Melissa Birol, Slawomir P. Wojcik, Andrew D. Miranker, and Elizabeth Rhoades. Identification of n-linked glycans as specific mediators of neuronal uptake of acetylated α-synuclein. *PLoS Biology*, 17(6):1–29, 2019.

[175] Nicholas J. Izzo, Agnes Staniszewski, Lillian To, Mauro Fa, Andrew F. Teich, Faisal Saeed, Harrison Wostein, Thomas Walko, Anisha Vaswani, Meghan Wardius, Zanobia Syed, Jessica Ravenscroft, Kelsie Mozzoni, Colleen Silky, Courtney Rehak, Raymond Yurko, Patricia Finn, Gary Look, Gilbert Rishton, Hank Safferstein, Miles Miller, Conrad Johanson, Edward Stopa, Manfred Windisch, Birgit Hutter-Paier, Mehrdad Shamloo, Ottavio Arancio, Harry LeVine, and Susan M. Catalano. Alzheimer's therapeutics targeting amyloid beta 1-42 oligomers I: Abeta 42 oligomer binding to specific neuronal receptors is displaced by drug candidates that improve cognitive deficits. *PLoS ONE*, 9(11), 2014.

[176] Hyun-Seok Hong, Izumi Maezawa, Nianhuan Yao, Bailing Xu, Diaz-Avalos Ruben, Sandeep Rana, Duy H. Hua, R. Holland Chen, Kit S. Lam, and Lee-Way Jin. Combining the Rapid MTT Formazan Exocytosis Assay and the MC65 Protection

Assay Led to the Discovery of Carbazole Analogs as Small-Molecule Inhibitors of Aβ Oligomer-Induced Cytotoxicity. *Brain Research*, 23(1):1–7, 2008.